AFRL-SR-AR-TR-04-

0634

REPORT DOCUMENTATION PAGE

1. AGENCY USE ONLY (Leave blank)	2. REPORT DATE	3. REPORT TYPE AND DATES COVERED
	11/30/04	Final performance: 5/15/00-5/14/04

4. TITLE AND SUBTITLE
Ultra-Stable Gallium Nitride and Infrared Laser Frequency Standards Based on Spectral Hole Burning

5. FUNDING NUMBERS
F49620 -00-1-0314

6. AUTHOR(S)
PI: Cone, Rufus L., Professor of Physics (406) 994 6175

7. PERFORMING ORGANIZATION NAME(S) AND ADDRESS(ES)
Physics Department, EPS 264
Montana State University
Bozeman, MT 59717-3840

Office of Grants and Contracts
Montana State University
Bozeman, MT 59717-3840

8. PERFORMING ORGANIZATION REPORT NUMBER

9. SPONSORING / MONITORING AGENCY NAME(S) AND ADDRESS(ES)
Dr. Gernot Pomrenke
Air Force Office of Scientific Research
Ballston Common Towers III
4015 Wilson Blvd, Room 713
Arlington VA 22203-1954

10. SPONSORING / MONITORING AGENCY REPORT NUMBER

11. SUPPLEMENTARY NOTES
The views, opinions and/or findings contained in this report are those of the author(s) and should not be construed as an official Department of the Air Force position, policy or decision, unless so designated by other documentation.

12a. DISTRIBUTION / AVAILABILITY STATEMENT
Approved for public release; distribution unlimited.

12b. DISTRIBUTION CODE

13. ABSTRACT ***(Maximum 200 Words)***

Our development of compact optical frequency standards and stable lasers opens new applications particularly to vibrometry and analog optical signal processing with high bandwidth and time-bandwidth products. Lasers are stabilized to 'spectral holes' as frequency references; devices deliver 20 Hz range stability potentially in compact packages. We stabilized diode lasers at 1.5 micron communication wavelengths, developed and characterized devices, and worked to develop compact packages for advanced systems. Hole burning materials were designed and identified that produce frequency references in the infrared, visible, and near ultraviolet spectral ranges. Frequency standards are programmable, readily mass produced, and transportable; multiple frequency values or intervals can be programmed in the same piece of material. We have state of the art facilities for spectroscopy, development, and characterization of optical materials. We have defined the limits of precision in optical spectroscopy of solids (73Hz). Scientific Materials Corporation of Bozeman, MT, is a partner in materials development, allowing for rapid refinement of new materials and material concepts. Training of optics professionals is a basic part of this project and encompasses undergraduate and graduate students and post-doctoral fellows. Graduates from our laboratory have become DoD contractors, industrial scientists, faculty, and scientists at national labs.

14. SUBJECT TERMS
Spectral Hole Burning, Laser Frequency Stabilization, Optical Coherent Transients, Optical Material, Diode Laser, 1.5 micron, spatial-spectral holography

15. NUMBER OF PAGES
89

16. PRICE CODE

17. SECURITY CLASSIFICATION OF REPORT	18. SECURITY CLASSIFICATION OF THIS PAGE	19. SECURITY CLASSIFICATION OF ABSTRACT	20. LIMITATION OF ABSTRACT
UNCLASSIFIED	UNCLASSIFIED	UNCLASSIFIED	UL

Final Report

for 15 May 2000 to 14 May 2004

submitted by

Rufus L. Cone, Principal Investigator
Physics Department
Montana State University
Bozeman, MT 59717
Telephone: 406-994-6175
FAX: 406-994-4452
Email: cone@montana.edu

AFOSR-DEPSCoR Agreement Number F49620 -00-1-0314

Ultra-Stable Gallium Nitride and Infrared Laser Frequency Standards Based on Spectral Hole Burning

submitted to

Dr. Gernot Pomrenke, Program Manager
AFOSR/NE
Directorate of Physics and Electronics
Air Force Office of Scientific Research
Ballston Common Towers III
4015 Wilson Blvd, Room 713
Arlington, VA 22203-1954

SUMMARY OF EFFORT

Relevance

Lasers, high bandwidth and high time-bandwidth product analog optical signal processing devices, quantum information, and optical data storage are applications areas for our lasers and spectral hole burning (SHB) materials. Our lasers stabilized to spectral holes are enabling technology for optical signal processing and a number of opto-electronic devices based on spectral hole burning and spatial-spectral holography.

We have transferred our designs and characterizations of hole burning materials to Scientific Materials Corporation of Bozeman, MT, a DoD SBIR contractor.

We have transferred laser stabilization techniques and spectral hole burning materials to MSU Spectrum Lab, Scientific Materials Corporation, and other DoD funded groups and have developed, refined, and characterized materials for both high bandwidth optical signal processors and high density optical memories based on spectral hole burning in support of DoD programs.

We collaborated with IBM Almaden Research Center and MSU Spectrum Lab.

Overview of Impacts on Montana Business and Other Montana Programs

This project impacts Montana business, commercial products under development, the Spectrum Lab at Montana State University which is the device oriented arm of our cooperative Montana-based spectral hole burning research activities, and other research groups in the Physics Department at Montana State University.

- Our stable laser devices are required for a number of Montana-critical applications. Our new lasers and laser systems are required for optical signal processing devices produced by Scientific Materials Corporation and MSU Spectrum Lab; for new initiatives at MSU in the high-profile computer technology based on quantum physics and called 'quantum computing,' 'quantum information,' or 'quantum cryptography;' and for military applications such as remote sensing of vibrations (laser vibrometry).

- We have provided enabling technology for the S^2CHIP optical signal processing program that Scientific Materials Corporation, Bozeman, MT, has with the US Missile Defense Agency (MDA) and US Army Space and Missile Defense Command (USA/SMDC). The name "S^2CHIP" stands for "Spatial-Spectral Coherent Holographic Integrating Processor."

- We have transferred our laser stabilization techniques and materials to MSU Spectrum Lab as enabling technology for (a) signal processors for the US Defense Advanced Research Projects Agency (DARPA), (b) the S^2CHIP for Army Missile Defense Agency/Space and Missile Defense Command, and (c) other Spectrum Lab projects funded by the US Government through cooperation with the University of Colorado.

The MSU Spectrum Lab highlights the two fundamental technologies responsible for Spectrum Lab's success:

- Spatial-spectral holography — relying on our materials
- Laser development and stabilization: Frequency locking to spectral holes — developed in our laboratory.

The S^2CHIP 'proof of concept' demonstration mentioned on page 3 was done in Autumn 2001,

- with Cone group stabilized lasers,
- in the Cone lab, and
- in a laser stabilization and hole burning material that the Cone group developed – $Er^{3+}:Y_2SO_5$.

S^2CHIP for RADAR

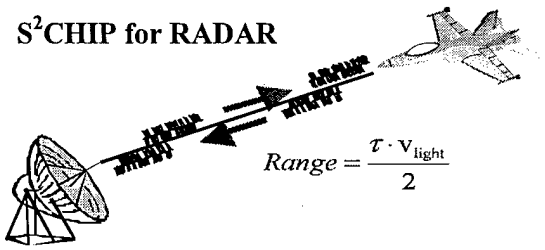

That experiment led to a family of high optical bandwidth and high time-bandwidth product analog optical signal processing devices.

Details are discussed beginning on page 6 of this report and in Applied Physics Letters:
Coherent Integration of 0.5 GHz Spectral Holograms at 1536 nm using Dynamic Bi-Phase Codes, Z. Cole, T. Böttger, Krishna Mohan, R. Reibel, W. R. Babbitt, R. L. Cone, and K. D. Merkel, Appl. Phys. Lett. **81**, 3525-3527 (2002).

Three US Patents Issued

1. United States Patent 6,407,831. *Coherent interaction of optical radiation beams with optical-electronic materials of generalized crystal symmetry.* Inventors: Rufus L. Cone (Bozeman, MT), Guangming Wang (Marlborough, MA), Yongchen Sun (Bozeman, MT), Randy W. Equall (Bozeman, MT), issued June 18, 2002.
2. United States Patent 6,516,014. *Programmable Frequency Reference for Laser Frequency Stabilization, and Arbitrary Optical Clock Generator, Using Persistent Spectral Hole Burning,* J. L. Carlsten, R. L. Cone, P. B. Sellin, N. M. Strickland, issued February 4, 2003.
3. United States Patent 6,654,394. *Laser Frequency Stabilizer Using Transient Spectral Hole Burning,* J. L. Carlsten, R. L. Cone, P. B. Sellin, N. M. Strickland, issued November 25, 2003.

Refereed Papers

Twenty published..

Conference Presentations

Seventeen invited and plenary talks & fifty contributed talks.

Conference Organization

Twelve conference program and organizing committees and conference sessions chaired.

CONFERENCE ORGANIZATION, **8th International Meeting on Hole Burning, Single Molecule, and Related Spectroscopies: Science and Applications – HBSM 2003**, July 27 to 31, 2003, Bozeman, MT. Rufus Cone, Randy Babbitt, and Aleks Rebane, together with Randy Equall of Scientific Materials Corporation, hosted the 8th International Meeting on Hole Burning, Single Molecule, and Related Spectroscopies: Science and Applications, 'HBSM 2003,' on July 26 - 31, 2003, in Bozeman, Montana. The conference was sponsored by The Physics Department, The Spectrum Lab, and Scientific Materials Corporation and was supported by Air Force Office of Scientific Research and Scientific Materials Corporation.

Accomplishments in the following areas are described on pages 6-67:

ACCOMPLISHMENTS

Our laser frequency stabilization to spectral hole frequency references has been applied to diode lasers in our laboratory, and our technology has been transferred to several Ti:Sapphire lasers, demonstrating that these concepts and material references are broadly applicable to other types of lasers.

Our laser technology has been fundamental to the development of the analog optical signal processing as epitomized by the S^2CHIP processor developed by MSU Spectrum Lab and Scientific Materials Corp. of Bozeman. Advantages compared to conventional signal processing, are a) high bandwidth, large time–bandwidth product, and large dynamic range operation, b) the ability to process waveforms that change from shot to shot, c) coherent integration or signal averaging of up many shots, and d) Doppler processing. Our laser technology has been adopted by a number of other groups who focus on development of similar devices.

External cavity diode lasers have typical free-running linewidths of 100 kHz to 1 MHz or more, and standard diode Fabry-Perot lasers have linewidths far far larger. Our stabilization techniques have improved linewidths dramatically to the 20 Hz region over millisecond time scales. This corresponds to stability of a part in 2×10^{13}.

Analog Optical Signal Processing Enabled by Lasers Stabilized to Spectral Holes

Coherent integration of 0.5 GHz spectral holograms at 1536 nm using dynamic biphase codes
Z. Cole, T. Böttger, Krishna Mohan, R. Reibel, W. R. Babbitt, R. L. Cone, and K. D. Merkel, Appl. Phys. Lett. **81**, 3525-3527 (2002).

This technology relies on our SHB materials and our laser stabilization in addition to the concepts of spatial-spectral holography under development by Spectrum Lab. This discussion illustrates the significant application of our stable lasers to important warfighting technology.

Spectral hole-burning-based optical processing devices are created for coherent integration of multiple high-bandwidth interference patterns in a spectral hole-burning medium. We developed the hole-burning medium, provided the laser and most of the processing apparatus, and this demonstration was carried out in our laboratory in collaboration with personnel of the Spectrum Laboratory at Montana State University. This was the first experimental demonstration of what has become the S^2CHIP system described in the introduction of this report. Spectrum Lab personnel have since advanced the performance to ~10 GHz bandwidth in a compact package slated for commercialization.

In this first implementation, 0.5 GHz spectral holographic gratings were dynamically accumulated in Er^{3+}:Y_2SiO_5 at 4.2 K using a 1536 nm laser frequency stabilized to a spectral hole, along with commercial off-the-shelf components. The processed data, representing time delays over 0.5–2.0 μs, were optically read out using a frequency-swept probe laser, an approach that makes possible the use of low-bandwidth, large-dynamic-range detectors and digitizers.

Applications of SHB analog optical signal processing devices include optical storage, processing, true-time delay, rf spectrum analysis, and quantum computing. In previous processing demonstrations, spatial–spectral holographic gratings were recorded and then coherently probed to stimulate the emission of an optical coherent transient signal representing the processed output.

The present approach enables SHB-based processing applications including RADAR discussed here, LIDAR, vibrometry, and radio astronomy. In RADAR range and Doppler processing, a coded rf waveform is transmitted, reflected by a target, and then received (with inevitable additive noise) after a delay τ_D. The delay can be accurately determined by modulating the transmitted and returned rf waveforms onto an optical carrier and illuminating a spectral hole-burning material that acts as a correlative signal processor. For a single processing shot, two time-ordered waveforms resonantly interfere in a frequency selective inhomogeneously broadened transition, resulting in a spectral holographic grating – a frequency-dependent population grating that includes the spectral product of the waveforms modified by a $1/\tau_D$ periodic component. The processed information persists for and may be readout within the optical transition lifetime T_1 . For multishot processing, with pulse repetition frequency of $1/\tau_{Rep}$, up to $N = T_1/\tau_{Rep}$ shots may be coherently integrated by the medium, given sufficient laser frequency stability over T_1, resulting in an accumulated spectral grating in the SHB processing material. For N coherent shots, all having a common delay, the primary $1/\tau_D$ grating component accumulates as $;N^{2\alpha}$, where $\alpha \leq 1$ for small N. For large N, the integration gain saturates due to population dynamics. For agile RADAR processing applications, where each transmitted waveform is a unique code, the material coherently integrates the processing sequence, recording a dynamically accumulated spectral grating. The primary $1/\tau_D$ component accumulates while the changing spectral features of the dynamic codes and additive noise are averaged. Coherent integration of spectral gratings is achieved with low optical input power at pulse repetition frequencies of 1 kHz to 1 MHz with presently available materials near 1550 nm and 800 nm. Further, Doppler processing is achieved by introducing multiple optical frequency shifted copies of the transmitted waveform into different spatial channels of the material and parallel processing the returned signal (nonshifted) in all channels. Accumulation of the $1/\tau_D$ grating component occurs only when the frequency shift closely matches the Doppler shift on the return signal. The reconfiguration of a spectral grating in a single spatial location is limited by T_1.

We experimentally demonstrated coherent integration of up to 800 shots over 0.5 GHz bandwidth at 1536 nm in an Er^{3+}:Y_2SiO_5 crystal maintained at 4.2 K. Each transmit waveform was a 200-bit long binary-phaseshift-keyed code. The code time-bandwidth product is a factor of ~7 higher than previous spectral holographic processing efforts. A frequency-swept probe measured processed time delays ranging from 0.5 to 2.0 ms. We report coherent integration dynamics and material parameters under these conditions. This demonstration utilized technologies developed through Montana State University collaborations, including a laser frequency stabilized to a transient spectral hole and a rare-earth-doped spectral hole-burning crystal, along with commercial components. In the processing sequence, a shot consisted of a randomly generated zero-mean waveform and its time-delayed replica, emulating a RADAR transmit and return waveform pair without additive noise. Shots were introduced at a repetition interval τ_{Rep} , with a fixed delay τ_D for $n = 1,2,...N$. To avoid coherent beating between consecutive shots, we set $\tau_{Rep} > 2T_2$, where T_2 is the coherence time of the transition.

We implemented a frequency-swept readout technique to probe the grating structure by frequency dependent transmission, rather than using the traditional brief pulse to stimulate a photon echo. The transmitted signal can be detected, digitized, and post-processed to extract the processed delay(s). Frequency-swept probing enables practical system development, with the following advantages: (1) use of currently available low bandwidth, large dynamic range detectors (~1 MHz and ~120 dB), and digitizers (~2.5 MS/s and ~16 bit) to extract delay information from high bandwidth gratings, and (2) use of low power lasers with electrooptic frequency tuning elements to provide reproducible, high-bandwidth frequency-swept probes. The frequency-sweep rate should be less than $1/(\tau_{D\max})^2$ to ensure sufficient temporal resolution, where $\tau_{D\max}$ is the maximum resolvable delay limited by T_2 . The required bandwidth of detection is just $1/\tau_{D\max}$ rather than the signal bandwidth B. The required sweep duration is $[B(\tau_{D\max})]^2$. For example, if $\tau_{D\max} = 1.0$ μs, a sweep rate of 1.0 MHz/μs and a detection bandwidth of 1 MHz $<< B$ is sufficient.

Experiments were performed in a 2 mm thick 0.005 at.% Er^{3+}:Y_2SiO_5 crystal grown by Scientific Materials Corporation, with $\alpha L = 1.8$ at the 1536.14 nm line center. The $^4I_{15/2}$ (1) → $^4I_{13/2}$ (1) transition of site 1 had a 0.5 GHz absorption profile. The integration time for the holographic processor is set by $T_1 = 11$ ms, the population lifetime of the excited state of the Er^{3+} ions. Material studies determined the optimum direction for an applied magnetic field to minimize the effects of spectral diffusion on the holographic grating. When a 3.0 T external field was applied parallel to the $\mathbf{D}_1$ axis, operation was practical at 4.2 K, a temperature that can be provided by closed-cycle cryocooler technology. The external cavity diode laser was stabilized to a regenerative spectral hole in a different spatial region of the same crystal. The stabilization occurs at the required wavelength and provides the required stability over T_1 . Thus, the processing and stabilization techniques can be transferred to other hole burning materials. The spectral hole was nominally 30 kHz wide and frequency stability of ~1 kHz (Allan deviation over an integration time of 10 ms) was achieved. Both processing and stabilization beams propagated parallel to the crystal **b** axis and were polarized along $\mathbf{D}_2$.

Figure 1 depicts the main experimental components. The stabilized laser—tuned to the absorption line center—was fiber coupled and split into a processing and probing beam. The processing beam was continuously biphase-shift-keyed modulated by an electro-optic phase modulator driven by a pulse pattern generator and then amplified. Each waveform S^n was modulated at 0.5 Gb/s. Between all S^n, the light was square wave modulated (...101010...) at 1 Gb/s. A chopper created a 4 ms off window in the processing beam to allow for probing 0.5 ms into this window. The probing beam was amplified and frequency swept by an acousto-optic modulator. The beams were

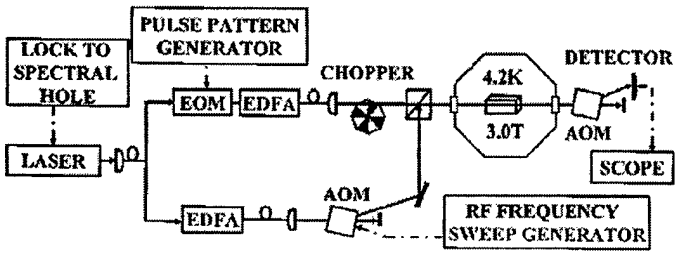

FIG. 1. Experimental schematic is shown: EOM—electro-optic modulator; EDFA—erbium-doped fiber amplifier; and AOM—acousto-optic modulator.

made collinear and focused to a ~50 μm (1/*e*2 diameter) spot in the crystal. The transmitted probe was deflected toward a 125 MHz bandwidth, ~50 dB dynamic range photodetector. For all experiments, each waveform was 400 ns long (200 bits at 2 ns/bit) with τ_{Rep} = 5 ms. The probe pulse was 10 mW and swept over ~15 MHz, shifted 165 MHz from the carrier at a sweep rate of 0.2083 MHz/μs. Post-processing of the transmitted probe consisted of filtering to minimize the low-frequency components of the unabsorbed probe envelope, performing a fast Fourier transform, and calculating its magnitude squared. Figure 2 plots post-processed data for N = 800 shots, where τ_D was varied from 0.5 to 2.0 μs in 0.1 μs increments using a 25 mW programming beam. The primary peak of each trace was normalized to the 0.5 ms peak. Analysis of the peaks, representing the extracted time delays, showed an arrival time accuracy of ~3 ns. The inset of Fig. 2 shows corresponding traces of the filtered transmitted probe, revealing the periodic $1/\tau_D$ structure and reduced grating strength with increasing delays due to coherence decay. For 25 mW and 40 mW excitation, a first-order fit of the non-normalized peaks to exp(-$2\tau_D/T_2$) results in a T_2 value of 0.82 ± 0.03 ms for these conditions.

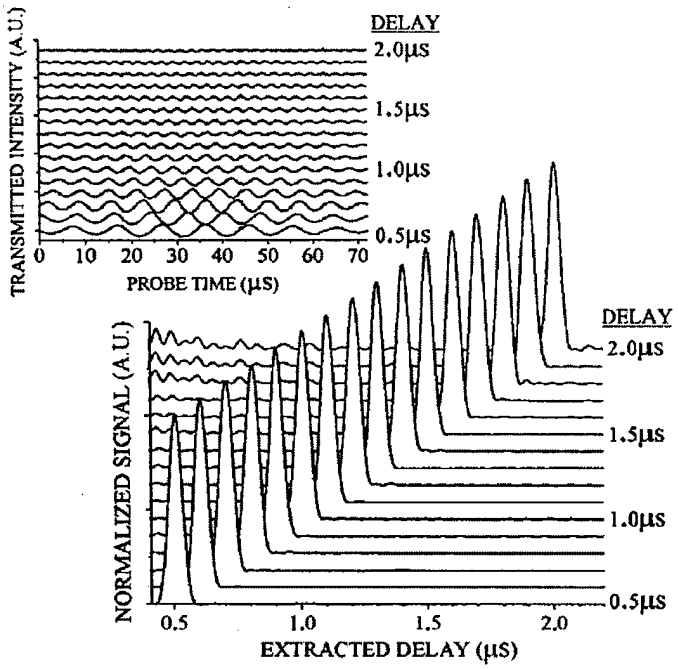

FIG. 2. Normalized traces of extracted time delay data are shown for processed time delay τ_D values ranging from 0.5 – 2.0 μs, after 800 shots using a 25 mW processing beam. The inset shows traces of the frequency-swept probe, which map the corresponding accumulated spectral gratings.

Figure 3(a) plots two examples of signal strength (log scale) versus extracted time delay (linear scale) when τ_D = 0.5 μs and N = 200 for 25 mW (thin line) and 40 mW (bold line) programming powers. In addition to the primary delay, there are nonlinear terms, or spurs, resulting in harmonics of each delay (and intermods if there are multiple delays). The second-harmonic observed here accumulates as $N^{4\beta}$. The grating strength and α and β depend on N, the optical programming power, coherence loss [∝exp(-2 τ_D /T_2)] during each shot, and population decay [∝ exp(-τ_{Rep}/T_1)] between shots. In Fig. 3(a), the primary peak and its second harmonic can be clearly observed and as expected increase with input power. Figure 3(a) is divided into four regions: I contains the primary peak representing the time delay τ_D ; II contains the right temporal correlation sidelobes; III contains the second harmonic of the primary peak; and IV contains the system background noise. There are residual low-frequency components due to imperfect post-processing of the unabsorbed probe, limiting absolute comparison between the regions in this demonstration; we

are, therefore, not including the left temporal sidelobe regions in our analysis. The peak temporal width of ~65 ns (full width at half maximum) is set by the probe bandwidth.

Figures 3(b) and 3(c) plot the root-mean-square (rms) values for regions I–IV (log scale) versus N (log scale) for a fixed $\tau_D = 0.5$ μs with (b) 25 mW or (c) 40 mW programming power. In Fig. 3(c), the higher programming power exhibits larger grating strength and stronger nonlinearities, as expected. Region I peaks of both Figs. 3(b) and 3(c) increase as $2\alpha \sim 1.8$ for the first 100 shots. The second harmonics in region III of Fig. 3(b) and 3(c) rise above the noise floor at $N = 70$ and $N = 30$, respectively, and both grow (for N <200) as $4\beta \sim 2.4$. The relatively flat nature of region II, particularly for the first 100 shots of Fig. 3(b), highlights the effects of coherent integration with dynamic codes. Improved performance is expected with wider bandwidth frequency-swept sources, detectors with larger dynamic range, and materials with higher bandwidths and longer coherence times.

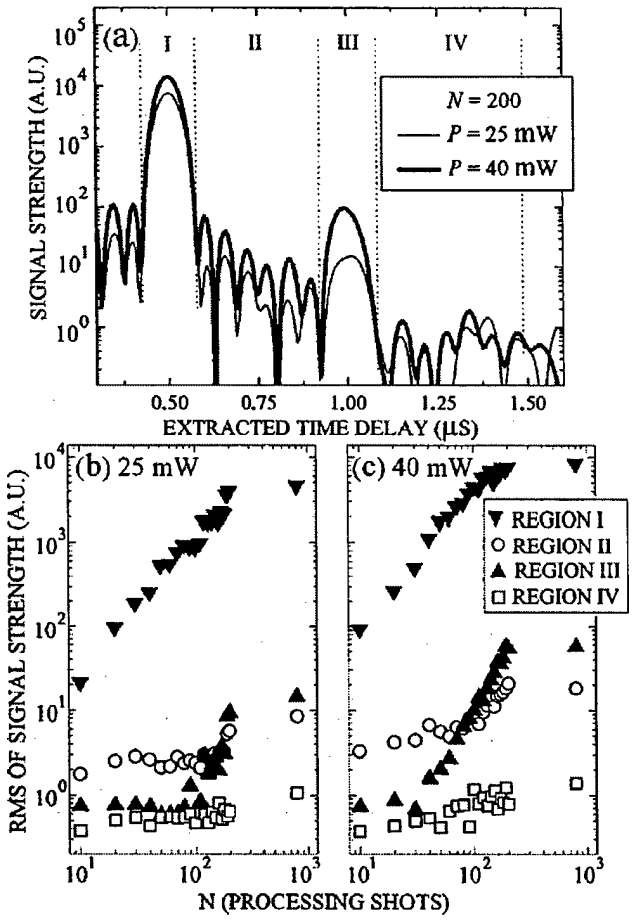

FIG. 3. (a) Traces of the extracted time delay are shown (log scale) for processed time delay $\tau_D = 0.5$ μs after N = 200 shots for 25 mW pulses (thin trace) and 40 mW pulses (bold trace). The data has four regions of interest: (I) the primary peak; (II) the right-hand side sidelobe region; (III) the second harmonic of the primary peak; and (IV) the background noise of the system. The rms values of regions I–IV vs N are shown in (b) for 25 mW and (c) for 40 mW programming pulses over a 4 ms integration time.

Adoption of these techniques offers the following for analog signal processing applications: (1) high bandwidth, large time–bandwidth product, and large dynamic range operation without high-bandwidth detectors and digitizers, (2) the ability to process waveforms that change from shot to shot, (3) coherent integration of up to $\sim T_1/\tau_{Rep}$ shots, or of two continuous signals correlated over a T_2 window for a time T_1, and (4) Doppler processing.

In summary, dynamic accumulation of spectral holographic gratings by coherent integration of up to 800 shots was demonstrated. The signal processing bandwidth was 0.5 GHz, limited by the crystal used. Performance in the 10 GHz range has now been achieved by Spectrum Lab in extensions of this

work. Time delays of 0.5 to 2.0 μs were processed and extracted with 3 ns accuracy in the initial work described here. The demonstration used a stabilized diode laser, 1550 nm telecom components, and a frequency-swept probe. Successful processing and frequency stabilization in crystals at 4.2 K make possible the use of closed-cycle cryocoolers, and enable practical, high performance, multi-GHz, analog correlative processors using spectral holography.

This signal processing demonstration has led directly to the development of processors for RADAR signals that exceed the state of the art for electronic processing.

Lasers Stabilized to Spectral Holes

Laser Stabilization at 1536 nm using Regenerative Spectral Hole Burning
P. B. Sellin, N. M. Strickland, T. Böttger, J. L. Carlsten, and R. L. Cone, Phys. Rev. B **63,** 155111-1 – 155111-7 (2001)

This development of stable lasers provided the basis for the processing application discussed above. Having the same material be used for the analog signal processing and the frequency reference for the laser provides important vibration immunity to devices.

This work also transferred our concepts to the important communication band at 1550 nm. That makes our work applicable in telecom devices and also means that the important component infrastructure developed by the telecom industry can be incorporated in our lasers and processors. A goal is to integrate and develop 'all optical' devices and connect all elements with optical fiber.

Laser frequency stabilization giving a 500 Hz root Allan variance for a 2 ms integration time with drift reduced to 7 kHz/min over several-minutes was achieved at 1536 nm. A continuously-regenerated spectral hole in the inhomogeneously broadened $^4I_{15/2}$ (1) → $^4I_{13/2}$ (1) optical absorption of an Er^{3+}:Y_2SiO_5 crystal was used as the short term frequency reference, while a new variation on the locking technique allowed simultaneous use of the inhomogeneously broadened absorption line as a long term reference. The reported frequency stability was achieved without vibration isolation. Spectral hole burning frequency stabilization provides ideal laser sources for high resolution spectroscopy, real time optical signal processing, and a range of applications requiring ultra-narrowband light sources or coherent detection; the time scale for stability and the compatibility with spectral hole burning devices make this technique complementary to other frequency references for laser stabilization.

Frequency stable lasers are required for applications such as

- solid state optoelectronic devices based on spectral hole burning (SHB) such as
  - GHz-scale time-domain optical signal processing
  - network packet switching,
- high resolution spectroscopy of solids, molecules, and atoms,
- precision laser ranging,
- long-baseline interferometry, including *laser vibrometry*
- gravitational wave detection,
- spatial coordination of satellite arrays,

- optical communication using coherent light detection,
- sensitive vibration monitoring devices, and
- a variety of other optical and fiber optical sensors.

Spectral holes provide alternatives that are complementary to precision atomic resonances or the reflection modes of Fabry-Perot optical cavities. Our demonstrations were carried out with crystals cooled to liquid helium temperatures, but higher temperature operation at 15 – 20 K with 1 kHz frequency stability can be projected for our Tm^{3+} or Er^{3+} doped and deuterated CaF_2 materials described below. Best performance with atomic resonances or Fabry-Perot cavities also typically requires liquid helium temperature.

The availability of ultra-narrow SHB resonances down to 15 Hz in rare earth doped crystals, the relative immunity of spectral holes to environmental disturbances such as vibrations, and the portability and compactness of a stable laser system using SHB references with a closed cycle cryocooler are important features that should enable application in a variety of fields beyond those normally associated with spectral hole burning.

Stabilization of the repetitive pulse trains from mode locked lasers to spectral holes also should be practical and will have applications in signal processing and in other contexts that require short pulses, "frequency combs," or optical clocks. The SHB frequency references are well suited to applications where multiple frequencies are required and where the programmability of SHB materials allows programmable frequency differences up to the multi-GHz range or, if disordered solids are used, to the THz range. With the development of suitable photon-gated (or two-photon) SHB materials, the production of long term secondary frequency standards based on SHB may become practical.

When stabilized laser sources are required for real time optical signal processing in SHB materials, the use of a second piece of the same signal processing material as a SHB frequency reference provides automatic frequency compatibility between the signal processing material and the stabilized laser source. The relative vibration immunity of the spectral holes provides an important simplification in system design and performance for either spectroscopy or SHB devices; this advantage is even greater when both the frequency reference and spectroscopic sample or SHB device are mounted on the same platform or sample holder. This has been demonstrated here for Er^{3+}:Y_2SiO_5. A stabilized laser of this type will be especially helpful, for example, in measurements of spectral diffusion using the stimulated photon echo technique.

The importance of stabilization in SHB signal processing is underscored by the observation that early moderate-speed demonstrations were limited by laser frequency jitter that led to a loss in signal fidelity. Those problems can occur at several levels: (a) uncontrolled phase variations between programming pulses when repeated pulse sequences are used for writing or refreshing spectral interference gratings, (b) the more extreme case where the jitter exceeds the Fourier width of the exciting pulses so that the processed pulses fail to overlap spectrally with the programming pulses, and (c) the case where the jitter exceeds the Fourier width of the exciting pulses so that the excitation pulses fail to overlap spectrally with the probe pulse in measurements of spectral diffusion. Lasers stabilized to spectral holes are already playing an

important role in proof-of-principle demonstrations of a variety of SHB devices at the MSU Spectrum Lab.

In our work, an Er^{3+}-doped SHB crystal has been used to demonstrate laser stabilization in the important 1.5 μm telecommunications band. We have shown that Er^{3+}-doped crystals have the frequency selectivity required for optical storage, real-time address header decoding for all-optical packet routing, and all-optical correlation. Since the laser can be stabilized to the same transition used in the device demonstrations, the requirements of frequency overlap, frequency and phase stability, and time scale of stabilization are all automatically fulfilled. The limits on device performance are set then by material parameters rather than by instability of the laser.

A transient spectral hole is continuously regenerated by the stabilized laser in the present work, and that provides a frequency reference at an arbitrarily chosen location in the inhomogeneous Er^{3+}:Y_2SiO_5 absorption profile. The stability of the laser is determined by the dynamical properties of the SHB material together with the design of the locking system.

To substantially improve the long-term frequency stability, we have extended the locking technique by using a combination of the error signal contributions from the spectral hole and the inhomogeneous line. The reduction of longer-term drift to 7 kHz/min over several minutes obtained with the new technique represents a substantial improvement over the 600 kHz/min we reported previously for stabilization to Tm^{3+}:YAG at 793 nm. [N. M. Strickland, P. B. Sellin, Y. Sun, J. L. Carlsten, and R. L. Cone, Phys. Rev. B **62**, 1473-1476 (2000).] Anticipated refinements to the feedback system and frequency modulators may be expected to provide further substantial improvement over both the long and short term stability reported here, which is already 1000 times better over important integration time scales than that for commercial lasers. This provides new capabilities to probe dynamics in the neighborhood of the active rare earth ions in SHB materials and to reveal small scale level structures and dynamics out to the tens of milliseconds scale or even longer.

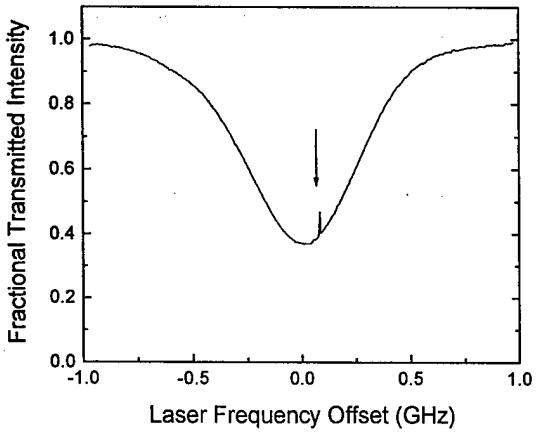

FIG. 4. Transmission spectrum of 0.005% Er^{3+}:Y_2SiO_5 scanned by a diode laser showing the entire inhomogeneously broadened absorption profile at zero applied field (B = 0 T). The arrow indicates a spectral hole burned by a second laser.

The SHB crystal frequency reference was an Er^{3+}:Y_2SiO_5 crystal with an Er^{3+} concentration of 0.005 atomic percent. This material exhibits transient spectral hole burning on the $^4I_{15/2}$ (1) → $^4I_{13/2}$ (1) transitions at 1536.14 nm (site 1) and 1538.57 nm (site 2) by population storage in the excited state of the optically active ion. The inhomogeneous linewidth Γ_{inh} = 500 MHz = 0.017 cm^{-1} is illustrated in Fig. 4 at left; a single spectral hole has been burned into the line in this illustration. The homogeneous linewidth Γ_h

of this Er^{3+} transition decreases substantially in applied magnetic fields, leading to narrower spectral hole widths. The homogeneous linewidth for this crystal was determined from the optical dephasing time T_2 obtained from two-pulse photon echo decay experiments at 1.6 K, and the measured value is $\Gamma_h \sim 5$ kHz. Stronger magnetic fields reduced the homogeneous line width to 78 Hz, and it is expected that further elucidation of the angular dependence of the Zeeman splittings will reveal a field direction that provides more rapid freezing out of electronic spin flips involving the excited component of the ground state and thus allow the linewidth to more closely approach the T_1 lifetime limited value of 15 Hz. Those Zeeman splitting experiments are under way.

Two frequency reference crystals were cut from the same crystal boule to give an absorption of ~50% at line center. Crystal dimensions were 5 mm along D_1, 6 mm along D_2 and 1 mm along b. Each crystal was oriented with its D_1-axis parallel to the magnetic field, the lasers' ***k***-vectors parallel to the b-axis, and the lasers polarized with ***E*** along D_2. Both crystals were immersed in superfluid helium at 1.6 K in a single dewar with a superconducting magnet that provided for adjustment of the magnetic field. The laser beams were spatially separated, and the crystals were masked so that each crystal was exposed to only one beam. The spectral holes were created with irradiances of 100 $\mu W/cm^2$ using ~3 mm beam diameters. Beam irradiance was controlled using a $\lambda/2$-plate and a prism polarizer.

The experimental apparatus is shown in Fig. 5 below. Two external cavity diode lasers in the Littman-Metcalf configuration were equipped with InGaAsP/InP quantum well diodes that had one facet angled to eliminate intra-cavity optical feedback. The Pound-Drever-Hall technique

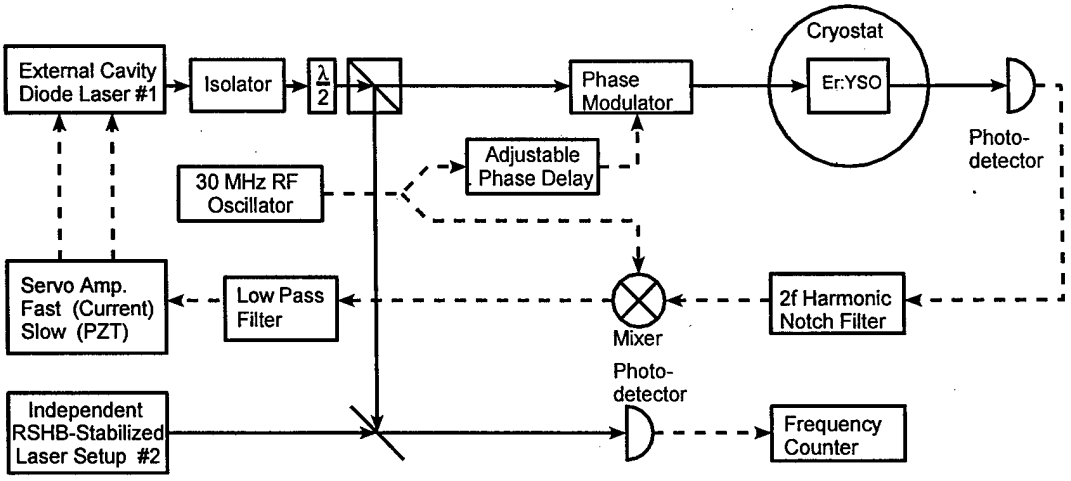

FIG. 5. Experimental apparatus for laser frequency locking to spectral holes and beat frequency measurement of laser stability by combining the beam from the laser shown and that from an independent second laser system.

was used for locking the laser frequency to the spectral hole. The error signal was derived from the spectral hole transmission using frequency modulation (FM) spectroscopy, with the two lasers modulated by external electro-optic modulators driven at 27 MHz and 30 MHz, respectively. These frequencies greatly exceeded the spectral hole widths but were far less than

the inhomogeneous absorption linewidth Γ_{inh} = 500 MHz. The primary laser side bands had a modulation index M = 0.4, and secondary side bands were small but observable. The sharp resonance of the spectral hole in the inhomogeneous absorption line creates a corresponding dispersion in the refractive index. Each laser burns a hole in its reference crystal, primarily at the carrier frequency but also at the frequencies of the FM side bands.

The FM error signal was processed by a servo loop that provided both fast corrections to the injection current of the laser diode and reduced bandwidth signals to the piezoelectric control of the laser's external diffraction grating. Control of the grating keeps the current servo within its operating limits. Due to laboratory constraints, the two lasers were on one table, and the reference crystals, magnet dewar, and locking beam detectors were on a separate table. Neither table was pneumatically floated, so the results reported here demonstrate the immunity of this locking technique to vibrations. By contrast, most other frequency references require extreme vibration isolation measures to reach this short-term stability.

Evaluation of the frequency stability of a single laser at sub MHz resolution is difficult if one lacks a frequency standard at the appropriate wavelength for comparison. For that reason, two independent lasers were constructed and locked to two separate SHB crystal references. The frequency stability was determined by beating unmodulated portions of the two stabilized laser beams on a photodiode detector, recording the beat frequency measured by a commercial frequency counter, and carrying out subsequent statistical analysis of the time dependence of the beats using a computer.

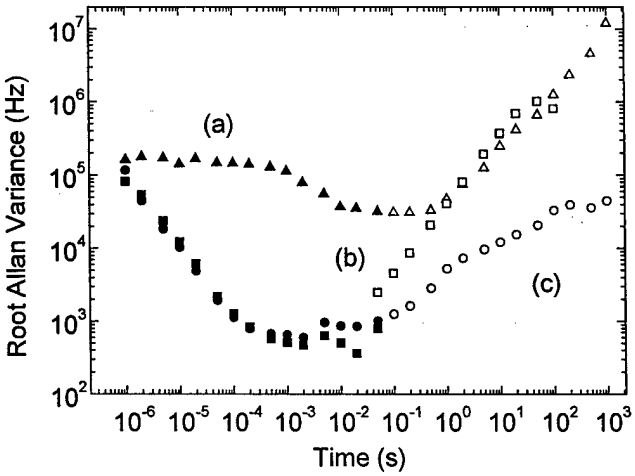

FIG. 6. Root Allan variance values for the beat between two lasers: (a) lasers free-running (triangles), (b) locked to spectral holes in different crystals using straight quadrature detection of the error signal at applied field B = 0.5 T (squares), and (c) locked to spectral holes using the strategy of intermediate phase detection of the combined error signal from the spectral hole and inhomogeneous line at applied field B = 0.2 T (circles).

The stability over broad time scales was characterized by the root Allan variance of the heterodyne beat frequency. Performance of the free running lasers is shown in Fig. 6 (a), while that of the lasers locked to regenerative spectral holes using the method that we reported last year is shown in Fig. 6 (b). Short term stabilization giving a 500 Hz root Allan variance for a 2 ms integration time was achieved with the conventional adjustment of the phase sensitive error signal, that is, with the detector signal and local oscillator in phase at the mixer. Under those conditions, the dominant contribution to the error signal comes from the spectral hole. Comparison of the curves in Fig. 6 (a) and (b) shows that slow frequency drift (integration times longer than 100 ms) of the stabilized lasers in these early experiments

approached that of the unstabilized laser. Much of this drift is attributable to slowly-varying DC voltage offsets in the feedback servo loop arising from residual amplitude modulation at the optical phase modulators and temperature drift in the feedback electronics and modulators. The servo offsets cause the laser to lock off-center to the spectral hole and consequently cause the regenerated spectral hole to drift continuously until the drift in the voltage offset undergoes a change of sign. Further development of the feedback servo system should substantially reduce these slowly-varying offsets and thus reduce this long-term drift.

A new locking strategy was devised to reduce drift by simultaneously exploiting the high resolution short term frequency reference of the spectral hole and the long term stability of the significantly broader inhomogeneous absorption line. Crystal transmission is increased at the frequency of the spectral hole, so the transmission property of the hole and inhomogeneous absorption line have opposite signs. Their pure absorptive and dispersive FM contributions also have opposite signs in simple limiting cases. The shape of the FM signals, however, also depends on the relationship between the modulation frequency ν_m and the width of the relevant spectral feature. There is broad latitude for making this choice, since the hole width $\sim 2\,\Gamma_h$ can be from 10^5 to 10^8 times narrower than the inhomogeneous line width Γ_{inh}. In the present case, the line widths of the hole contribution and inhomogeneous line contribution lie at opposite extremes relative to the modulation frequency: $\Gamma_h << \nu_m << \Gamma_{inh}$. The two contributions to the error signal at line center are then strongly phase dependent and are maximized for different quadratures – the dispersive case for the spectral hole and absorptive case for the inhomogeneous profile. For a phase angle of $\phi = 0°$ the inhomogeneous line signal is negligible and the locking signal is derived primarily from the spectral hole and for a phase angle of $\phi = 90°$ the signal from the inhomogeneous line is maximized, but the contribution from the spectral hole has vanished at the line center of the hole. By choosing an intermediate phase $0° < \phi < 90°$, both contributions to the error signal contribute to locking stability; a steeply sloped signal from the spectral hole drives the short term stability while at the same time a signal of lower slope from the inhomogeneous line opposes long term drift.

With this procedure, the introduction of a static DC offset in the servo loop leads to an equilibrium lock point where a balance occurs between the sloping contribution from the inhomogeneous line and the DC offset. While not a perfect solution, this is preferable to the original situation where a DC offset caused the locking to be displaced toward one side of the hole and consequently caused a steady drift in hole position and laser frequency as regenerative hole burning took place asymmetrically. Drift in hole position and hence in laser frequency can still occur with the present strategy if the DC offset is slowly varying, but the impacts on stability are reduced. This tendency to settle into an equilibrium position instead of continuing to drift not only improves the long-term frequency stability but also provides a means to choose an arbitrary frequency within the inhomogeneous absorption profile as the stabilization frequency. To adjust the locking frequency, either the DC offset level or the local oscillator phase (and hence the contribution of the inhomogeneous line to the error signal slope) may be adjusted. The system initially drifts towards and then settles at the equilibrium frequency, where the offset cancels the FM signal. This behavior was verified by computer simulation and by direct observation using a probe laser to monitor the position of the spectral hole and the locked laser within the inhomogeneous line.

The impact of this new hybrid locking strategy on frequency stability is shown in the root Allan variance plot in Fig. 6 (c) above. There is no degradation of the short-term stability, and the long-term stability is improved dramatically for integration times of 100 ms to greater than 1000 s, with the improvement exceeding two orders of magnitude at the longer times.

Evolution of the heterodyne beat frequency over a period of 30 minutes (1800 s) is shown in Fig. 7 (a) when both lasers were free running and in Fig. 7 (b) when both lasers were locked using the new strategy. For integration times of 1 s and longer, the drift has been reduced to about 7 kHz/min over several minutes. The inherent sub-MHz free-running stability of the lasers is already sufficient for many spectroscopic applications, but an improvement over the free running case of about two orders of magnitude has been accomplished for time scales of 100 μs - 10 ms and for times longer than one minute. Minimum root Allan variances of 200 Hz have been recorded, although the 500 Hz value shown is typical for performance at this stage of system development.

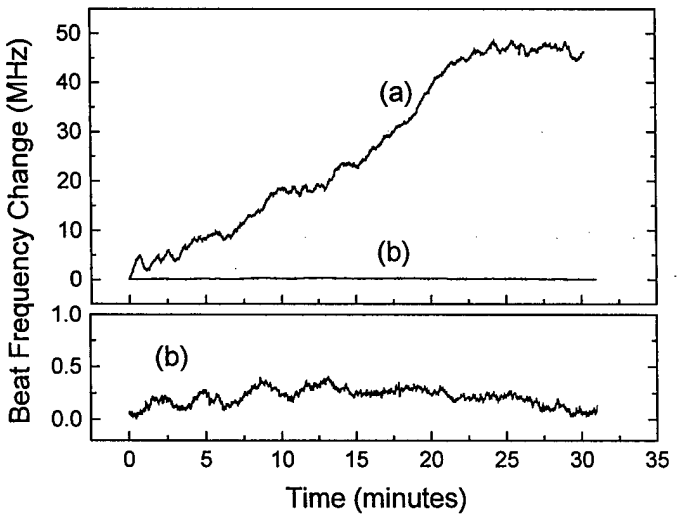

FIG. 7. Change in heterodyne beat signal between (a) free-running and (b) independently locked lasers to separate spectral holes and inhomogeneous lines in different crystals at field B = 0.2 T.

For somewhat stronger long-term resistance to drift, the modulation frequency could be increased to provide a larger inhomogeneous line contribution to the slope at the desired locking frequency; this increases the amplitude of the contribution from the inhomogeneous line with little effect on the contribution from the spectral hole.

The Er^{3+}:Y_2SiO_5 homogeneous resonance width in a magnetic field of 0.2 to 0.5 T is narrower than that from the preceding work on Tm^{3+}:YAG, so it might be expected to provide lower short-term root Allan variance values than Tm^{3+}:YAG using the same technique and apparatus. In this case, however, the $4f^{11}$ electron configuration of the Er^{3+} ion leads to strong Er^{3+} magnetic moments, whereas the Tm^{3+} ion with configuration $4f^{10}$ has an electronic singlet ground state with 'quenched' angular momentum and no first order magnetic moment. Electron spin flips of nearby Er^{3+}-ions in the ground state as well as nuclear spin flip-flops by Y^{3+} nuclei lead to fluctuations in the local fields and thus to measurable spectral diffusion of the Er^{3+}-ion population that makes up the spectral hole frequency reference. The 0.2 to 0.5 T applied magnetic field reduces electron spin flips by reducing thermal population of the upper component of the Er^{3+} Kramers doublet ground state, but it does not eliminate them completely. It also suppresses the far weaker spectral diffusion due to Y^{3+} (or Er^{3+}) nuclear spin flip-flops. Evolution of the spectral hole width by spectral diffusion limits the currently achieved frequency

stability of the hole on time scales longer than 2 ms and hence of the locked laser. Detailed studies of the spectral diffusion phenomena are being carried out both to improve laser stabilization performance and to improve these materials for other spatial-spectral holography applications.

Further sources that limit stability are residual amplitude modulation produced by the electro-optic phase modulator and thermally induced drift in the locking circuitry and modulator, all of which introduce variable offsets to the error-signal, causing the laser to lock slightly off the center of the spectral hole. In the previous implementation this produced unrestrained long-term frequency drift of the spectral hole. With the new method reported here, it results instead in smaller changes to the equilibrium lock point in the inhomogeneous line profile. As noted above, further improvements from passively and actively stabilizing the temperature of the feedback electronics are expected to improve system performance.

Time-domain spectroscopy and a wide range of proposed SHB optical devices are based on the photon echo and stimulated photon echo, the capabilities of these techniques can be improved with the level of frequency stabilization reported here. For optimal exploitation of the stimulated photon echo, laser frequency stability to better than the spectral width of the broadest excitation pulse, or in the limiting case to better than a homogeneous linewidth, is required for the storage time of the material, which is defined by the decay time of a transient spectral hole for the transition being probed. With lasers stabilized to spectral holes, this requirement is naturally and automatically met.

We demonstrated this improvement by measuring stimulated photon echoes on the $^4I_{15/2}$ (1) $\rightarrow$ $^4I_{13/2}$ (1) site (1) transition of Er^{3+}:Y_2SiO_5 using a stabilized 1536 nm laser, an Er-doped fiber amplifier, and the echo apparatus described previously. Approximately 5 mW of unmodulated continuous-wave laser power was available for producing echo excitation pulses after continuous wave amplification of the laser by the Er-doped fiber amplifier, which was located outside the servo loop for laser stabilization. A portion of the un-amplified laser output was used to frequency-lock the laser to a regenerative transient spectral hole in the same transition as described above. Echo excitation pulses were produced using two acousto-optic modulators in series to improve the on/off contrast ratio and to cancel any net shift in the laser frequency, since the Er^{3+}:Y_2SiO_5 spectral lines are narrow. The resulting photon echo signal was gated from the transmitted beam by a third acousto-optic modulator to discriminate against the exciting pulses. The echo was detected with a fast InGaAs-photodiode. To generate stimulated photon echoes, three 2 μs excitation pulses were incident on the crystal, with the delay t_{12} between the first and second pulses fixed at 19 μs. The strength of the stimulated echo was measured as a function of the delay t_{23} between the second and third pulses.

With the laser frequency locked to a transient spectral hole, photon echoes could be measured consistently for t_{23} delay times of several hundreds of microseconds, giving the data in Fig. 6b. The limiting factor for measuring echoes with longer t_{23} delay times was the detector signal-to-noise ratio, rather than laser frequency jitter, even though additional jitter may have been introduced by the Er-doped fiber amplifier. After 800 μs total delay time the stimulated echo signal was buried in the noise. In contrast, when the stimulated echo decay was measured with the laser free running, the reproducibility of the stimulated echo became unreliable after only

200 μs. All the data points were single-shot acquisitions of the stimulated photon echo without thresholding to reject low-intensity echoes. Frequency jitter was the cause of the echo signal amplitude fluctuations when a free-running laser was used, since occasionally an optimum echo was produced when the laser frequency of the third pulse happened to match that of the first two.

The concept of laser frequency stabilization using regenerative transient spectral hole burning has been extended to the technologically important 1.5 μm wavelength region. Stable laser sources based on this method improve both spectroscopic capability and the performance of SHB devices such as all-optical network routers and address header decoders. Moreover, by stabilizing the laser source to the same SHB material already employed in the SHB device, system complexity is significantly reduced. A hybrid method to control long-term frequency drift has been demonstrated, using an intermediate phase delay in the phase sensitive detection of the frequency locking error signal that exploits contributions from the narrow spectral hole and from the inhomogeneous absorption profile. This stabilization method is particularly well suited for spectroscopy and for optical data processing devices based on time-domain spectral hole burning. Substantial improvement in stimulated photon-echo reproducibility was demonstrated, showing the impact of this technique on spectroscopy of rare earth materials.

Reviews of Laser Stabilization to Spectral Holes

These and other developments in our laboratory were summarized in an invited review,

Semiconductor Lasers Stabilized to Spectral Holes in Rare Earth Crystals, R. L. Cone, T. Böttger, G. J. Pryde, N.M. Strickland, Y. Sun, P. B. Sellin, and J. L. Carlsten, in Physics and Simulation of Optoelectronic Devices IX, Yasuhiko Arakawa, Peter Blood, Marek Osinski, Editors, Proceedings of SPIE Vol. **4283**, 335-346 (2001).

Our work on laser stabilization to spectral holes was also a feature in **Optics in 2001** published by the Optical Society of America.

Semiconductor Lasers Stabilized to Spectral Holes in Rare-Earth Crystals, Thomas Böttger, Geoffrey J. Pryde, Nicholas M. Strickland, Peter B. Sellin, and Rufus L. Cone, Optics & Photonics News, **12,** #12, 23 (2001).

Models Developed for Laser Stabilization to Spectral Holes

Several generations of models of the process of laser stabilization to spectral holes have been developed by us and reported in these publications.

- Thomas Böttger, Y. Sun, G.J. Pryde, G. Reinemer, and R.L. Cone, J. Lumin. **94-95**, 565-568 (2001).
- *Numerical modeling of laser stabilization by regenerative spectral hole burning,* G. J. Pryde, T. Böttger, and R. L. Cone, J. Lumin. **94-95**, 587-591 (2001).
- *Semiconductor lasers stabilized to spectral holes in rare earth crystals to a part in 10^{13} and their application to devices and spectroscopy,* G. J. Pryde, T. Böttger, R. L. Cone, and R. C. C. Ward, J. Lumin. **98**, 309-315 (2002).

Details of the models are given below.

First Numerical Model of Laser Stabilization by Regenerative Spectral Hole Burning

Our regenerative transient spectral hole frequency references have provided relative optical stability on the 10^{-13} scale over tens of ms and longer. These references are comparatively insensitive to vibration and, unlike traditional Fabry-Perot cavities, atomic references or gated spectral holes, the reference shape and position can depend on the laser input as well as the material properties. Numerical modeling of a frequency stabilization system incorporating regenerative spectral holes has been carried out, and the importance of the specific spectral hole burning material has been considered. It was shown that for intervals shorter than the spectral hole lifetime, the hole reference is similar to a Fabry-Perot cavity reference. For periods longer than the hole lifetime, the performance of the spectral hole reference can be affected by uncompensated offsets in the stabilization system caused by the environment.

The SHB frequency references can be grouped into three categories.

- Regenerative (or transient) spectral holes have a lifetime limited by the T_1 of the optical transition or a bottleneck state. For the materials described in this report, this time is typically 10 ms.
- Persistent spectral holes have a lifetime which is much longer than the optical T_1. Persistent holes arise from photophysical or photochemical hole burning, or long-lived metastable states such as the Eu^{3+} nuclear spin states.
- Gated spectral holes require application of some physical process, such as an electric field or another optical field, as well as the usual optical field for hole burning to occur.

In the SHB materials explored to date, regenerative spectral holes are orders of magnitude narrower in frequency than persistent holes at the 1.5 μm telecommunications wavelengths and at 793 nm; both of those wavelengths are important for a variety of SHB-based optical signal processors. The absence of narrower persistent holes at these wavelengths represents the current state of materials development. Narrow, gated SHB materials have been under development as we describe below but have not yet been realized. Persistent holes with widths as narrow as 100 Hz and lifetimes of weeks do exist for the $^7F_0$ • $^5D_0$ transition at ~ 580 nm in Eu^{3+}:Y_2SiO_5.

Much of our attention is focused on regenerative holes in the context of signal processing devices. We subsequently refer to regenerative spectral holes with the acronym RSHB.

Since regenerative and persistent spectral holes are ungated, there exists potential for modification of the hole spectrum by the incident probe laser field. This is a fundamental difference between ungated SHB frequency references and the more familiar Fabry-Perot or atomic references, and our models explicitly take this into account. There is in general an interplay between the system noise and the properties of the SHB that determines how an ungated spectral hole will perform as a frequency reference. Therefore, the optimization of a laser stabilization system incorporating ungated SHB references is a more complex problem than for traditional frequency references.

We describe in the next few pages our first numerical approach to the problem of determining and optimizing the performance of RSHB frequency references. The same technique can be employed, with slight modifications, to examine persistent hole burning references as well. The

numerical modeling draws on techniques familiar in the frequency stabilization community: a time-dependent frequency, the spectral noise density, and feedback control theory. The spectral hole is represented by population rate equations, the noise by a spectral noise density (with optional time domain additions such as long timescale drift), and spectral diffusion processes by repeated convolution of the hole spectrum with a Gaussian broadening function. The shape of the inhomogeneous line is also considered as a factor that can be included in the calculation, since experimentally it can provide improved absolute stability. The modeling is based on a typical Pound-Drever-Hall experimental stabilization system, such as the one used in parallel experimental efforts.

The most significant complication of the time-dependent hole spectrum is the inability to treat the numerical modeling strictly in the frequency domain, as is usually done with Fabry-Perot references, for example. Consequently, a hybrid time- and frequency-domain approach must be adopted. This technique will be described in more detail elsewhere. In brief, it is convenient to group noise in the system into stationary (time-independent mean) and non-stationary (time-dependent mean) processes, where these terms are expanded to include deterministic as well as stochastic noise. Examples of stationary processes are white frequency noise and sinusoidal frequency modulations; examples of non-stationary processes are random walk frequency noise and deterministic linear frequency drift. The stationary processes are then treated using the spectral hole as a time-dependent filter and the non-stationary processes that are not easily treated by the hybrid model are considered entirely in the time domain.

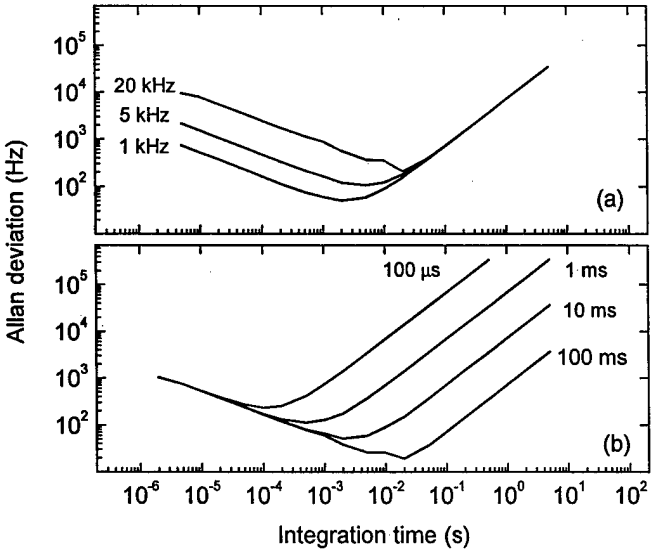

FIG. 8. Variation of computed laser stability, as measured by the Allan deviation, as a function of (a) the spectral hole width, with hole lifetime = 10 ms and (b) the hole lifetime, with hole width = 1 kHz. In both cases, the input noise is 140 Hz/• Hz of white frequency noise and 1 MHz/second linear frequency drift.

Following the standard approach in frequency stabilization literature, the noise on the laser is described by the time-dependent instantaneous frequency deviation. The interaction of the laser and the ions is taken into account through the use of a population rate equation, rather than the use of the full optical Bloch equations. This approximation is valid in the condition that the Rabi frequency is smaller than the homogeneous linewidth of the transition. The interpretation of this approximation is that the laser is weakly probing the absorption of the ions rather than coherently driving them. This situation corresponds to the usual condition in the associated experiments, where the Rabi frequency is deliberately made small so as not to power broaden the spectral hole.

The effects on stabilized laser performance of the hole width, hole lifetime and rate of spectral diffusion were examined for several characteristic noise types, including white frequency noise introduced through noise on the laser electronics or random fluctuations in the laser cavity and also linear frequency drift, which can arise from a variety of sources including offsets in the laser electronics. Figure 8 shows the effect of the hole width and hole lifetime of the RSHB reference, for white noise and linear frequency drift. It can be seen that the hole lifetime dictates the short-term performance of the system in a manner similar to a Fabry-Perot cavity. Over longer times, the hole lifetime has a part to play. As expected, when the hole lifetime is increased for a specific hole width, the long-term performance of the system is greatly improved. This is because the 'memory time' of the spectral hole is being increased – it remains a valid frequency reference for longer periods. The numerical model has also been used to examine the effect of spectral diffusion, which acts to reduce the memory of the system; the effective memory time is reduced if the ions' population diffuses rapidly compared to the hole lifetime.

The results of the model compare favorably with the experimental results achieved. Figure 9 shows the stability achieved experimentally, using two different SHB materials, $Er^{3+}:Y_2SiO_5$, which exhibits RSHB and $Er^{3+}:CaF_2:D^-$, which exhibits persistent SHB. These materials have contrasting properties in the sense that the first has narrow (~ 1 kHz) holes and a T_1 limited lifetime of 13 ms, whilst the second has broad (~ 40 MHz) holes but a lifetime that is effectively infinite on the time scale of the experiment. It can be seen that the persistent SHB material is better for suppressing long-term drifts in the experiment, observable over long integration times in the Allan deviation, while holes in $Er^{3+}:Y_2SiO_5$ suppress the short time scale noise more effectively.

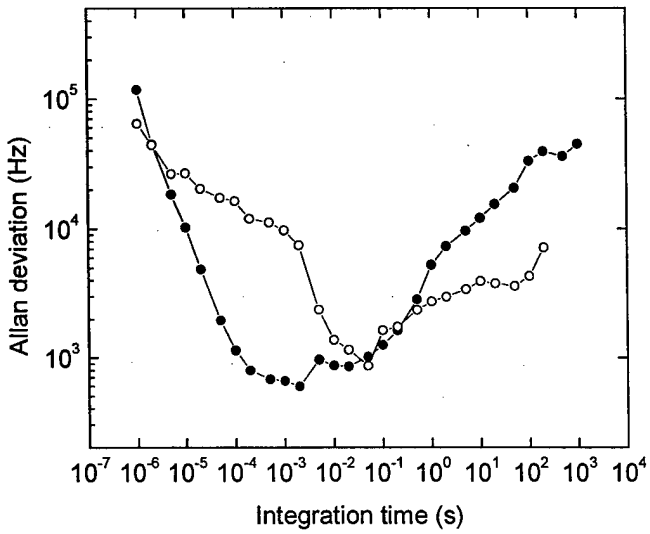

FIG. 9. Experimentally measured Allan deviations for independent lasers locked to separate spectral holes in the $^4I_{15/2}$ • $^4I_{13/2}$ transition of the RSHB material $Er^{3+}:Y_2SiO_5$ (filled circles) and the persistent SHB $Er^{3+}:CaF_2:D^-$ (unfilled circles).

A more complex model has been developed that treats the problem exclusively in the time domain from the standpoint of the electric field and incorporates the full optical Bloch equations, allowing the low intensity approximation to be surpassed. Treatment of the electric field of the laser allows for calculations of two-time correlations in the manner of quantum noise problems and gives access to numerical predictions for the performance of lasers locked to spectral holes and used for interferometry and advanced spectroscopy. This treatment of the problem from the point of the electric field will be reported in full elsewhere.

A simplified version of the electric field model highlights the similarities and differences, already discussed, between the RSHB reference and a Fabry-Perot cavity. The optical Bloch equations were used to calculate the noise frequency dependence of the Pound-Drever-Hall reference signal recovered from a regenerated spectral hole. The result of this calculation is compared with calculations for a Fabry-Perot reference cavity in Fig. 10. The hole width is chosen to be coincident with the width of the Fabry-Perot resonance. It can be seen that for frequencies greater than the inverse hole lifetime, the spectral hole and the Fabry-Perot exhibit a similar frequency response. At lower frequencies, the response of the hole is rolled off relative to the cavity. This is the reason behind the lifetime-dependent stabilization performance at longer time scales, as shown in Fig. 8 (b). It can be shown from feedback control theory that the servo electronics can be designed to compensate this rolloff and suppress noise on the laser or electronics with substantial low frequency components. However, servo gain cannot compensate low frequency noise on the reference itself, so passive reduction of this noise becomes essential for good long-term performance of RSHB references with short hole lifetimes. Of course, linear frequency drift can be removed after the fact, as with lasers stabilized to traditional references.

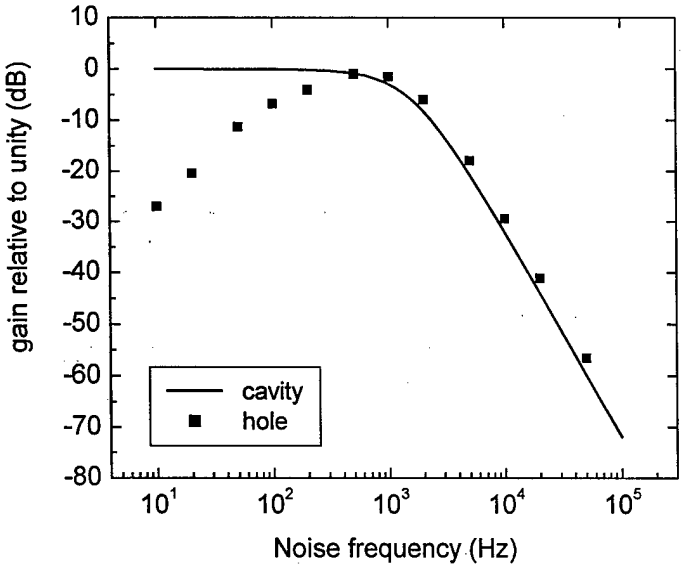

FIG. 10. Calculated AC response of (a) a Fabry-Perot cavity with 10 kHz linewidth and (b) a regenerated spectral hole with 10 kHz hole width and 10 ms hole lifetime.

In conclusion, numerical modeling of RSHB frequency references has shown that, on time scales shorter than and corresponding to the hole lifetime, regenerative spectral hole frequency references are functionally equivalent to Fabry-Perot cavities. The narrow hole widths of 1 kHz (and potentially better) that are available in RSHB references results in precise frequency stabilization, with the added benefits of compactness and insensitivity to vibrations. Over longer time scales, the gain of the reference rolls off, imposing the requirement for ultimate performance that the reference be passively stabilized against low frequency noise components. Narrow, persistent spectral hole references are far less sensitive to roll off at much lower frequency and gated spectral hole references under development will not roll off at all. The results of the model are in agreement with experimental observations and have allowed rapid experimental system optimization. Continued materials development, based on model predictions, will result in even more precise frequency stabilization to regenerative and persistent SHB frequency references in the near future.

Improved Hybrid Time- and Frequency-Domain Numerical Model of Laser Stabilization to Regenerative Spectral Holes

Spectral hole burning frequency references using regenerative or persistent spectral holes are qualitatively different from other references, such as Fabry-Perot cavities or gas absorption cells, since the reference hole can, in general, be modified by the laser probing it. This dynamic interplay between the reference and the laser cannot be described by the traditional frequency-domain techniques of feedback control theory, since the hole spectrum may be time-dependent.

A hybrid time- and frequency-domain numerical model and a more complicated time-domain only numerical model have been developed to investigate the dependence of the laser stability on materials and system parameters and to speed optimization of the experimental demonstrations. These simulations use rate equations and the optical Bloch equations respectively to represent the interaction of the material with the optical field. In these models, stochastic and deterministic noise are provided as inputs, along with the material parameters and varying degrees of system detail, such as the frequency- or time-dependent servo response. The input noise can either be mathematically generated or derived from the measured spectral noise density of the experimental system. The stability of the system, characterized by the Allan deviation or spectral noise density, is examined as material or system parameters are varied in turn. Furthermore, the output of the simulations can be used as an input for other spectroscopic or optical processing models, such as the simulation of coherent transient pulse sequences.

Stabilization of lasers to regenerative spectral holes - where the hole lifetime is of the order of the optical T_1 - has been of particular interest, since to date, the lowest experimental Allan deviations have been achieved in this regime. It has been found that the hole width, governed by a combination of homogeneous linewidth and the probing Rabi frequency, dictates the stability over short integration times, while the stability measured over integration times longer than the hole lifetime is governed by the hole lifetime or rate of spectral diffusion, parameters that characterize the memory time of the reference. Employing the time-domain model, which describes the material in terms of the optical Bloch equations, we obtained the frequency-dependent response of the error signal. This is shown in Fig. 11, where it is compared with

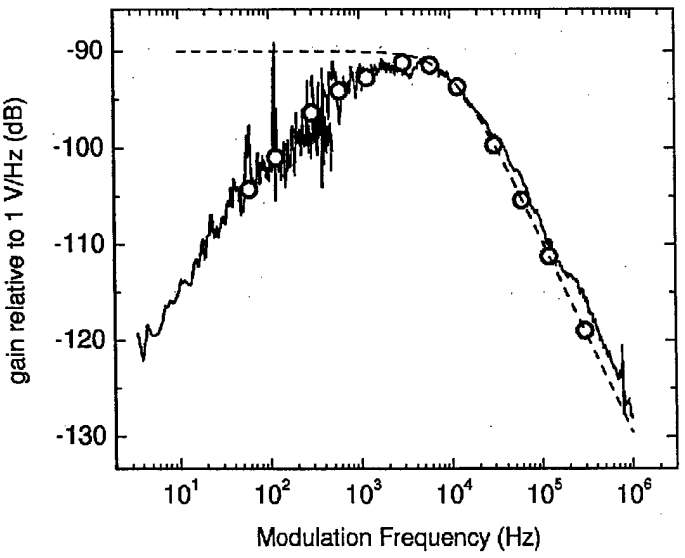

FIG. 11. Frequency response of the error signal generated from a regenerative spectral hole frequency reference: experimental measurement in Er^{3+}:Y_2SiO_5 (solid line) and the model (open circles), compared with the calculated response of a Fabry-Perot cavity with the same linewidth (dashed line), scaled for comparison.

the response of a Fabry-Perot cavity of the same spectral width and with the experimentally measured spectrum for the regenerative hole burning material Er^{3+}:Y_2SiO_5. The experimental result was obtained by probing a regenerative spectral hole in Er^{3+}:Y_2SiO_5 with the stabilized laser. Phase-modulation sidebands were swept over the frequency range of interest and the phase modulation spectrum recorded. This spectrum was scaled by a factor proportional to the inverse modulation frequency, for comparison with the calculated responses for the hole and cavity, since the latter assume frequency- rather than phase-modulation. Since the phase modulation signal goes to zero at DC, the signal-to-noise ratio imposes a lower limit on the measurable error signal response. The low frequency response of the hole can be inferred beyond this limit by taking the ratio of the spectral noise density measured relative to the regenerative spectral hole and that measured relative to a static reference, in this case, a 150 MHz FWHM inhomogeneous line in isotopically purified Er^{3+}:$LiYF_4$. This measurement is the source of the experimental data in Fig. 11 at frequencies below 300 Hz. The narrow features in the low frequency error signal response are artifacts of this technique.

Over the range of the measurement, the model and experiment agree, and they are both in coincidence with the response of a Fabry-Perot cavity. It is clear that the high-frequency rolloff is close to 20 dB/decade, which is ideal for servo design since the accumulated phase shift from the reference is limited to 90•• At lower frequencies, the predicted rolloff of the gain is observed, consistent with the idea that the system is losing its memory as a frequency reference because of the limited hole lifetime. In principle, this can be partially compensated by servo gain and the issues associated with compensation are presently under investigation.

The modeling has led to understanding of the process of stabilization to regenerative spectral holes and identification of the ideal hole burning material – one with long-lived, narrow spectral holes and no spectral diffusion. In addition, it allows investigation of the effect of varying locking system parameters for a given spectral hole frequency reference, leading to optimization of the stabilization experiments.

Stabilization of Diode Lasers at 1537 nm to Regenerative Spectral Holes in KTP

Single-frequency diode lasers have been stabilized to 200 Hz at 1.5 microns using narrow spectral holes in the absorption lines of Er^{3+}:KTP. Potassium titanyl phosphate, $KTiOPO_4$ (KTP), is an important nonlinear electro-optic material primarily used as frequency doubling crystals and for optical waveguides. We achieved 200 Hz laser stabilization utilizing Er^{3+}: KTP crystals grown at Oxford University with an Er^{3+} concentration of 0.004 at. percent as a spectral hole burning frequency reference. The crystal was oriented with its a-axis parallel to an external magnetic field and its b-axis parallel to the laser **k**-vector. The lowest energy $^4I_{15/2} \rightarrow {}^4I_{13/2}$ Er^{3+} transition has been observed to exhibit six distinct sites near 1537 nm. The site with the strongest absorption, located at 1536.87 nm (6506.69 cm^{-1}), exhibits transient spectral hole burning by population storage in the excited state of the optically active Er^{3+} ion; laser stabilization experiments were performed using the absorption transition between the lowest Zeeman split levels. Fig. 12 (a) shows the transmission through the ~ 2 GHz (FWHM) wide inhomogeneously broadened line for a magnetic field of B = 0.25 T and temperature T = 1.9 K. The origin of the shoulder appearing at higher frequency is most likely due to absorption from a spectrally similar site, as indicated by fluorescence decay experiments. A narrow spectral hole, indicated by an

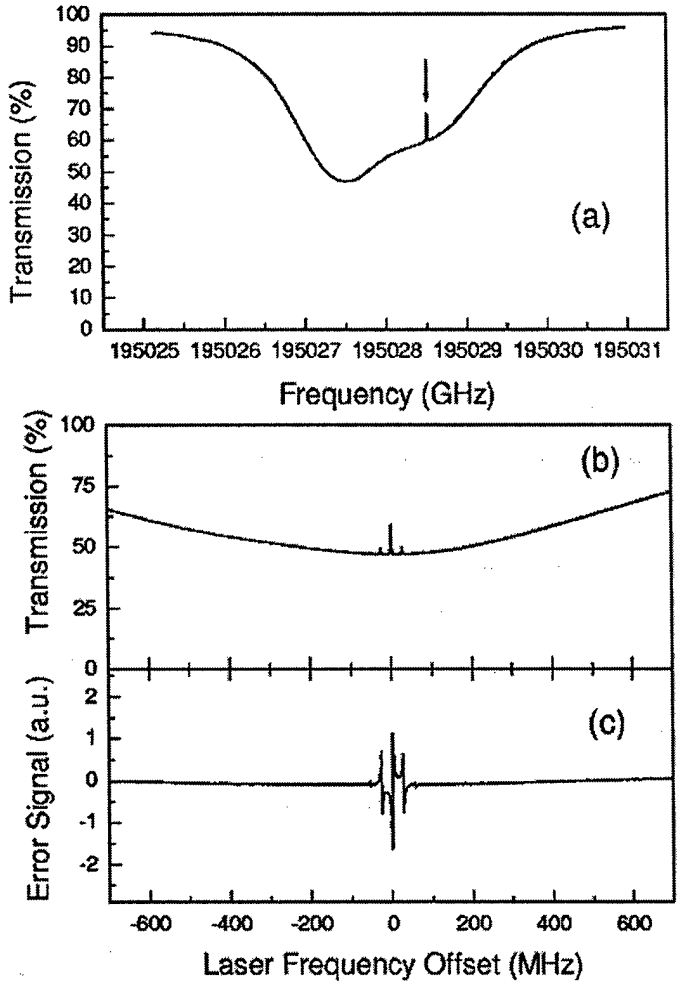

FIG. 12. (a) Transmission spectrum of 0.004 % Er^{3+}:KTP at 1537 nm showing the entire inhomogeneously broadened $^4I_{15/2} \rightarrow {}^4I_{13/2}$ optical absorption scanned by a diode probe laser. The arrow indicates a spectral hole, which has been burned by a second laser. (b) Transmission of a phase-modulated probe laser through a single spectral hole created by a second laser, using an applied magnetic field of B = 0.25 T. (c) Demodulated FM-error signal derived from the spectral hole in (b).

arrow, has been prepared by a second laser and can be placed anywhere within the inhomogeneously broadened line. The homogeneous linewidth has been characterized using two pulse photon echoes measured as a function of delay time between the two excitation pulses. The measured dephasing time corresponds to a homogenous linewidth of 2 - 3 kHz for small magnetic fields below B = 0.4 T.

Two external cavity lasers in the Littman-Metcalf configuration equipped with quantum well InGaAsP/InP single angled faceted laser diodes have been stabilized using the conventional Pound-Drever-Hall technique. The lasers were modulated with modulation index M ~ 0.4 at 27 MHz and 30 MHz, respectively, values greatly exceeding the spectral hole width. The error signal was derived from the spectral hole transmission exploiting frequency modulation (FM) spectroscopy. Fig. 12 (b) shows the transmission through a spectral hole burned by a second laser and Fig. 12 (c) the corresponding demodulated FM error signal probed with a phase-modulated laser; detector signal and local oscillator are in phase. For active laser frequency stabilization the error signal is applied to a fast servo loop providing rapid modulation of the injection current of the laser diode whereas a slow servo loop makes corrections to the piezoelectrically-driven feedback prism plate of the external laser cavity. To obtain a good signal to noise ratio in the detection under low laser locking irradiance, it is beneficial to choose a large frequency reference crystal. Crystal dimensions were 12.87 mm along a, 14.89 mm along c, with a 5.18 mm optical path along b; both lasers were locked to the same crystal. To avoid spatial overlap or interaction of the two

independently locked laser beams, a mask with separated 4 mm apertures was placed over the crystal. A small magnetic field of B ~ 0.25 T has been conveniently applied by sandwiching the sample holder between two permanent Nd-Fe-B magnet disks of diameter 2.5 cm, greatly simplifying the experimental apparatus. The mounted crystal was immersed in liquid helium at T = 1.9 K.

The laser irradiance of ~ 100 $\mu W/cm^2$ at the crystal was split from the laser beam using a $\lambda/2$-plate/ prism-polarizer combination, leaving most of the laser output power to be used for experiments requiring a stabilized source or to saturate an Erbium doped fiber amplifier for higher power applications. Using higher irradiance at the locking crystal leads to a deeper spectral hole, which in turn becomes since there is less saturation of material absorption in the wings of a hole than at the center. During active stabilization, each laser burns a spatially and spectrally separated transient spectral hole into the inhomogeneously broadened absorption profile. Error signal feedback to each laser leads to a continuous regeneration of the transient spectral hole until a balance between spontaneous hole relaxation and hole burning occurs.

Relative frequency stability of the two stabilized lasers was characterized by the statistical Allan standard deviation of the optical beat frequency since no absolute frequency reference was available. The beat signal from a photodiode was measured with a frequency counter and recorded over time with a computer at 50 ms time intervals. Allan deviations for integration times up to 50 ms were directly measured with the frequency counter, whereas for longer integration times the Allan deviation was calculated from the recorded heterodyne beat frequency data.

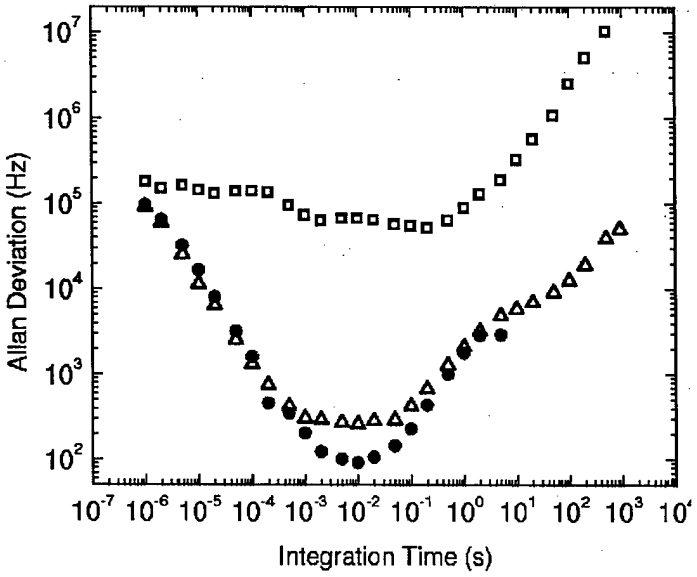

FIG. 13. Allan deviation for the heterodyne beat frequency between two lasers: lasers free-running (squares), independently locked to transient spectral holes in the $^4I_{15/2} \rightarrow {}^4I_{13/2}$ transition in Er^{3+}: KTP at 1537nm (triangles) and model prediction of stabilization in Er^{3+}: KTP (circles).

The joint Allan deviation for the free running lasers and actively stabilized lasers is shown in Fig. 13. With the laser locked to transient spectral holes in Er^{3+}: KTP an improvement in the Allan deviation over the free running lasers to 250 Hz has been achieved for integration times between 1 ms and 100 ms, demonstrating the potential of Er^{3+}: KTP at the current stage of system development. During quiet periods, Allan deviations of 200 Hz at 10 ms integration time have been measured. The structure of the Allan deviation curve is reproducible. Long-term linear drift of the laser evidenced by an upturn of the Allan deviation at longer integration times has been greatly reduced by choosing an

intermediate phase setting at the mixer between detector signal and local oscillator. This technique combines the excellent short-term stability of the spectral hole with the good long-term stability of the inhomogeneous line; long term drift of the beat frequency between the two lasers has been suppressed to ~ 10 kHz per minute. The demonstrated short-term stability shows a clear improvement compared to the earlier results using transient spectral holes in Er^{3+}:Y_2SiO_5 and is the best result achieved in Er^{3+}-doped compounds. As in the case of Er^{3+}:Y_2SiO_5, spectral diffusion plays a significant role in the achieved performance. Even though the transient spectral hole provides a narrow (few kHz) wide reference, the narrow hole width cannot be fully exploited over longer periods because of the T_1-limited hole lifetime. In addition, the strong Er^{3+} ion magnetic moments are perturbed by local field fluctuations due to electron spin flip-flops between nearby Er^{3+} ions in the ground state. These perturbations lead to a broadening of the homogeneous linewidth over time. The small applied magnetic field of B = 0.25 T slows this spectral diffusion process by thermally depopulating the upper Zeeman component of the Er^{3+}-ion ground state but does not eliminate it completely.

Technical limitations are also set by reflections inside the electro-optic modulators, temperature dependent residual amplitude modulation at the electro optic modulators, and voltage offsets created in the electronic servo loop. Since a transient spectral hole is a dynamic reference, any voltage offsets introduced to the error signal baseline cause the lock frequency to shift and consequently introduce long-term laser drift since the laser is modifying its own reference. Further improvements can be expected from passive and active temperature stabilization in order to minimize and stabilize voltage offsets. Environmental disturbances due to vibration and acoustical noise sources have been partially addressed by floating the optical table and covering the experiment by the acoustical enclosure. The 250 Hz improvement in stabilization performance for Er:KTP relative to $Er^{3+}Y_2SiO_5$ is due to a combination of three factors: extra vibrational and acoustical isolation, reduced noise in system components such as electronics, and the subtle differences in regenerative holeburning material. Materials studies to date suggest that the last contribution is minor.

The hybrid model of laser stabilization to regenerative spectral holes, described several pages earlier, was used to compute the predicted Allan deviation for locking in Er^{3+}:KTP, based on the measured spectral noise density of the unstabilized laser and the known materials and system parameters. The results of this computation are compared with the experimentally measured Allan deviation in Fig. 13. It can be seen that there is good agreement between the computed and measured values for shorter and longer integration times. Over the range of integration times from 1 ms to 100 ms, where the measured Allan deviation is a minimum, there is some divergence of the computed values from the measured values. This deviation is attributed to a reduced spectral noise density of the unstabilized laser, over the relevant integration times, at the time that it was recorded, compared to the time that the directly measured Allan deviation was acquired. The narrow (~ 5 kHz) spectral hole in Er^{3+}:KTP results in high gain, leading to excellent suppression of the noise over short integration times. Over longer integration times, the limited lifetime of the hole causes the reference to lose its frequency memory and the effects of drift and other slow fluctuations begin to dominate the Allan deviation curve. The effective hole lifetime used in the modeling is 10 ms, which is in agreement with our experiments.

Stabilization of diode lasers at 1523 nm to Persistent Spectral Holes

Programmable Sub-kHz Laser Frequency Stabilization at 1523 nm using Persistent Spectral Hole Burning, Thomas Böttger, G. J. Pryde, and R. L. Cone, Opt. Lett. **28**, 200-202 (2003).

Diode laser frequency stability of 2 kHz to 680 Hz over 20 ms to 500 s has been demonstrated at 1523 nm in the technologically important communication band using *persistent* spectral holes in the inhomogeneously broadened Er^{3+} $^4I_{15/2} \rightarrow {}^4I_{13/2}$ optical absorption of Er^{3+}:D^-:CaF_2. Laser frequency stabilization was realized without vibrational or acoustical isolation of either the laser or spectral hole frequency reference, providing the means for implementing a versatile, compact, stable source.

Persistent spectral holes can have lifetimes ranging from several weeks to months or longer; consequently, they can serve as long-term secondary frequency standards. We have recently reported compact vibration-insensitive laser stabilization in regenerative spectral hole burning materials and demonstrated a persistent spectral hole frequency reference. We reported improved performance to longer integration times for diode lasers stabilized to persistent spectral holes at 1523 nm in Er^{3+}:D^-:CaF_2, which we believe is the first example of a programmable frequency reference material in the spectral region at 1.5 μm. Although the ideal persistent spectral hole burning material at 1.5 μm is not yet available, these results highlight the concept of using a persistent spectral hole for laser frequency stabilization.

Many scientific and device applications require frequency stability at the achieved and anticipated levels. Lasers stabilized to spectral holes already find important application in coherent transient spectroscopy and optical devices and are a key component of optical correlators with improved time-bandwidth products. Besides applications related to spectral hole burning, simple stable laser systems like ours, which does not require vibration or acoustic isolation, open up 1.5 μm technology for a new variety of uses, such as eyesafe laser radar, remote vibrometry, and interferometry in the field. Anticipated system performance will extend the use to ultrahigh resolution spectroscopy, quantum optics research, electromagnetically induced transparency (EIT), optical clocks, metrology, and other applications requiring ultra-narrow band light sources or coherent detection.

The material Er^{3+}:D^-:CaF_2, to our knowledge, is the only material yet known to show persistent spectral hole burning at 1.5 μm. Deuteride (D^-) ions introduced into a 0.05 at. % Er^{3+} doped CaF_2 crystal both interstitially and by substitution for F^- ions in the vicinity of Er^{3+} ions give rise to additional Er^{3+} $^4I_{15/2} \rightarrow {}^4I_{13/2}$ absorption lines. The lines at 1523 nm from the R center exhibit persistent hole burning by optically induced D^- ion migration. Spectral holes of full width at half maximum (FWHM) of ~ 40 MHz showed no measurable degradation over forty-eight hours. The activation energy deduced from those results suggests that the hole lifetime could be indefinitely long for samples held at liquid helium temperature. The material Er^{3+}:D^-:CaF_2 should be practical as a frequency reference up to a temperature of 15 K where the hole width reaches 200 MHz (FWHM), and that enables simpler operation with a cryocooler. Wavelength versatility can be achieved by replacing the Er^{3+} ions with other rare earth ions, since the hole burning mechanism is a property of the host, rather than being dopant-specific.

Figure 14 (a) shows a transmission spectrum of Er^{3+}:D^-:CaF_2 and illustrates a number of spectral holes programmed in the inhomogeneous absorption line of the R center. Laser beat frequencies, pulse spectra, holograms, or data can be recorded and read out at a later time or location as long as the sample temperature is maintained.

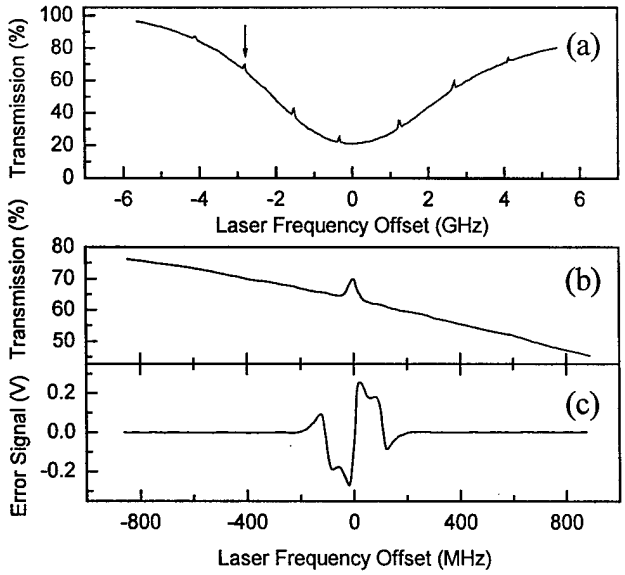

Fig. 14. (a) Transmission spectrum of Er^{3+}:D^-:CaF_2 at 1523 nm. A number of spectral holes have been burned into the inhomogeneously broadened $^4I_{15/2} \rightarrow {}^4I_{13/2}$ transition demonstrating the programmability of the material. The arrow indicates a spectral hole that is enlarged in (b). (c) Demodulated FM-error signal derived from the spectral hole in (b).

Laser frequency stabilization was implemented using frequency modulation (FM) spectroscopy to sense the center of a spectral hole in much the same way as for a Fabry-Perot frequency reference. The experimental setup was similar to that previously reported. Two independent external cavity diode lasers were phase-modulated with modulation index of M = 0.4 and modulation frequencies of 93 MHz and 109.5 MHz, respectively, values chosen to lie well outside the ~ 40 MHz (FWHM) spectral holes. Figure 14 (b) shows a transmission spectrum through a single spectral hole and the corresponding demodulated FM error signal [Fig. 14 (c)]. Diode laser injection current and piezo-driven feedback prism plate provided fast and slow frequency corrections. Both stable laser and modulator systems – each 10 cm x 20 cm, the optical cryostat, locking electronics, and laser diagnostics were fitted on a tabletop breadboard without vibrational or acoustical isolation. Miniaturization of this apparatus is feasible with waveguide-based external cavity diode lasers and electro-optic modulators, leading to a compact system with size limited by the required cryocooler.

Each laser was independently stabilized to a separate reference crystal immersed in a single cryostat at T = 1.9 K. Since width and depth of the programmed persistent spectral hole determine the slope of the error signal for active laser frequency stabilization, careful preparation of the initial persistent spectral hole was important. An increase in hole width as a function of burn time was observed, resulting from the longer hole burning time for ion centers having only partial frequency overlap with the laser and consequently a lower effective transition probability than centers resonant with the laser. This implies a tradeoff between hole depth and hole width has to be made, limiting error signal slope and signal-to-noise ratio for detection. Good locking results were achieved using persistent holes of ~ 40 MHz (FWHM) and a depth corresponding to

a change in transmission by ~ 5 percent, prepared by illuminating the sample for 20 seconds with incident light intensities of ~ 300 $\mu W/cm^2$. Since the hole width was much wider than the unstabilized laser linewidth, no active stabilization was required during hole preparation. For materials with narrower persistent spectral holes, it will be necessary to reduce the laser linewidth by bootstrapping the hole burning and stabilization procedure. To minimize continuous modification of the hole while maintaining a good signal to noise ratio on the locking detector during active stabilization, a beam spot diameter of 4.8 mm and a low irradiance of ~ 30 $\mu W/cm^2$ were required at the sample. An additional factor of twenty in signal to noise ratio should be achievable with a larger illuminated area of ~ 20 mm.

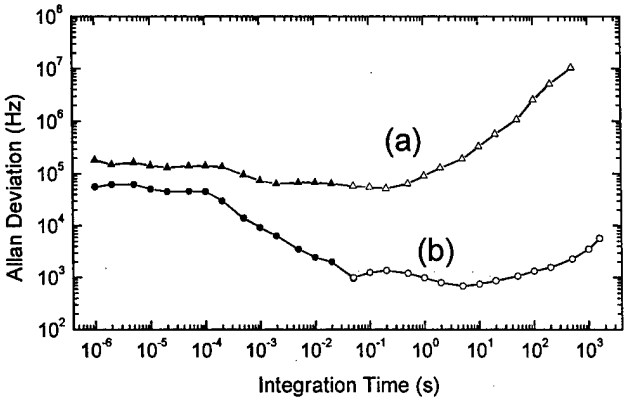

Fig. 15. Allan deviation for the heterodyne beat frequency between two lasers: (a) free-running (triangles), (b) independently locked to persistent spectral holes in the $^4I_{15/2} \rightarrow {}^4I_{13/2}$ transition in Er^{3+}: D^-:CaF_2 at 1523nm (circles). Filled symbols, 300 sample Allan deviations measured directly by a frequency counter; open symbols, values computed from the beat-frequency data of Fig. 16.

Laser frequency stability was characterized using the Allan deviation of the beat frequency between the two lasers. Figure 15 contrasts measurements for (a) the free running lasers with (b) that for the lasers stabilized to spectral holes. The free running lasers already show excellent frequency stability sufficient for many applications. With the lasers locked to the ~ 40 MHz (FWHM) persistent spectral holes an improvement of more than three orders of magnitude was achieved for integration times greater than 300 s, while an order of magnitude was achieved for integration times of 2 ms. Allan deviations down to 680 Hz were attained over a wide range of integration times without requiring vibration isolation of the laser or the crystal frequency reference, demonstrating laser frequency stabilization to better than 6 parts in 10^5 of the ~ 40 MHz hole width.

Characterization and optimization of spectral hole burning references by experiment and simulation have shown that the Allan deviation over short integration times is determined by the width of the spectral hole, whereas stabilization over long integration times is determined by the lifetime of the spectral hole. In Er^{3+}:D^-:CaF_2 the stability over short ($< 10^{-2}$ s) integration times is limited by the relatively low gain of the reference arising from the broad hole and the reduced laser power used to probe it. Nevertheless, the long lifetime of the persistent Er^{3+}:D^-:CaF_2 spectral holes leads to good medium- and long-term stability demonstrated in Fig. 16, where the change in beat frequency between the (a) free running and (b) actively stabilized lasers is shown. Laser frequency drift has been reduced to only a few kHz per minute, limited in this implementation by modifications of the spectral hole by continuous exposure to the probing laser. All Allan deviation values increased by ~ 100 Hz over a period of 10 minutes due to this process. Limiting the exposure of the spectral hole by decreasing the irradiance or periodically

(rather than continuously) probing the reference could substantially improve the performance. The long-term stability of the *persistent* spectral hole itself is primarily limited by temperature fluctuations. A measured frequency shift of the hole with temperature of 1.6 kHz / K at 1.5 K implies Hertz stability of the reference if the temperature is maintained at the milliKelvin level.

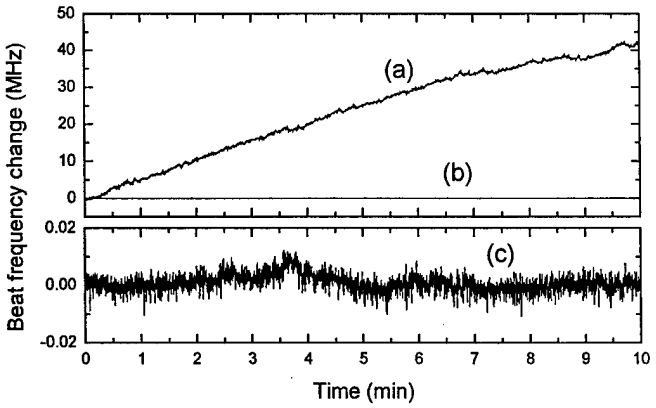

Fig. 16. Change in heterodyne beat frequency between (a) free running lasers and (b) lasers independently locked to persistent spectral holes in separate crystals over a period of 10 minutes, (c) expanded view of data shown in (b), counter gate time was 50 ms.

The material $Er^{3+}:D^{-}:CaF_2$ is not ideal but illustrates the concept of using a *persistent* spectral hole for laser frequency stabilization. Development of persistent hole burning material with lower quantum efficiency for hole burning and with narrower hole widths should significantly improve performance. Gated spectral hole burning materials are being designed to eliminate continued hole burning; a gated hole burning material requires a second laser field or physical process for hole burning to occur and is therefore impervious to hole burning during reading.

Technical limitations were also set by thermally dependent residual amplitude modulation at the electro-optic modulator and voltage offsets in the feedback loop adding to long-term laser drift.

With this experiment we extended the performance of *persistent* spectral holes as programmable laser frequency references to the important 1.5 μm optical communication window, achieving sub-kilohertz laser frequency stability over broader time scales. A compact laser frequency stabilization system that utilizes inexpensive diode lasers has been demonstrated. The system is not limited to low optical power applications, since Erbium doped fiber amplifiers or injection locked high power laser diodes can be used to boost the output power to several watts or more.

Additional more suitable spectral hole burning materials for laser frequency stabilization and spectral hole burning based optical processing are under continuous development, facilitating the stabilization of other sources and improving the versatility of the technique.

Laser Stabilization at 410 nm to Gated Spectral Holes in $Eu^{2+}:CaF_2$

Spectral holes at 410 nm in $Eu^{2+}:CaF_2$ were successfully burned with a tunable GaN external cavity diode laser similar to those used in the experiments described above. Stabilization of the diode laser to gated spectral holes is still under way.

The material optimization discussions of pages 45-65 are relevant to Eu^{2+} materials and provide insight for increasing the efficiency of gated spectral hole burning.

Material Optimization for Laser Frequency References

Material Optimization of Er^{3+}:Y_2SiO_5 at 1.5 μm for Optical Processing, Memory, and Laser Frequency Stabilization Applications,
Thomas Böttger, Y. Sun, C. W. Thiel, and R. L. Cone, Proceedings of SPIE , Vol. 4988, 51-61 (2003).

The material Er^{3+}:Y_2SiO_5 is one of the most important materials for laser stabilization and for spatial-spectral holographic devices using spectral hole burning in the important 1.5 μm communication band. Extensive measurements have been carried out to evaluate and improve this material. Site-selective absorption and emission spectroscopy identified the spectral hole burning transitions. Excited state T_1 lifetimes were measured. The effects of crystal temperature, Er^{3+}-dopant concentration, magnetic field strength, and crystal orientation on spectral diffusion were explored using stimulated photon echo spectroscopy, which is the "prototype" interaction mechanism for spatial-spectral holographic device applications.

The performance of Er^{3+}:Y_2SiO_5 and related Er^{3+} materials has been dramatically enhanced by reducing the effect of spectral diffusion on the coherence lifetime T_2 through fundamental material design coupled with the application of an external magnetic field oriented along specific directions. A preferred magnetic field orientation that maximized T_2 by minimizing the effects of spectral diffusion was determined using the results of angle-dependent Zeeman spectroscopy. The observed linewidth broadening due to spectral diffusion was successfully modeled by considering the effect of one-phonon (direct) processes on Er^{3+} - Er^{3+} interactions. The reported studies improved our understanding of Er^{3+} materials, explored the range of conditions and material parameters required to optimize performance for specific applications, and enabled measurement of the *narrowest* optical resonance ever observed in a solid—with a homogeneous linewidth of 73 Hz. With the optimized materials and operating conditions, photon echoes were observed up to temperatures of 5 K, enabling 0.5 GHz bandwidth optical signal processing at 4.2 K and providing the possibility for operation with a closed-cycle cryocooler.

In Er^{3+}:Y_2SiO_5, SHB at 1.5 μm occurs for the lowest $^4I_{15/2} \rightarrow {}^4I_{13/2}$ transition by population storage in the long-lived $^4I_{13/2}$ excited state. The host crystal Y_2SiO_5 (also called yttrium silicate or YSO and sometimes YOS) belongs to the space group C_{2h}^6 (C2/c, number 15) with eight formula units per monoclinic cell. The Y^{3+} ions occupy two crystallographically inequivalent sites of C_1 symmetry and the Er^{3+} ions substitute for Y^{3+} host ions at both crystallographic sites without charge compensation. All crystals were grown by Scientific Materials Corp. (Bozeman, MT) using the Czochralski method and were transparent and colorless. There are 3 mutually perpendicular optical extinction axes in Y_2SiO_5; the ***b***-axis is parallel to the ⟨010⟩ direction and the $\boldsymbol{D_1}$ and $\boldsymbol{D_2}$ axes correspond to the optical extinction directions when the crystal is viewed along ⟨010⟩ between crossed polarizers. All crystals were x-ray oriented, cut perpendicular to the three optical extinction axes, and polished to optical quality.

Site-selective spectroscopy experiments with continuously tunable external cavity diode lasers (ECDL) were used to identify the $^4I_{15/2}$ ground state and $^4I_{13/2}$ excited state crystal field levels for both Er^{3+} sites and to identify relevant spectral hole burning transitions at 1.5 μm. Absorption measurements located the excited-state crystal field levels, and site-selective fluorescence

unambiguously assigned the excited and ground state level structure to Er^{3+} ions occupying either crystallographically inequivalent Y^{3+} site.

For absorption measurements, a 2 % Er^{3+}:Y_2SiO_5 crystal was held at low temperature (2 K) to ensure that only the lowest crystal field level Z_1 of the $^4I_{15/2}$ ground J-multiplet was significantly populated. The crystal was aligned with its ***b***-axis parallel to the light propagation direction, a Glan-Thompson polarizer was used to select the light polarization, and light transmitted through the crystal was analyzed with a 1.0 m spectrometer and detected with a cooled germanium detector. Atmospheric water vapor lines were used to precisely calibrate the wavelength of the absorption spectrum. Calibration for other measurements was verified using a narrowband external cavity diode laser (ECDL) as a marker whose wavelength was determined with an accuracy of ± 100 MHz using a Burleigh WA 1500 wavemeter.

Absorption lines to the crystal field levels of the $^4I_{13/2}$ J-multiplet are shown in Fig. 17. The sharp well-resolved lines determined 13 of the 14 levels in the $^4I_{13/2}$ J-multiplets for the two sites. The absorption lines from the two Er^{3+} sites are interspersed, with each site experiencing different crystal field splittings.

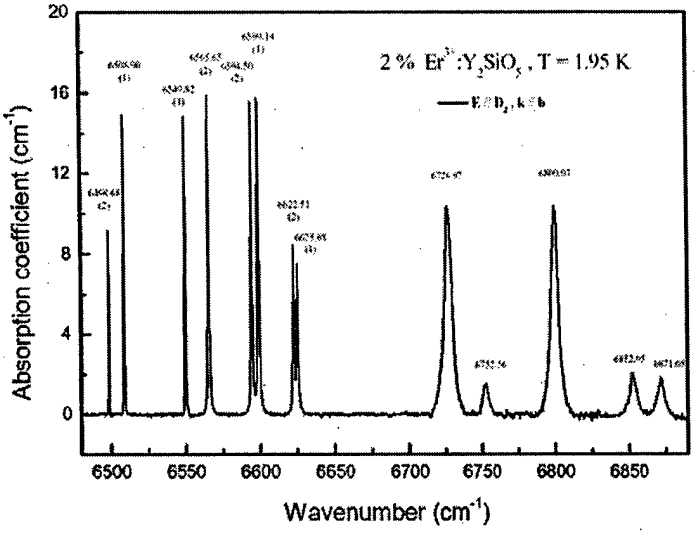

FIG 17. Polarized absorption spectrum of 2% Er^{3+}:Y_2SiO_5 for E//D_2 at T = 2 K. Line centers and crystallographic site assignments (in parenthesis) are given.

Two distinct fluorescence spectra, each corresponding to a specific crystallographic site, were observed when pumping each absorption line with the narrowband ECDL, allowing the crystal field levels of the $^4I_{15/2}$ and $^4I_{13/2}$ multiplets to be assigned to site 1 or site 2; line centers and site assignments are indicated in Fig. 17. The limited tuning range of the ECDL used in these experiments prevented pumping levels above $^4I_{13/2}$:Y_4 so that levels above 6700 cm^{-1} could not be assigned. A complete report and discussion of these measurements will be presented elsewhere.

Knowledge of the excited state lifetime T_1 is important since it establishes the ultimate limit for the coherence lifetime T_2 through the relation $T_2 \leq 2T_1$ and establishes the spectral hole lifetime for population storage in the excited state. The fluorescence dynamics of the metastable $^4I_{13/2}$:Y_1 excited state were investigated for Er^{3+} in both crystallographic sites. Figure 18 shows the measured $^4I_{13/2}$:$Y_1 \rightarrow {}^4I_{15/2}$:$Z_1$ fluorescence decay for site 1 at a temperature of 10 K. The decays were exponential over three decades and exponential least-squares fits gave fluorescence lifetimes T_1 = 11.4 ms for site 1 and T_1 = 9.2 ms for site 2. The ultra-low Er^{3+} concentration of 0.001 % used in our experiments minimized the effect of

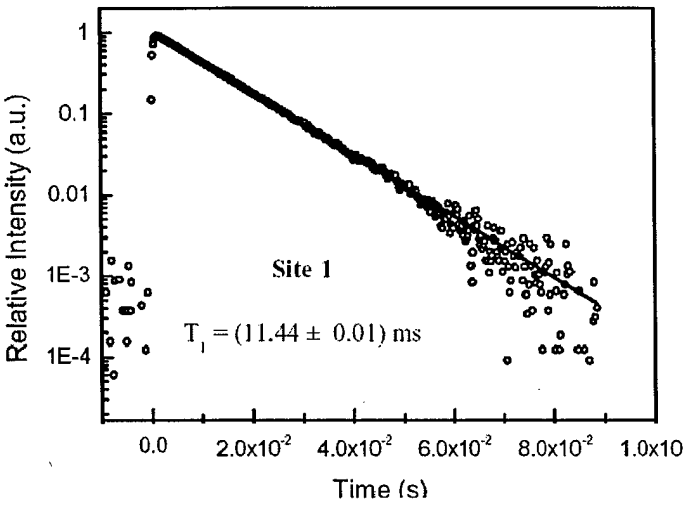

FIG. 18. Fluorescence decay of site 1 for the 0.001 % Er^{3+}:Y_2SiO_5 $^4I_{13/2}(Y_1) \rightarrow {}^4I_{15/2}(Z_1)$ transition at T = 10 K.

radiation trapping on the observed fluorescence lifetimes. The nearly negligible effect of radiation trapping was confirmed by the minimal effect of temperature and excitation energy on the observed lifetimes; hence, these measured values establish an upper limit for the fluorescence lifetime of the $^4I_{15/2}$:Y_1 level in Er^{3+}:Y_2SiO_5 materials.

Optical interactions with rare-earth-activated materials rely on the macroscopic polarization created by the combined response of the individual rare-earth ions in the material. The macroscopic polarization and resulting material response depend on the phase relationships between the individual ions. To enhance processing time or storage density, the coherence time should be maximized under practical operating conditions. For Er^{3+} optical centers, loss of phase coherence between the ions is induced by random perturbations of the energy levels involved in the optical transition, a process that also contributes to spectral diffusion. In Er^{3+}:Y_2SiO_5, the primary source for dephasing is the magnetic dipole-dipole interaction between the large magnetic moments of the Er^{3+} ions' electronic states. The energy of each Er^{3+} ion depends on the orientation of all other Er^{3+} moments in the crystal; therefore, whenever an Er^{3+} ion undergoes a spin flip, it perturbs the energy levels of the other ions in its environment. To achieve long coherence lifetimes, it is necessary to suppress the spin flips of all Er^{3+} ions in the crystal, including both the optically active Er^{3+} ions that are directly probed by the laser as well as all remaining non-resonant Er^{3+} ions in the environment. The application of an external magnetic field lifts the Kramers degeneracy, "freezing out" spin flips through the preferential occupation of the lower energy spin state. The ratio of the level splitting to the available thermal energy $g\mu_B B/kT$ is a key variable influencing the microscopic dynamics in Er^{3+}:Y_2SiO_5. Maximizing the level splitting at a particular applied field requires knowledge of the anisotropy of the ground and excited state Er^{3+} magnetic moments at each site. As a fundamental part of the material optimization strategy, this magnetic anisotropy was measured using Zeeman spectroscopy as a function of magnetic field orientation to determine the relevant ground and excited state g-values.

Simultaneously maximizing the g-values for the ground and excited states of all ions that influence the optical dephasing was challenging due to the complex crystal structure of Er^{3+}:Y_2SiO_5, which has two distinct crystallographic sites, each exhibiting the lowest C_1 site symmetry. Additional complexity arises from the magnetic inequivalence of the multiple orientations that occur for each of the crystallographic sites within the unit cell. The results of Zeeman spectroscopy identified a preferred magnetic field orientation at an angle of $\Phi \sim 140^\circ$

with respect to the D_1-axis in the D_1-D_2 plane. This direction minimizes the spin flips of ions at both site 1 and site 2. A full report of these measurements will be given elsewhere.

Two-pulse photon echo experiments were performed as a function of magnetic field orientation to measure the optical dephasing and to confirm the elaborate predictions derived from the Zeeman experiments. Optical dephasing for site 1 in a 0.001 % Er^{3+}:Y_2SiO_5 crystal was measured as a function of magnetic field orientation in the D_1-D_2 plane at 1.6 K with a magnetic field of 3 T. The experimental apparatus and conditions were the same as for stimulated photon echo spectroscopy described below. Under these experimental conditions, linewidth values spanned over two orders of magnitude from 400 Hz to 50 kHz as the magnetic field orientation was varied, highlighting the leading role of Er^{3+} spin flips as a source of optical dephasing. As predicted by our optimization strategy, the narrowest homogeneous linewidths of ~ 400 Hz were observed for magnetic field orientations of $\Phi \sim 140^\circ - 160^\circ$ with respect to the D_1-axis in the D_1-D_2 plane. This confirms that the spectral diffusion may be suppressed using knowledge of the magnetic anisotropy to select orientations that simultaneously maximize the level splittings of both site 1 and site 2. The two-pulse echo results demonstrated further that non-resonant "environment" ions at both crystallographic sites contribute to dephasing and must be considered in the selection of the preferred external magnetic field orientation. An additional criterion for choosing the magnetic field direction is to maximize the number of magnetically equivalent Er^{3+} ions to enhance the interaction with the resonant optical field. For Er^{3+}:Y_2SiO_5, applying the magnetic field in the D_1-D_2 plane, which contains the preferred direction discussed above, increases the number of ions resonant with the laser by a factor of two compared to an arbitrary field orientation. A full discussion of these measurements will be presented elsewhere.

Intrinsic frequency selectivity of SHB materials enables the storage and manipulation of information encoded in the spectral or temporal properties of the light field. To analyze the material response over timescales appropriate for SHB applications, we extensively characterized the evolution of the coherence lifetime and spectral hole linewidth, both of which vary with time due to the presence of spectral diffusion in Er^{3+}:Y_2SiO_5. The angle-dependent Zeeman spectroscopy and two-pulse photon echo decay experiments identified preferred directions for the magnetic field that minimized dephasing induced from neighboring ions of site 1 and site 2. Additional information on the Er^{3+} dynamics was extracted by studying the dephasing of the optical center with stimulated photon echo spectroscopy. This method was ideal for investigating the effect of spectral diffusion on the linewidth over the timescales of interest for practical SHB device applications. These measurements also guided the choice of Er^{3+} concentration, magnetic field strength, and operating temperature for optimizing the material and provided insight into the microscopic spin dynamics. The Er^{3+}:Y_2SiO_5 crystals were aligned with the light propagating along the b-axis and with the magnetic field along D_1. The experimental apparatus is depicted in Fig. 19. The laser (ECDL) output power of ~ 1.8 mW was amplified by an Erbium doped fiber amplifier to 35 mW. An acousto-optic modulator (AOM) gated the photon echo pulse-sequence from the amplified laser beam. For most experiments, the beam was focused inside the crystal to a waist of radius ~ 25 μm. Typical π/2-pulse widths were ~ 500 ns, giving a ~ 2 MHz spectral width that minimized the sensitivity of the measurements to laser frequency fluctuations. The observed photon echo signals were detected using a photodiode.

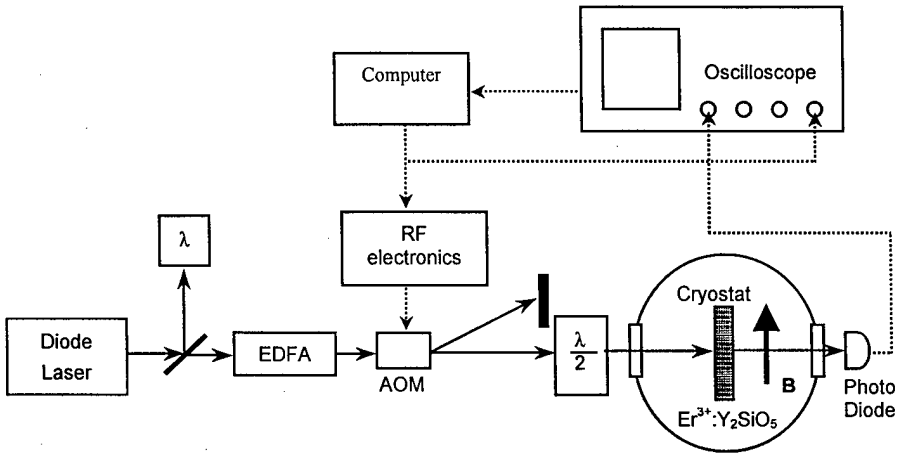

FIG. 19. Experimental setup for measuring two-pulse photon echoes and stimulated echoes.

The stimulated photon echo employs a three-pulse sequence and can be thought of as a modified two-pulse echo with a pulse delay of t_{12}, where the second π-pulse is broken up into two $\pi/2$-pulses that are separated by the waiting time T_W. Figure 20 shows an actual stimulated photon echo pulse sequence. As in the two-pulse echo case, the first pulse prepares the ions by placing each ion in a coherent superposition of the ground and excited state. During the delay t_{12}, the phase of the superposition state evolves according to the ion's instantaneous transition frequency. The second pulse stores each ion's total accumulated phase as a population difference between the ground and excited states. Thus, a frequency dependent population grating is produced between the ground and excited states with a period given by $1/t_{12}$. This grating decays due to population decay with the lifetime of the excited state T_1. In addition, spin-flips of other Er^{3+} ions in the crystal cause frequency shifts in the levels of the individual ions that make up the population grating. These frequency shifts tend to smear out the grating (i.e. spectral diffusion) and therefore lead to a loss of the stored coherence. When a short $\pi/2$-pulse is applied after the waiting time T_W, the remaining coherence stored in the population grating is rephased after an additional time delay of t_{12} and a stimulated photon echo is emitted. The stimulated photon echo intensity contains information about dephasing during the two t_{12} delays and spectral diffusion and population decay during T_W. Systematic measurements of the stimulated echo intensity I were made as t_{12} was varied for different T_W to map out the time evolution of the effective homogeneous linewidth Γ_{eff} as excited ions underwent spectral diffusion.

A specific spectral diffusion model has been incorporated into the echo decay function, enabling us to significantly extend previous data analysis methods. In this model, a generalized form of the echo decay function

$$I(t_{12},T_W) = A \cdot \exp\left\{-\frac{2T_W}{T_1}\right\} \cdot \exp\left\{-4t_{12}\pi\,\Gamma_{eff}(t_{12},T_W)\right\} \qquad (1)$$

describes the stimulated echo intensity, where the constant homogeneous linewidth is replaced by a time-dependent effective linewidth $\Gamma_{eff}(t_{12},T_W)$ that incorporates the effect of spectral

diffusion. If we specifically consider the spectral diffusion resulting from spin flips, the effective linewidth is given by

$$\Gamma_{eff}(t_{12},T_W)=\Gamma_0+\tfrac{1}{2}\Gamma_1\left[R\,t_{12}+\{1-\exp(-RT_W)\}\right], \quad (2)$$

following the approach of Mims. In this expression, Γ_0 is the initial homogeneous linewidth in the absence of spectral diffusion, Γ_1 is the maximum contribution of spectral diffusion to the homogeneous linewidth, and R is the rate of perturbations causing the spectral diffusion. This

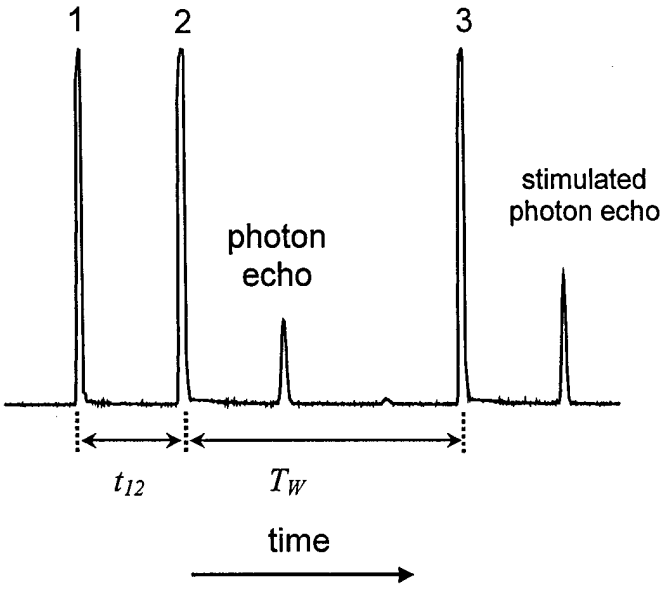

FIG. 20. A typical stimulated photon echo pulse sequence. The first two excitation pulses are separated by a time delay t_{12} and pulse 2 and 3 are separated by the waiting time T_W. The stimulated photon echo occurs at a time delay t_{12} after pulse 3, a two-pulse echo can be observed at a time delay t_{12} after pulse 2; note that the excitation pulse area is ~ $\pi/2$ for each of the three pulses, causing the stimulated photon echo to be stronger than the two-pulse photon echo.

expression is valid in the limit $Rt_{12} \ll 1$; for the limit $Rt_{12} \gg 1$, the effective linewidth is expected to be independent of T_W. Analyzing the behavior of the physical parameters R and Γ_1 extracted from the data using this approach provides direct insight into the microscopic dynamics causing the spin flips and also allows the effect of spectral diffusion to be predicted and explained for a wide range of operating conditions. The underlying theory as well as experimental detail will be presented elsewhere.

If we analyze the spectral diffusion that occurs during T_W, Eq. (2) simplifies to

$$\Gamma_{eff}(T_W)=\Gamma_0+\tfrac{1}{2}\Gamma_1\left[1-\exp\{-RT_W\}\right], \quad (3)$$

allowing the effective homogeneous linewidth to be modeled as a function of T_W from the stimulated echo decay curves. This expression represents the effective initial linewidth for very short t_{12} and also approximately describes the behavior of the effective linewidth for cases where the linewidth is dominated by spectral diffusion during the waiting time, as is the case for large T_W. In the long time limit, Eq. (1) and Eq. (3) predict simple exponential decays with a saturated

effective linewidth given by $\Gamma_0 + \frac{1}{2}\Gamma_1$, where the factor of $\frac{1}{2}$ enters because spectral diffusion during the waiting time only produces dephasing for the last t_{12} section of the echo sequence. It is important to note that the corresponding absorption linewidth is a Lorentzian with a full width at half maximum given by $\Gamma_0 + \Gamma_1$.

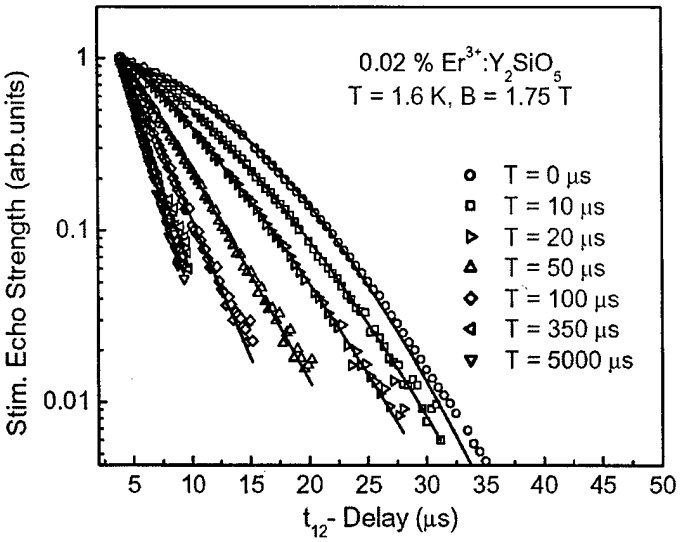

FIG. 21. Stimulated photon echo decays for 0.02% Er^{3+}:Y_2SiO_5 in a magnetic field of B = 1.75 T at 1.6 K as the waiting time is varied between 0 μs and 10000 μs; ***B*** // ***D*****1**. Solid lines are least-square fits to Eq. (1), with Γ_{eff} given by Eq. (2).

Figure 21 shows typical stimulated photon echo decays for 0.02 % Er^{3+}:Y_2SiO_5 in a magnetic field of 1.75 T and at 1.6 K as T_W was varied from 0 μs (equivalent to a two-pulse photon echo decay) to 5000 μs. Stimulated photon echo decays for short waiting times were non-exponential, indicating the rapidly increasing effect of spectral diffusion occurring on the time scale of the echo sequence. Longer waiting times yielded exponential decays, and the observed decay constants saturated at values determined by the temperature, concentration, magnetic field, and field direction. The solid lines are fits to the data points using Eq. (1) with Γ_{eff} given by Eq. (2); they gave good agreement, allowing the time evolution of the linewidth to be extracted as the waiting time T_W was varied. It should be noted that this model tends to underestimate the echo intensity at large values of t_{12}, as can be seen by a small deviation of the fit from the data for the first three curves (T_W = 0 μs, 7 μs, 15 μs). For these decay curves, the value of t_{12} approaches $1/R$, corresponding to a significant probability for each perturber to undergo multiple spin flips during the t_{12} sections of the echo sequence. Perturbers that undergo multiple spin flips have a reduced effect on the optical dephasing since the dephasing induced by subsequent flips tends to cancel, reducing the net effect. This causes the echo intensity to decay more slowly as t_{12} approaches $1/R$, an effect similar to "motional narrowing" in NMR.

Representative results of the stimulated echo analysis are shown in Fig. 22 for a 0.02 % Er^{3+}:Y_2SiO_5 sample, where the evolution of the effective linewidth is mapped as a function of T_W for a variety of magnetic fields from 0.8 T up to 3 T at 1.6 K. Solid lines in Fig. 22 are least-squares fits to the data using Eq. (3). Each case shows excellent agreement. The presence of spectral diffusion is clearly observed in the significant broadening of the linewidth as T_W is increased. For these measurements, a plateau was reached after several hundred microseconds where the contribution of spectral diffusion to the linewidth reached its saturated value. As shown in Fig. 22, a larger magnetic field dramatically suppresses linewidth broadening, illustrating how the magnetic field strength may be chosen to reduce the linewidth to a particular level required for a given application.

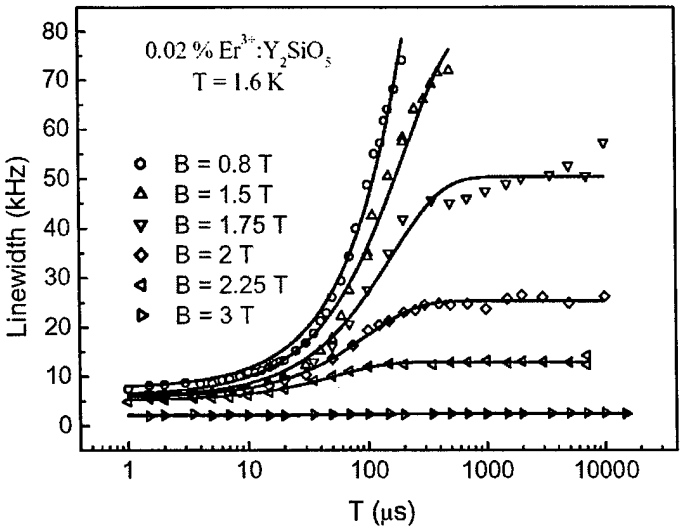

FIG 22. Evolution of the effective linewidth of site 1 in 0.02 % Er^{3+}:Y_2SiO_5 at 1.6 K as the waiting time T_W is varied in a stimulated photon echo experiment. The magnetic field varies from B = 0.8 T to B = 3 T between data sets; $\boldsymbol{B} \,//\, \boldsymbol{D_1}$. Solid lines are least-squares fits to the data using Eq. (3).

To understand and predict the behavior of the spectral diffusion as a function of magnetic field and temperature, we employed a specific model based on the spin-flip dynamics in the material. The spectral diffusion parameters Γ_1 and R may be modeled by considering the magnitude of the dipole-dipole interactions between Er^{3+} ions and the physical mechanism driving the spin flips. The model predicts saturation of the linewidth when all spins deviating from thermal equilibrium have flipped. The saturated linewidth value $\Gamma_1(B,T)$ for long T_W is related to the size of the average deviation of the population from equilibrium and is given by

$$\Gamma_1(B,T) = \Gamma_{max}\,\mathrm{sech}^2\left(\frac{g\mu_B B}{2kT}\right), \tag{4}$$

where g is the g-value of the ground state Kramers doublet, μ_B the Bohr magneton, B the magnetic field, k the Boltzmann constant, T the temperature, and Γ_{max} is determined by the magnitude of the dipole-dipole interaction between Er^{3+} ions. It is important to note that, for magnetic dipole-dipole interactions between ions randomly distributed in the crystal lattice, Γ_{max} may be calculated from knowledge of the crystal structure and the magnitude of the dipole moments in the ground and excited states. The ratio $\Delta E_g / 2kT = g\mu_B B / 2kT$ between the ground state energy level splitting ΔE_g and the thermal energy available to the ions kT determines the saturation level of the homogeneous linewidth Γ_1. If the splitting is large compared to the thermal energy, deviations of the spin population from thermal equilibrium will be small and therefore only make a negligible contribution to the spectral diffusion of the optical center. The spectral diffusion rate R represents the sum of the upward and downward spin-flip transition rates and is given by the spin-lattice relaxation rate that describes how fast the spin population returns to thermal equilibrium. To model the behavior of R, we must explicitly incorporate the mechanism driving the spin flips. If we attribute the driving mechanism to the one-phonon (direct) absorption and emission process between the two Zeeman levels, the relaxation rate for Kramers ions as a function of magnetic field and temperature is given by

$$R(B,T) = R_0 + \alpha(g\mu_B)^3 B^5 \coth\left(\frac{g\mu_B B}{kT}\right), \tag{5}$$

where α is a constant determined by the phonon coupling, R_0 is the spin-flip rate at zero magnetic field, and all remaining quantities are the same as in Eq. (4). Physically, R_0 corresponds to the minimum spin-lattice relaxation rate, and it results from mechanisms that have negligible

dependence on the applied magnetic field strength over the range studied, such as two-phonon interactions with higher energy electronic states. Over the temperature and magnetic field ranges studied here, R_0 typically represents a small contribution to the observed rates. The spin-lattice relaxation rate described by Eq. (5) grows rapidly with increasing magnetic field strength due to an increase of the accessible density of phonon states at energies degenerate with the splitting of the Zeeman levels and an increase in the magnetic-field-induced wavefunction mixing of crystal field levels.

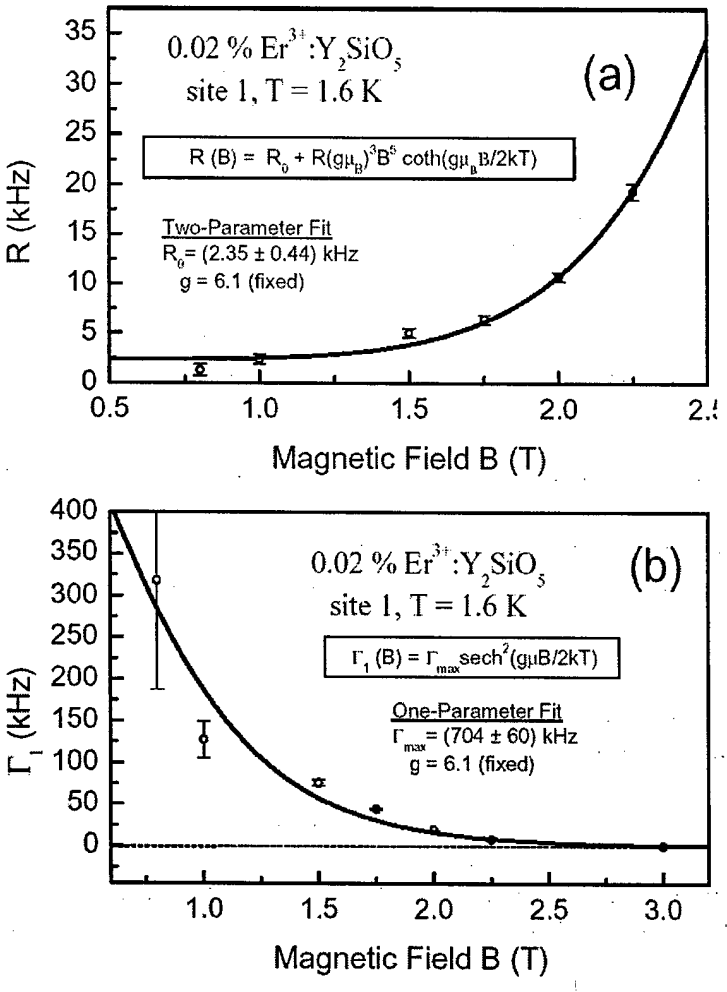

FIG. 23. (a) Measured relaxation rate R and (b) saturated spectral diffusion linewidth Γ_1 as a function of magnetic field for 0.02% Er^{3+}:Y_2SiO_5 at 1.6 K; $\boldsymbol{B} // \boldsymbol{D_1}$. Solid lines are least-squares fits using equations Eq. (5) and Eq. (4), respectively.

Field dependent linewidth saturation values $\Gamma_1(B)$ and relaxation rates $R(B)$ obtained from the fits shown in Fig. 21 are plotted with error bars as a function of magnetic field in Fig. 23. The solid lines are least-squares fits to the magnetic field dependent saturated linewidth $\Gamma_1(B)$ and rate $R(B)$ using Eq. (4) and Eq. (5), respectively. Both fits give excellent agreement and fitting parameters are shown in the figure. For these fits, the exact measured g-value of g = 6.1 for site 1 with $\boldsymbol{B} // \boldsymbol{D_1}$ was used, clearly indicating that the spectral diffusion was dominated by spin flips of environment ions occupying site 1. Spin flips of site 2 were "frozen out" due to the much larger ground state energy level splitting for this $\boldsymbol{B} // \boldsymbol{D_1}$ direction (g = 14.7). We also observed that spectral diffusion of site 1 can be dominated by spin flips from either site 1 or site 2 for different magnetic field orientations, consistent with the measured magnetic anisotropy.

Spectral diffusion was also investigated at elevated temperatures. In a 0.005% Er^{3+}:Y_2SiO_5 crystal held at T = 4.2 K in a field of B =3 T, spectral diffusion was evident as Γ_{eff} broadened from ~ 20 kHz to ~ 110 kHz within the first 20 μs and then saturated. Stimulated echoes were consistently measurable over the entire lifetime of the excited state for waiting times up to

T_W = 10 ms. These optimized material properties, coupled with a laser stabilized to a spectral hole frequency reference, enabled high bandwidth (0.5 GHz) signal processing in that crystal at 4.2 K, providing the possibility for operation with a closed-cycle cryocooler.

The success of this analysis allows us to not only identify the source of spectral diffusion as Er^{3+} ions residing at site 1, but also allows us to identify the specific mechanism responsible for the spectral diffusion as spin flips driven by the one-phonon process. It should be noted that spectral diffusion due to Y^{3+} ion nuclear spin flips, with rates on the order of a few Hz, occurs on a timescale longer than our stimulated photon echo measurements, but is expected to contribute significantly to the linewidth broadening on timescales of hundreds of milliseconds or longer. By extending this analysis to related materials, new insight into the physical mechanisms that influence each material's behavior may be gained.

Guided by our material optimization strategy that suppresses optical dephasing, we investigated the material coherence time (or homogeneous linewidth) under optimum experimental operating conditions in the crystal with 0.001 atomic percent Er^{3+} concentration. Dephasing for site 1 was characterized using two-pulse photon echo measurements with a magnetic field of 7 T applied in the $\boldsymbol{D_1}$-$\boldsymbol{D_2}$ plane and with the laser propagation direction along the $\boldsymbol{b}$-axis. The magnetic field was oriented along the preferred direction of $\boldsymbol{\Phi} = 140^\circ$ with respect to the $\boldsymbol{D_1}$ crystal axis. To "freeze out" the thermal population in the upper Zeeman level of the ground state, the sample was immersed in a liquid helium bath held at 1.5 K. Under these conditions, two-pulse echo decays gave a dephasing time of T_2 = 4.38 ms, corresponding to an optical homogeneous linewidth of 73 Hz. This is the longest optical dephasing time ever measured in any solid-state material, with the corresponding linewidth being the narrowest optical resonance. Residual contributions to this narrow linewidth are population decay, excitation induced dephasing (instantaneous spectral diffusion), and contributions from the ^{89}Y nuclear spin fluctuations. The excited state lifetime T_1 = 11.4 ms establishes the ultimate limit of 14 Hz for the homogeneous linewidth in Er^{3+}:Y_2SiO_5. Further measurements are required to separate other individual contributions, which may include fluctuations in laser frequency stability, fluctuations of the earth's magnetic field, or stray electromagnetic fields in the laboratory as suggested by the results of Equall *et. al.*, where a linewidth of Γ_{hom} = 122 Hz was measured in Eu^{3+}:Y_2SiO_5.

Optical material design and the choice of practical operating conditions require a complex balance of many factors that must be simultaneously satisfied for each specific application. Developing a buffer memory, for example, might require high spectral bandwidth and strong optical transition dipoles for high Rabi frequencies, while ultra-dense data storage might require longer coherence and spectral hole lifetimes. Applications requiring maximum signal sensitivity and compactness may benefit from higher dopant concentrations to increase the interaction strength; however, the higher concentrations also increase the spectral diffusion, resulting in broader homogeneous linewidths and shorter coherence lifetimes. Every device implementation must be analyzed to determine an optimal balance between design parameters as diverse as optical wavelength, absorption strength, Rabi frequency, coherence lifetime, inhomogeneous linewidth, hole burning efficiency, spectral hole lifetime, laser power, operating temperature, and magnetic field strength.

This work explored aspects of rare-earth-activated materials that are critical for SHB-enabled optical technologies. These experimental studies provide the basis for theoretical understanding of how the material properties are affected by the operating conditions. Both the advanced modeling and the determination of the static and dynamic optical properties have been illustrated here. By fully understanding the behavior of spectral diffusion and its effect on material performance, precise operating conditions and material composition can be chosen to meet specific requirements for each device application.

Based on the experimental evidence and our understanding of the material physics, an optimization strategy was developed that is also applicable to similar Er^{3+} materials and other paramagnetic ions. To minimize dephasing, the g-values must be simultaneously maximized in both the ground and excited states for all crystallographic sites in the material. In addition, the site exhibiting the longest T_1 lifetime and strongest absorption should be used for SHB applications. Magnetic field strength and operating temperature can then be employed to "freeze out" the thermal spin population in upper Zeeman levels. The magnetic field should also be oriented so that a minimum of magnetically inequivalent site orientations is present in the crystal. The Er^{3+} concentration can be adjusted to increase Er^{3+} - Er^{3+} ion distances and reduce spectral diffusion while balancing the necessity for sufficient optical absorption.

This study led to significant material optimization that allowed the demonstration described earlier of high bandwidth optical signal processing at T = 4.2 K and also enabled the measurement of what we believe to be the narrowest optical resonance in a solid with a homogeneous linewidth of 73 Hz.

Other Er^{3+} Materials

Characterization and optimization of spectral hole burning frequency references for laser stabilization, both by experiment and simulation, has demonstrated that narrow holes lead to a high signal to noise ratio and consequently to the good short term stability needed for devices. Materials combining long-lived holes and minimal spectral diffusion provide good stability over integration times of hundreds of seconds or longer. Spectroscopic investigation of Er^{3+}:Y_2SiO_5 and other materials demonstrated that hole widths can be made much less than a kilohertz and can potentially reach the lifetime limit of approximately 10 Hz. Locking has been demonstrated for six materials, and many other materials are characterized. Further development of crystals with both narrow and long-lived holes is in progress, including 100 Hz holes lasting for weeks, and has lead to higher performance and stability over a longer integration times.

Frequency reference crystals have been developed that are capable of providing long-term portable references with spectral holes persisting above liquid Nitrogen temperatures. The holes can be programmed at arbitrary positions within the inhomogeneous profile, which has been custom tailored in width to values between 0.2 and 270 GHz by altering the crystal composition. Still broader ranges available in glasses, as we are showing in another project.

The 1.5 μm $^4I_{15/2} \leftrightarrow {}^4I_{13/2}$ transitions of Er^{3+} materials provide exciting possibilities for accelerating the development of practical hole burning technologies by incorporating the established telecommunications equipment infrastructure that operates in this same spectral band. These wavelengths are also 'eye safe,' opening additional applications. Toward this goal, in Sec. 2 we report the progress made in the study of Er^{3+} doped Y_2SiO_5 (YSO), Y_2O_3, $YAlO_3$, YAG, $CaWO_4$, and $SrWO_4$ samples.

Photon echo, stimulated photon echo, and other characterization measurements have been carried out on the $^4I_{15/2} \leftrightarrow {}^4I_{13/2}$ transition Er^{3+} in a range of oxide crystals. This transition occurs in the 1.5 μm region, coinciding with the telecommunications band. The properties of this transition were examined for materials including Y_2SiO_5, Y_2O_3, $LiNbO_3$, YAG, $YAlO_3$, $CaWO_4$, and $SrWO_4$.

In these materials, Er^{3+} was doped at very low concentration (~10 ppm) to minimize dephasing and spectral diffusion induced by mutual Er-Er spin flips. The coherence properties for 0.005% Er^{3+}:YSO have been reported earlier where the dephasing time T_2 was measured to be as long as 580 μs. To further reduce the Er-Er dephasing, we examined an even more dilute 0.001% Er^{3+} doped sample. For this sample, the dephasing time was measured to be as long as 6.4 ms at B=70 kG and T=1.5 K, corresponding to a homogeneous linewidth Γ_h of ~50 Hz. The large g-factor of Er^{3+} in this material allows the Er-Er spin-flip induced dephasing to be frozen out at moderate magnetic field. At a typical field achieved using simple button-sized Nd-Fe-B magnets (2.5 kG), the Er-Er induced dephasing is suppressed enough that the homogeneous linewidth is as narrow as Γ_h~2.5kHz.

The Y_2O_3 host is another low nuclear magnetic moment material similar to YSO. However, because of the higher symmetry of the crystal (T_h), in addition to the two crystallographically inequivalent Er^{3+} sites, there are also six magnetically inequivalent site orientations for the C_2 site and four magnetically inequivalent site orientations for the C_{3i} site. Measurements of the coherence properties of the C_2 site showed that they are similar to the properties observed in YSO, with a similar narrowing of the homogeneous line observed for applied magnetic fields. For the 0.005% Er^{3+}:Y_2O_3 sample, very strong photon echoes were observed even in a magnetic field as weak as a few hundred Gauss.

In the search for materials with large inhomogeneous to homogeneous linewidth ratios Γ_{inh}/Γ_h, 0.06% Er^{3+}:$LiNbO_3$ has proven to be of particular interest. We have found that this material has a large inhomogeneous linewidth of Γ_{inh} = 250 GHz, and a homogeneous linewidth as narrow as Γ_h =4 kHz at 1.5 K for B=5 kG along the c-axis. Increasing the magnetic field strength results in a further narrowing of the homogeneous linewidth, reaching a limit of 2 kHz for a field of 20 kG along the c-axis. These properties correspond to Γ_{inh}/Γ_h greater than 10^8, making this an interesting material for spatial-spectral holographic applications where a large Γ_{inh}/Γ_h determines the time bandwidth product for signal processing. The homogenous linewidth was also measured across the inhomogenous absorption profile by shifting the laser to excite at every 10 GHz interval, revealing that the homogeneous linewidth Γ_h is constant across the entire inhomogeneous line.

In Table I we present all the coherence parameters discussed above, as well as the transition wavelengths and the Γ_{inh}/Γ_h ratio as a measure of the time-bandwidth product. We have found that for those applications where low field is a prerequisite, the YSO and Y_2O_3 hosts provide excellent candidates, while applications that require very high bandwidth would benefit from the properties of materials such as $LiNbO_3$. In addition, the properties of Er^{3+} doped $YAlO_3$, YAG, $CaWO_4$, and $SrWO_4$ were studied and given in Table I. Lengthening of T_2 with the magnetic field was also observed in these materials. All materials have similar oscillator strength except for Er:$SrWO_4$ where it was an order of magnitude smaller than the other materials.

			H_0=0		Saturated values in magnetic field		
Material, Er conc.	Wavelength (nm)	Γ_{inh} (GHz)	T_M (μs)	x	T_M (μs)	x	Γ_{inh}/Γ_h
Y_2SiO_5, 0.001%	1536.14, site 1 1538.57, site 2	0.5	3.3	1	>2000	1.0	$3x10^6$
Y_2O_3, 0.005%	1535.28 nm	1	18	1.85	105	1.4	$3 x10^5$
$LiNbO_3$, 0.06%	1531.52 nm	200			170	2.0	$1 x10^8$
$YAlO_3$, 0.005%	1514.38 nm	1			265	2.2	$8 x10^5$
$CaWO_4$, 0.005%	1532.30 nm	1			140	1.5	$4.4 x10^5$
$SrWO_4$, 0.05%	1533.55 nm	1			72	1.0	$2.2 x10^5$
YAG, 0.1%	1526.97 nm	30			75	1.5	$7 x10^6$

Table I. Summary of material parameters for Er^{3+} doped oxides. The dephasing times are parameters in the Mims decay expression, $I = I_0 \exp(-(4t/T_M)^x)$. The Mims dephasing time T_M plays a role similar to the conventional optical T_2.

Photon Gated Spectral Hole Burning – Relation of Rare Earth Ions to Band Structure

- *Systematics of 4f Electron Energies Relative to Host Bands by Resonant Photoemission of Rare Earth Ions in Aluminum Garnets,* C. W. Thiel, H. Cruguel, H. Wu, Y. Sun, G. J. Lapeyre, R. L. Cone, R. W. Equall, and R. M. Macfarlane, Phys. Rev. B **64**, 085107 (2001).
- *Systematics of 4f electron energies relative to host bands by resonant photoemission of rare earth doped optical materials,* C. W. Thiel, H. Cruguel, Y. Sun, G. J. Lapeyre, R. M. Macfarlane, R. W. Equall, and R. L. Cone, J. Lumin. **94-95**, 1-6 (2001).

- *Recent progress in developing new rare earth materials for hole burning and coherent transient applications,* Y. Sun, C. W. Thiel, R. L. Cone, R. W. Equall, and R. L. Hutcheson, J. Lumin. **98**, 281-287 (2002).
- *Progress in Relating Rare Earth Ion 4f and 5d Energy Levels to Host Bands in Optical Materials for Hole Burning, Quantum Information, and Phosphors,* C. W. Thiel, Y. Sun, and R. L. Cone, Journal of Modern Optics **49**, 2399-2411 (2002).

Our work on relating ion levels to host band structure was also a feature in **Optics in 2001** published by the Optical Society of America.

- *Relating Localized Electronic States to Host Band Structure in Rare-Earth-Activated Optical Materials,* Charles W. Thiel, Herve Cruguel, Huasheng Wu, Yongchen Sun, Gerald J. Lapeyre, Rufus L. Cone, Randy W. Equall, and Roger M. Macfarlane, Optics & Photonics News, **12,** #12, 64 (2001).

Photon-gated spectral hole burning is a two-photon process in which the first photon provides the spectral selectivity by exciting the ion, and a second "gating" photon is required to enable a persistent hole burning mechanism. This gated hole burning process provides a method for non-destructive readout of the information stored in the absorption profile since hole burning only occurs when the gating photons are present. One mechanism that is well-suited to photon-gating is two-step photoionization. The steps involved in this mechanism are illustrated in Fig. 24. In the first step, a laser selectively excites a $4f^N$ to $4f^N$ transition of ions at frequencies where spectral holes are to be burned. Next, the gating photons selectively excite the ions that are in their upper $4f^N$ state to a $4f^{N-1}5d$ state. Because of the large oscillator strength and broad absorption of the $4f^N$ to $4f^{N-1}5d$ transition, either a second laser or even possibly a filtered broadband lamp could be used as the source of gating photons to excite the ions into the $4f^{N-1}5d$ state. If the $4f^{N-1}5d$ state is within the conduction band of the host, the 5d electron may relax into the conduction band and diffuse away from the rare earth ion to become trapped at an electron acceptor site in the lattice (lattice defects or doped acceptor impurities). Since the valence of the excited rare earth ion has changed, it is permanently removed from the absorption, producing a persistent spectral hole.

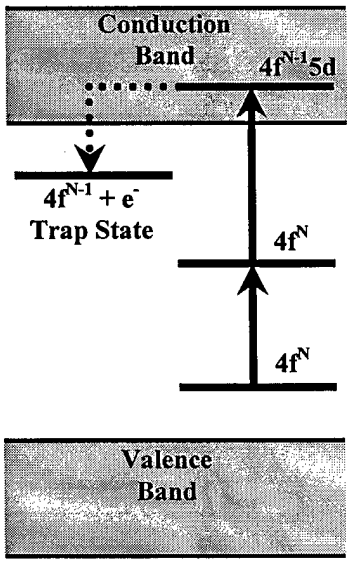

FIG 24. Energy level diagram illustrating the photon-gated photoionization spectral hole burning process in rare-earth-activated materials.

Photon-gated spectral hole burning has important applications including laser frequency stabilization, optical coherent transient data processing, and optical memories. In the laser frequency stabilization applications, a narrow spectral hole burned at the desired laser frequency may be used as a reference to stabilize the laser. These stable lasers have many applications in both fundamental research, where they enable measurements over long time scales with Hertz-level resolution, and technological applications such as measuring precise distances through interferometry. Photon-gated hole burning is of particular interest for laser stabilization since it prevents the laser from modifying the spectral hole during the locking process. In optical data processing and memory applications, photon-gated hole burning would provide a mechanism for "programming" the material by modifying the absorption spectrum while providing for non-destructive readout by avoiding hole burning from probe photons.

Photon-gated hole burning may also prove useful in proposed architectures for quantum information applications that employ entangled states of rare earth ions in a crystal. Some of these techniques involve generating spectral features that correspond to groups of strongly coupled ions in the lattice. This is done by using hole burning to selectively remove ions from the absorption spectrum until only the coupled ions remain. In these methods, photon-gating potentially could be used to permanently remove the undesired ions from the absorption spectrum when preparing the material.

To optimize photon-gated hole burning, it is necessary to develop a complete picture of the electronic structure of rare-earth-activated insulators that incorporates the interactions between the rare earth ion and the electronic states of the host material. Understanding these interactions between and how they influence basic material properties can enhance or inhibit performance. Although the general properties of rare earth ions' electronic states and transitions are well understood and their theoretical description is well established, much less is known regarding the relationships between the energy levels of the ions and the electronic band states of the crystal lattice.

To improve our fundamental physical understanding of these phenomena as well as to provide new information of practical significance for technological applications, we have carried out a systematic study of the relative energies and the interaction dynamics of the rare earth energy levels and the host bands in optical materials.

The first step in developing practical photon-gated photoionization hole burning materials for each of these applications is to determine the energies of the $4f^{N-1}5d$ states relative to the host conduction band as well as the energies of the $4f^N$ ground states relative to the host valence band. For the ionization hole burning process to produce stable, long-lived spectral holes, it is expected that the $4f^N$ ground state must have an energy higher than the valence band states. The reason is that, if there are occupied valence states at higher energy than the $4f^N$ ground state, an electron from the ligand ions, whose valence states primarily contribute to the valence band, can relax into the "hole" on the ionized rare earth, returning the rare earth to its original valence and filling the spectral hole. In addition, it is important to know the energy of the $4f^{N-1}5d$ states relative to the conduction band to determine which levels are degenerate with conduction band states and what corresponding gating wavelength is required to produce ionization. Among other materials, we have applied this approach to rare-earth-doped $YAlO_3$, where the energies of the rare earth

$4f^N$ and $4f^{N-1}5d$ states relative to the host band states were determined and discussed within the context of photon-gated photoionization hole burning. By extending these methods to additional materials, candidate photoionization hole burning materials may be identified and analyzed.

We employed both conventional electron photoemission and resonant photoemission to measure the relative energies of the $4f^N$ and host valence band states in optical materials. Photoemission allows the energies of occupied electronic states to be independently measured relative to an absolute energy reference and complements optical methods, which measure energy differences between electronic states in the material. By determining the energies of electronic states using photoemission, features that appear, or do not appear, in the optical spectra may be unambiguously interpreted in terms of energy differences and transition probabilities—two properties that are difficult to deconvolve from the optical spectra alone. Furthermore, resonant photoemission spectroscopy allows the rare earth 4f electron photoemission to be clearly identified and separated from the host spectrum by using synchrotron radiation to probe resonances in the rare earth photoemission cross-section. Because the precise energy of the photoemission resonance is an atomic property that is unique to each ion and valence state, resonant photoemission may be used to separate and identify each rare earth ion and rare earth valence state present within a material. By observing the systematic changes in the relative energies for different states, ions, and host materials, insight is gained into electron transfer, luminescence quenching, and ion valence stability.

We have shown that a simple two-parameter empirical model accurately describes the binding energies of the $4f^N$ states for all rare earth ions in materials ranging from ionic insulators to covalent metals. Since the model only requires two parameters to describe the effect of the host material, measurements on just two ions in a material can be used to predict the energies of all other rare earth ions in that material. In some materials, measurements on a single ion and the host material itself are sufficient to determine the energies of the remaining ions. This empirical approach provides an important tool for practical material development and may provide fundamental information about the material when viewed within the theoretical frameworks that describe the effect of the material on the rare earth binding energies.

The practical utility of an empirical model stimulated our recent work in applying a simple two-parameter model to the description, analysis, and extrapolation of binding energies. The form of this empirical model was motivated by the extensive work that has been done over the last century using an electrostatic point-charge model for the effect of the lattice on the electron binding energies. In this picture, the binding energies of an ion's electrons are viewed as being the free-ion values shifted through interactions with the lattice. These effects include the Madelung potential of the lattice site, the polarizability of the material, inter-atomic repulsive energies, and smaller effects such as Van der Waal's energies. A further complication in optical materials is that the active ion is commonly an impurity rather than a normal lattice constituent; thus, the local distortion of the lattice induced by the presence of the impurity can cause a significant change in the site's Madelung potential that results in a corresponding shift in the binding energies. This picture leads to an empirical model of the form $E_{4f} = I - E_L + \alpha_R(R-R_0)$, where E_{4f} is the 4f electron binding energy relative to a free electron in vacuum, I is the free-ion ionization potential, E_L is a binding energy shift experienced by all rare earth ions in a material, and $\alpha_R(R-R_0)$ represents an ion dependent shift in binding energy when the substituted rare

earth's ionic radius R deviates from the normal host ion's radius R_0. These definitions are chosen so that E_L represents a parameter that may be directly measured from the host lattice itself, since it is just the binding energy shift experienced by the normal lattice constituent. If we wish to reference the binding energies relative to another energy such as the valence band maximum, an additional term may be explicitly included in the model to subtract off the reference energy, or the reference energy may be included implicitly in the definition of E_L. For ionic materials where the electrostatic point-charge model is most appropriate, the parameters in this model may be directly estimated using the theoretical model of Pedrini et. al. if sufficient information is available for both the lattice and the effect of the impurity-induced distortion. In covalent materials such as the metals, chemical considerations have also led to a model for the binding energies in which the free-ion values are shifted because of the redistribution of charge and electrostatic shielding that occurs in the solid. In this picture, it is the variation in the effective nuclear charge experienced by the valence electrons that produces an ion-dependent binding energy shift in the material. Within this framework, the ionic radius that enters into the empirical model may be viewed as an estimate for the effective nuclear charge experienced by the valence electrons of the rare earth ion; hence, the model is also successful for describing covalent materials.

Although the empirical model can be shown to be an approximate expression for the binding energy in ionic and covalent materials, the extremely simple form of the model lends itself to an even more basic perspective. Specifically, we may view the empirical model as just the first two terms of a Taylor's series expansion for *any* effect of the lattice on the binding energy, where the expansion variable is the ionic radius of the ion—a physical parameter that directly influences the ion's environment. This simple interpretation may provide some insight into why the model applies to such a wide range of materials and cautions against too stringent an interpretation of the empirical parameters within a specific theoretical framework.

Another implication of this view is that perhaps another variable may be chosen when performing the expansion. To explore this possibility, we may consider a model of the form $E_{4f} = I - E_L + \alpha_A(A - A_0)$, where E_{4f}, I, and E_L have the same meaning as previously, and $\alpha_A(A - A_0)$ represents an ion dependent shift in binding energy that simply depends on the ion's atomic number A. In this model, a value of $A_0 = 67$ is chosen so that E_L has approximately the same value and interpretation as in previous work that used trivalent yttrium as the ionic radius reference. The choice of atomic number as the variable to describe the ion-dependence is motivated by the simplicity and generality of the expression as well as indications that it may represent an appropriate description for more covalent materials. Because the ionic radius is nearly linear as a function of atomic number, this form of the model gives nearly identical predictions for the 4f electron binding energies, with deviations smaller than the experimental accuracies currently achievable by any experimental method. As an example, in Fig. 25 the two models are compared to the measured 4f electron binding energies in the elemental rare earth metals from Lang et. al. The rare earth metals represent the most accurately known set of 4f binding energies available since the experimental features are much sharper in the metals than in other materials. Furthermore, the magnitude of the ion dependent term is nearly 2.5 times larger in the metals than in the other materials that have been studied; therefore, the metals represent an extreme case in which the differences between the two forms of the model are maximized. In Fig. 25, the circles are experimental binding energies (relative to the Fermi energy), the solid line

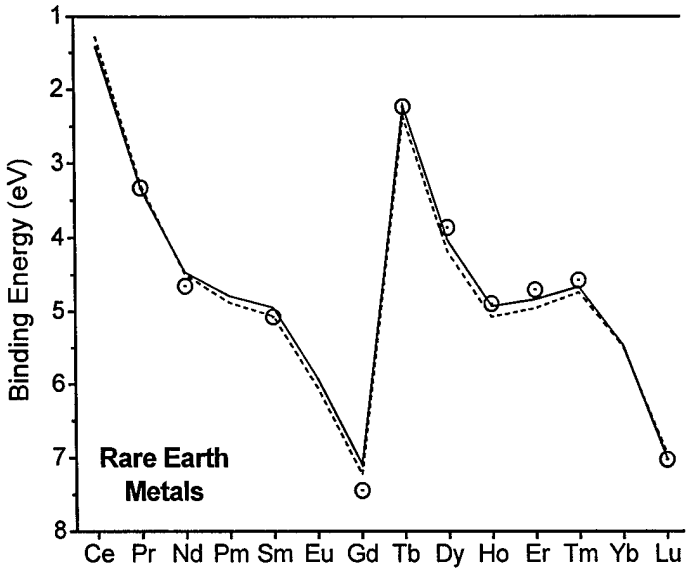

FIG 25. Comparison of empirical 4f electron binding energy models. Circles represent measured 4f electron binding energies relative to the Fermi energy in the elemental rare-earth metals. The dotted line is the fit of the empirical model using the ions' atomic numbers. The solid line is the fit of the empirical model using the ions' radii.

is the fit of the model using the ionic radius, and the dotted line is the fit of the model using the atomic number. Comparison of the two fits indicates that both expressions describe the binding energies equally well to within the experimental accuracy, with an approximate relationship between the parameters of $\alpha_A \approx -0.013\alpha_R$— a correspondence that also approximately holds for the other materials that we have studied. The agreement between the two forms of the model is expected to be even closer for the majority of optical materials, implying that either form may be used interchangeably as an empirical expression for the 4f electron binding energies.

The two forms of the empirical model each present different advantages and disadvantages. The use of ionic radius in the model has a clearer physical interpretation and may be directly related to theoretical models in ionic materials. However, ambiguity may arise because the ionic radius depends on both the environment of the ion and the degree of covalency in the bonding. Using the atomic number in the model provides a simple approach in which there is no ambiguity. However, this approach is more difficult to directly relate to theoretical models. Another advantage of the atomic number approach is that it allows a straightforward comparison of the parameters obtained from different materials regardless of the nature of the environment or the bonding. This might permit material trends to be more easily identified and analyzed. Thus, the choice of a particular form of the empirical model primarily depends on the intended application.

In both the empirical and theoretical models for the rare earth electron binding energies, the free-ion ionization potentials play an important role. Unfortunately, many of the existing ionization potential values have relatively large uncertainties that directly affect the accuracy of models that incorporate them. We suggested that improved estimates for the free-ion ionization potentials might be obtained by comparing experimental electron energies in solids to the empirical model for the binding energies. With the goal of improving the accuracy of the empirical model, we have analyzed the systematic deviations between experimental energies and the empirical model to obtain a set of "effective" free-ion ionization potentials as listed in Table II. These values were obtained by analyzing the available experimental energies of rare earth ions in the garnets, the rare earth metals, the rare earth fluorides, La_2S_3, and $YAlO_3$. Deviations between the

measured binding energies and the fit of the model were simply viewed as arising from a combination of the experimental error of each measurement and the error in the model due to uncertainties in the free-ion ionization potentials. Thus, by choosing ionization potentials that give perfect agreement between the model and the experimental data points, a set of new estimates for the free-ion ionization potentials are obtained from each material that have an uncertainty approximately equal to the experimental error. The estimated ionization potentials from each material were then averaged together with the experimental values for the free ions to obtain the best final estimates, where each experimental value was weighted by its uncertainty in the averaging process using the standard statistical method. The effective ionization potentials obtained from this procedure are presented in Table II, along with the corresponding uncertainty in each value.

Rare Earth Ion	*Effective Ionization Potential (eV)*	*Estimated Error (eV)*
Ce^{3+}	36.757	±0.005
Pr^{3+}	38.98	±0.02
Nd^{3+}	40.52	±0.14
Pm^{3+}	41.0	±0.6
Sm^{3+}	41.51	±0.14
Eu^{3+}	42.94	±0.29
Gd^{3+}	44.40	±0.12
Tb^{3+}	39.37	±0.07
Dy^{3+}	41.35	±0.12
Ho^{3+}	42.47	±0.12
Er^{3+}	42.56	±0.12
Tm^{3+}	42.52	±0.12
Yb^{3+}	43.53	±0.09
Lu^{3+}	45.25	±0.03

Table II. Effective free-ion ionization potentials for the trivalent rare earth ions determined from the systematic deviations between the experimental 4f electron binding energies in optical materials and the empirical model for the binding energies. The errors were determined from the experimental errors of the measurements that contributed to each estimate.

To demonstrate the impact of these effective ionization potential parameters on the $4f^N$ binding energy model, the fit of the empirical model using these new values is shown for yttrium aluminum garnet in Fig. 26. The circles represent experimental binding energies, the dotted line is the fit of the model using the free-ion ionization potentials, and the solid line is the fit using the effective ionization potentials from Table II. Only the values for europium and gadolinium are significantly different (the free-ion values for those two ions had large uncertainties), with the remaining ions only experiencing modest shifts. However, the estimated uncertainties were improved for nearly all of the ions—an important result for the empirical model since the errors

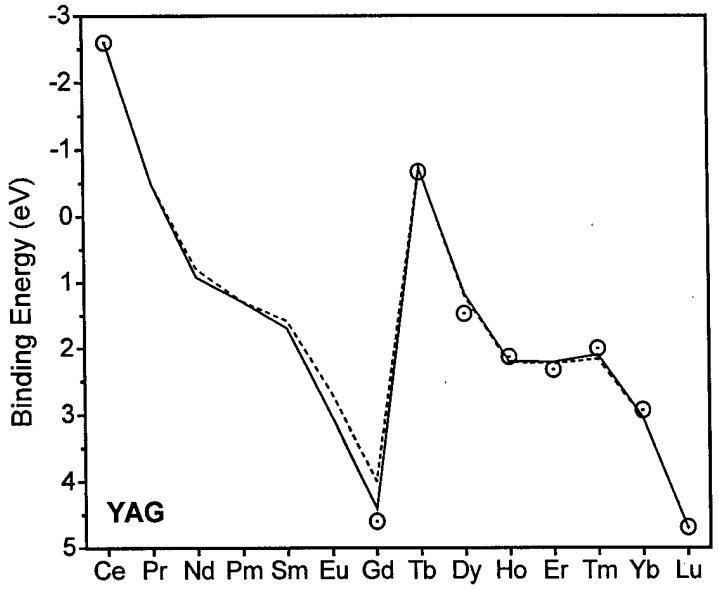

FIG. 26. Comparison of the empirical model using the free-ion ionization potentials and using the effective ionization potential values from Table 1. Circles represent average experimental 4f electron binding energies relative to the valence band maximum in yttrium aluminum garnet. The dotted line is the fit of the binding energy model using the free-ion ionization potentials. The solid line is the fit of the binding energy model using our empirical values for the ionization potentials given in Table II.

must be incorporated as weighting factors in the fitting process. By comparing the two curves to the experimental data, we can clearly see that the large deviation previously observed for the gadolinium binding energy was primarily due to the error in the free-ion ionization potential used in the model. For rare earths whose measured free-ion ionization potentials are relatively uncertain, such as gadolinium, these effective values may represent improved estimates for the free-ion values. However, care must be taken when interpreting the precise meaning of these effective ionization potentials since, in addition to representing corrections to values for the free ions, they may also include corrections for any systematic deviations inherent in the empirical model itself. In any case, these values represent a significant improvement in the accuracy of the empirical model, with future work on additional materials promising to provide even greater improvements.

The $4f^{N-1}5d$ states of the rare earth ions are important for many applications, some of which were outlined above. To obtain fundamental information about each material and evaluate its suitability for particular applications, we wish to determine the energies of the $4f^{N-1}5d$ states relative to the host band states. These relative energies may be determined by combining the measured or predicted binding energies of the $4f^N$ states relative to the host bands and the measured energy differences between the $4f^N$ and $4f^{N-1}5d$ states. The barycenters of the $4f^N$ to $4f^{N-1}5d$ transition energies, which exhibit large variations from material to material, may be determined from the absorption spectra of each rare earth ion in the host material. As an example of this procedure, the binding energies of the lowest $4f^{N-1}5d$ states in yttrium aluminum garnet were determined, as shown in Fig. 27 by the triangles. The circles represent the average of the measured $4f^N$ binding energies from the literature, and the solid line is the fit of the empirical model using the effective ionization potentials from Table II. These $4f^N$ energies were combined with the $4f^N$ to $4f^{N-1}5d$ transition energies to obtain the $4f^{N-1}5d$ binding energies. These binding energies may be interpreted as the energy required to remove the 5d electron from

the $4f^{N-1}5d$ configuration, leaving the tetravalent ion with a $4f^{N-1}$ configuration in the lowest energy state.

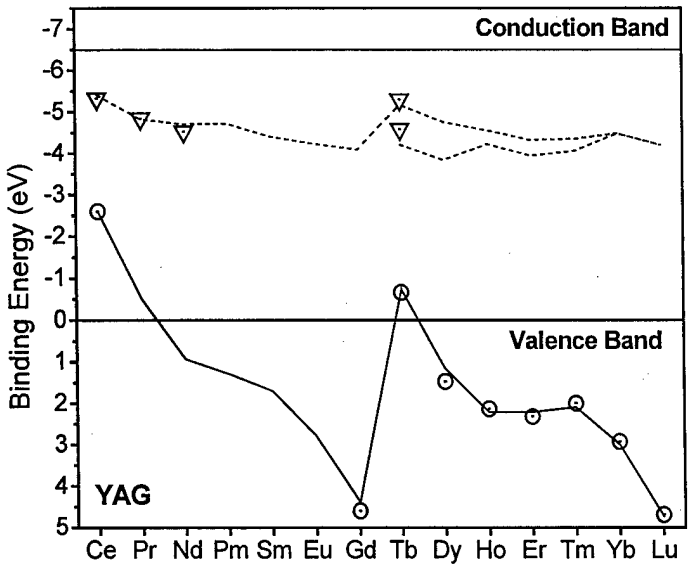

FIG. 27. The $4f^N$ and $4f^{N-1}5d$ binding energies in rare-earth-activated yttrium aluminum garnet (YAG) relative to the host valence band. Circles represent average measured $4f^N$ binding energies and the solid line is the fit of the $4f^N$ binding energy model using the effective ionization potentials from Table II. Triangles represent $4f^{N-1}5d$ binding energies determined from the $4f^N$ binding energy model and measured $4f^N$ to $4f^{N-1}5d$ transition energies. The dotted lines represent the model for the $4f^{N-1}5d$ binding energies; the upper line corresponds to the lowest energy high-spin state and the lower line corresponds to the lowest energy low-spin state.

By incorporating existing empirical models for the $4f^N$ to $4f^{N-1}5d$ transition energies into the $4f^N$ binding energy model, we may obtain an empirical model that describes both the $4f^N$ and $4f^{N-1}5d$ binding energies of all rare earth ions in a host material. Several models for the $4f^N$ to $4f^{N-1}5d$ transition energies have been applied to the study of optical materials over the last four decades. Recently, Dorenbos has compiled experimental measurements for hundreds of materials, and by comparing these experimental values with the theoretical models for the transition energies, has developed a simple empirical model in which only a single material dependent energy shift is required to determine the lowest $4f^N$ to $4f^{N-1}5d$ transition for all rare earth ions. Thus, by combining the empirical model for the $4f^N$ to $4f^{N-1}5d$ transition energies with the model for the $4f^N$ binding energies, a simple model is obtained that describes both the $4f^N$ and $4f^{N-1}5d$ binding energies in a material using only three empirical parameters. This is shown in Fig. 27 for yttrium aluminum garnet by the dotted lines. For the second half-series, the lower and upper dotted lines represent the barycenters of the lowest energy high-spin and low-spin $4f^{N-1}5d$ levels, respectively.

It is important to note that, in contrast to the $4f^N$ energies, the $4f^{N-1}5d$ binding energies have similar values for all of the rare earth ions. This similarity is expected since the large variation in $4f^N$ to $4f^{N-1}5d$ transition energy arises primarily from the strong electron correlation in the $4f^N$ configuration, with the energy of the 5d valence state only weakly influenced by the nature of the tetravalent $4f^{N-1}$ core. However, we do observe variation of as much as 1 eV across the rare earth series, indicating that the 5d levels cannot be taken to have exactly the same absolute binding energies.

The success of this model implies that, once the $4f^N$ energies are known, a single binding energy measurement of a rare earth ion's lowest $4f^{N-1}5d$ state in a material is sufficient to predict the energy of the lowest $4f^{N-1}5d$ states for all the remaining ions. This picture provides important insight into the behavior of the $4f^{N-1}5d$ luminescence in optical materials and is a powerful tool for the development of new optical materials, with particular significance in the search for photon-gated spectral hole burning materials.

One of the primary goals of our work is to search for material dependent trends in the relative energies of the rare earth $4f^N$ states and the host band states. Although this work is in its early stages, several important trends have been identified in the materials so far studied.

Recently, a series of rare earth garnets have been studied for concentrations ranging from a few percent to the stoichiometric compounds. In these materials, it was found that the host valence band and the 4f electron binding energies were not affected by the rare earth ion concentration, maintaining the same values across the entire range of concentrations to within the experimental accuracy. In addition, measurements on the aluminum, gallium, and iron garnets indicated that the 4f electron energies maintained the same absolute binding energies, while the valence band was shifted to reduced binding energies going from aluminum to gallium to iron. Thus, in these materials, the systematic shifts between the $4f^N$ energies and the host bands arise entirely from shifts of the host bands. We might also expect similar composition dependent trends to be observed in related ternary compounds such as $YAlO_3$.

When examining a wider range of materials, simple trends may be observed in the empirical parameters that describe the $4f^N$ binding energies. For example, when comparing chemically similar materials such as $Y_3Al_5O_{12}$ and $YAlO_3$, we have observed that the variations in the binding energies of the $4f^N$ electron energies between the materials arise almost entirely from the ion-dependent term in the model (α_R or α_A), with the same binding energy shift parameter (E_L) observed. However, when comparing results from chemically different materials, such as the oxides and fluorides, both parameters in the model can vary significantly. By identifying simple trends such as these, insight is gained into the behavior of the $4f^N$ energies in different materials. This insight can be extremely important for understanding the optical properties of rare earth materials and for guiding the development of materials for applications such as hole burning, quantum information, and phosphors.

Two examples provide additional examples of specific development of gated hole burning materials exploiting the perspectives gained from the ion level relationships to the band structure.

Development of Photon Gated Hole Burning in Oxide Materials including $YAlO_3$
Y. Sun, C. W. Thiel, R. L. Cone, R. W. Equall, and R. L. Hutcheson, J. Lumin. **98**, 281-287 (2002).

Recently, using photoemission spectroscopy and synchrotron radiation, we have measured the $4f^N$ ground state energies relative to the host valence band for several rare earth doped garnets, including YAG. This work has led to the development of empirical models for describing the relative energies of the $4f^N$ and $4f^{N-1}5d^1$ states of the rare earth ions in rare earth activated

materials. The application of this information to the development of photon-gated hole burning materials, with new results for rare earth doped $YAlO_3$, is given as an example.

Many proposed technological applications of persistent spectral hole burning are enabled by the spectral multiplexing capability of the materials, measured by the large Γ_{inh}/Γ_h ratios that may be achieved for the $4f^N$ to $4f^N$ transitions of the trivalent rare earth ions doped into inorganic insulators. In addition to the need for excellent coherence properties, many applications benefit from a mechanism for probing the population distribution of the optical transition without perturbing the population through further hole burning. Photon-gated hole burning provides a mechanism for non-destructive readout by employing a process that requires two photons of different frequencies. One such process is two-step photoionization hole burning: the first photon generates a population distribution in the $4f^N$ to $4f^N$ optical transition and the second photon photoionizes the population in the excited state, permanently removing them from the absorption. Thus, when the second photon is present, information may be "written" into the rare earth ions' population; when the second photon is not present, the information may be read back without the partial erasure associated with non-gated hole burning mechanisms.

Direct photoionization of highly localized $4f^N$ states is generally a very weak process for trivalent rare earth ions. The limited spatial overlap between the host conduction band states and the localized rare earth states implies the need for a spatially extended intermediate state, such as $4f^{N-1}5d^1$ to provide efficient ionization. Efficient excitation of rare earth ions into the $4f^{N-1}5d^1$ state is made possible by (a) the large cross-section of the parity-allowed transition from the upper $4f^N$ state that is involved in the hole burning to the $4f^{N-1}5d^1$ state and the (b) the long $4f^N$ lifetimes. For ionization to occur, the excited $4f^{N-1}5d^1$ state must have an absolute energy above the host conduction band; then the 5d electron may relax into a conduction band state and move to a trap. If deep electron trap states are present in the lattice, the mobile electrons in the conduction band may become trapped away from the ionized rare earth ion, providing a mechanism for permanent gated hole burning.

To determine the second-step photon energy needed to photoionize the rare earth ion, the energy of the rare earth ion's states relative to the host band states must be measured. Our measurements of the energy of the $4f^N$ ground states relative to the host crystal's valence band by resonant and conventional electron photoemission spectroscopy, combined with the host band gap and $4f^{N-1}5d^1$ transition energies from ultraviolet spectroscopy experiments have been used to locate the energies of the $4f^{N-1}5d^1$ states relative to the host conduction band.

It is well known that the crystal $YAlO_3$ forms both stable and transient color centers under ultraviolet irradiation, indicating the presence of deep trap states in the lattice. The abundance of electron trap states and the excellent optical properties of rare earth doped $YAlO_3$ suggested that it would be a good candidate for photoionization hole burning. With this motivation, the rare earth energy levels were located relative to the host band states for rare earth doped $YAlO_3$, as shown in Fig. 28. Resonant photoemission spectroscopy was used to measure the $4f^N$ energy of Tb^{3+} relative to the valence band and to determine the absolute energy of the valence band maximum in $YAlO_3$. This work was carried out on the Iowa State/Montana State ERG/Seya beam line at the University of Wisconsin-Madison Synchrotron Radiation Center. The $4f^N$ energies of Ce^{3+} and Lu^{3+} were determined by applying the techniques developed by us to

analyze x-ray photoemission spectra. Using the empirical model for the $4f^N$ binding energies, these measured energies (circles in Fig. 28) allow the $4f^N$ energies of the remaining rare earth ions to be accurately predicted, as shown by the solid line in Fig. 28. These results predict that, among the trivalent rare earth ions, only Ce^{3+} and Tb^{3+} have $4f^N$ ground state energies above the host valence band. This has important implications for choosing an active ion for photon-gated hole burning. Ions with their $4f^N$ ground state energy degenerate with valence band states are unlikely to form stable tetravalent ions after photoionization since higher energy valence band electrons would rapidly relax into the lower energy $4f^N$ state, returning the ion to a trivalent state and making them poor candidates for efficient photoionization hole burning materials. Thus, since the $4f^N$ to $4f^N$ transitions of Ce^{3+} are not easily accessible, Tb^{3+} represents the best candidate for photon-gated hole burning in $YAlO_3$.

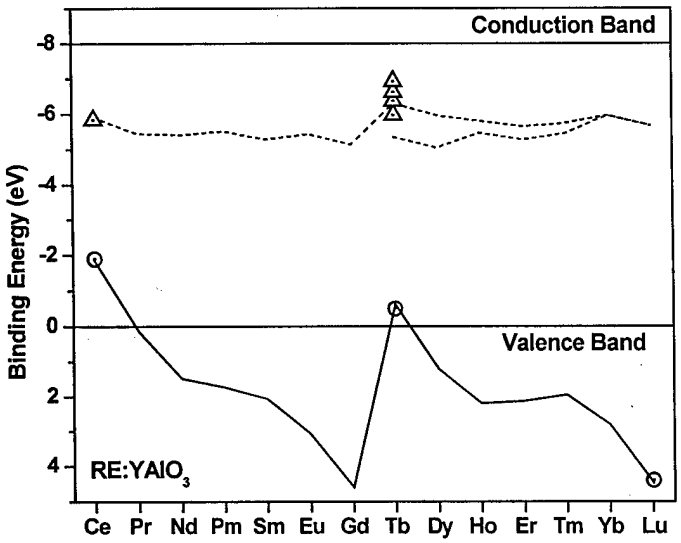

FIG. 28. Systematic behavior of 4f and 5d electron binding energies relative to host bands for trivalent rare-earth ions in $YAlO_3$. Circles represent measured 4f binding energies of the $4f^N$ ground states and triangles represent measured 5d binding energies for the lowest energy $4f^{N-1}5d^1$ states. The solid line is the model for the 4f binding energies and the dotted line is the model for the 5d binding energies. For the second half-series, the lower and upper dotted lines represent the barycenters of the lowest energy high-spin and low-spin $4f^{N-1}5d^1$ levels, respectively.

The energies of the $4f^7 5d^1$ states were determined from the ultraviolet absorption of Tb^{3+}:$YAlO_3$ for energies up to 57000 cm^{-1}. Four $4f^8$ to $4f^7 5d^1$ transitions were observed within this range: the lowest energy transition observed was a weak spin-forbidden transition at 42930 cm^{-1} (a high-spin $4f^7 5d^1$ state), while intense spin-allowed transitions were observed at 46060 cm^{-1}, 48060 cm^{-1}, and 50500 cm^{-1} (low-spin $4f^7 5d^1$ states). These energies are indicated in Fig. 28 by the triangles. The lowest energy $5d^1$ state of Ce^{3+} is also indicated in Fig. 28. In addition, estimates for the lowest $4f^{N-1}5d^1$ states of the remaining ions are indicated by the dotted lines in Fig. 28, where the lower and upper dotted lines for the second half series indicate the energies of the high-spin and low-spin $4f^{N-1}5d^1$ states, respectively. These estimates were obtained by combining our model for the $4f^N$ ground state binding energies with the model and parameters of Dorenbos for estimating the lowest $4f^{N-1}5d^1$ transitions in a material. These energies represent the relative energies required to remove the 5d electron from the $4f^{N-1}5d^1$ states of the trivalent rare earth ions in $YAlO_3$. These energies show only a weak variation of less than 1 eV across the rare earth series, indicating that the absolute energies of the 5d electrons are nearly constant for the lowest $4f^{N-1}5d^1$ states of the trivalent ions in $YAlO_3$.

To locate these states relative to the host conduction band, the host band gap energy is required. The fundamental band gap of $YAlO_3$ is estimated to be 8.0 eV from optical absorption and reflectivity measurements. This gives an estimate of 7.5 eV for the direct photoionization threshold of Tb^{3+}, with all of the observed $4f^75d^1$ states lying significantly below the bottom of the host conduction band. Thus, if the blue $^7F_6$ to $^5D_4$ transition at 20562 cm^{-1} in $YAlO_3$ was used as the hole burning transition, a second 4.9 eV gating photon would be required to directly photoionize the excited Tb^{3+} ion. Since no $4f^75d^1$ level was observed at this energy, an even greater energy would be required to excite to an upper lying $4f^75d^1$ state within the conduction band. These results suggest that $YAlO_3$ would present an inconvenient choice for a photon-gated hole burning material.

By the application of these methods to new materials, candidates for photoionization-gated hole burning in inorganic materials are identified and analyzed. Precise knowledge of the energy level structure, including the host band states, provides detailed insight into candidate materials and into the photoionization process, enabling a material's performance, or lack of performance, to be quantitatively characterized. Insight from each material can be used to understand the performance of current photon-gated hole burning materials as well as to logically and intelligently inspire development of new materials. This information is also relevant to the design of phosphors and scintillators where the technological impacts are significant.

Development of Tb^{3+} Gated Spectral Hole Burning Materials

Additional work has been carried out on a varied group of Tb^{3+}-doped oxide materials listed in Table III at the bottom of this page. Work on fluoride hosts is described on the next pages.

Crystal	$^7F_6(4f^8)$ to $^5D_4(4f^8)$	$^7F_6(4f^8)$ to $^9E(4f^75d)$ or $T_2(4f^75d)$	$^7F_6(4f^8)$ to $^7E(4f^75d)$ or $^7T_2(4f^75d)$
Tb^{3+}:$LiYF_4$	20553 cm^{-1}	38824 cm^{-1}	46860 cm^{-1}
Tb^{3+}:$LuPO_4$	~20500 cm^{-1}	37082 cm^{-1}	44376 cm^{-1}
Tb^{3+}:$ScPO_4$	~20500 cm^{-1}	36454 cm^{-1}	43536 cm^{-1}
Tb^{3+}:YPO_4	~20500 cm^{-1}	37273 cm^{-1}	44552 cm^{-1}
Tb^{3+}:YAG	20515 cm^{-1}	30236 cm^{-1}	35496 cm^{-1}
Tb^{3+}:Y_2SiO_5	20586 cm^{-1}	~38400 cm^{-1}	40750 cm^{-1}
Tb^{3+}:$Y_2Si_2O_7$	20657 cm^{-1}	34782 cm^{-1}	~41600 cm^{-1}
Tb^{3+}:$YAlO_3$	20562 cm^{-1}	42404 cm^{-1}	~45400 cm^{-1}

Table III. Summary of material parameters for candidate Tb^{3+}-doped oxide crystals. The second column indicates the hole burning transition energy and the third and fourth columns indicate possible gating energies involving parity-allowed interconfiguration transitions of the Tb^{3+} ions.

Study of Gated Spectral Hole Burning and Energy Level Structure of Tb^{3+}:$LiYF_4$
C. W. Thiel, Y. Sun, R. W. Equall, and R. L. Cone, J. Lumin. **107**, 236-244 (2004).

To investigate the potential for photon-gated hole burning through two-step photoionization in Tb^{3+}:$LiYF_4$, energies of the $4f^8$ and $4f^75d$ levels relative to the host band states were determined. From x-ray photoemission spectroscopy, the $4f^8$ ground-state binding energy was found to be in the band gap at 2.9 eV above the valence band maximum. The effects of electron-lattice coupling on ionization processes were considered, and it was determined that the level at 54950 cm^{-1} is the lowest $4f^75d$ state that will produce ionization. Those results were extended to other rare-earth ions in $LiYF_4$. High-resolution spectral hole burning on the $^7F_6$ to $^5D_4$ transition displayed hole/anti-hole structure attributed to population redistribution among the Tb^{3+} hyperfine levels with additional sidebands due to ^7Li and ^{19}F nuclear spin flips.

In the search for material systems that access new parameter spaces and extend the capabilities of spectral hole burning device applications, crystals doped with Tb^{3+} provide several interesting properties. Those systems received little attention in the past due to the need for blue dye lasers to access the $^7F_6$ to $^5D_4$ transition; however, rapidly expanding capabilities of semiconductor lasers in this spectral region led us to explore Tb^{3+}. In addition to the demonstrated capability for efficient and long-lived spectral hole burning through population redistribution among the nuclear hyperfine levels, the existence of stable tetravalent Tb^{4+} states and the relatively low energies of the $4f^75d$ levels suggest that Tb^{3+} materials are good candidates for photon-gated photoionization.

As an initial step in exploring the capabilities for photoionization hole burning of Tb^{3+}, we determined the location of the $4f^8$ and $4f^75d$ levels relative to the host band states in $LiYF_4$ using a combination of x-ray photoemission spectroscopy and ultraviolet absorption spectroscopy. These results also provide insight into the energies of other rare-earth ions relative to the band states in $LiYF_4$ and are important for understanding luminescence quenching and excited-state absorption due to ionization in these materials. We examined hyperfine population hole burning in this material to elucidate the hyperfine structure and investigate the structure and spectral diffusion broadening of the spectral holes.

The energy levels, magnetic properties, and coherence properties of the $^7F_6$ to $^5D_4$ transition of Tb^{3+}:$LiYF_4$ have been extensively studied and are well understood. Using photon echo spectroscopy, the effects of instantaneous spectral diffusion, applied magnetic fields, and nuclear modulation have all been characterized, indicating a fundamental homogeneous linewidth as narrow as 28 kHz at temperatures of 1.3 K with an applied magnetic field of 4.2 T. The hyperfine spectral hole-burning dynamics have also been studied, showing that the hole-burning quantum efficiency is 2% with hole lifetimes as long as 10 minutes for fields of 4.6 T. In the earlier studies, hole/anti-hole structure and hole widths were obscured by the limited spectral resolution of the pulsed dye laser system used there. Consequently, we have re-examined the hyperfine hole burning with higher resolution to determine hole widths and structure.

For the spectral hole-burning experiments reported here, a 1% Tb^{3+}:$LiYF_4$ crystal was immersed in liquid helium at 1.6 K in an Oxford Instruments SpectroMag cryostat that provided magnetic field strengths up to B = 8 T. Both the magnetic field and light polarization were aligned along

the crystal c-axis. A frequency-doubled external cavity diode laser with a linewidth of ~1 MHz and a power of ~10 mW at the crystal was used to burn a spectral hole in the lowest energy $^7F_6$ to $^5D_4$ transition. The hole was then probed by scanning the laser across the absorption line with the intensity attenuated by a neutral density filter with OD = 3. The intensities of the laser and the transmitted light were detected simultaneously during the scan using PIN photodiodes to determine the absorption, and transmission through an interferometer with a free spectral range of 112.5 MHz was used to monitor the laser frequency.

The typical hole-burning spectrum shown in Fig. 29 (a) for a magnetic field of 1.66 T demonstrates the complex side-hole and anti-hole structure caused by redistribution of population among the hyperfine levels. The ^{159}Tb nuclear spin I = 3/2 results in four hyperfine levels that, for this magnetic field strength, are equally spaced by 3.13 GHz in the ground state and 0.85 GHz in the excited state. From these splittings, the positions of all side-holes and anti-holes may be predicted, as shown in Fig. 29 (a). Comparing the predicted positions to the observed structure, we find that the overall agreement is quite good. However, small deviations are clearly observed, perhaps indicating the influence of quadrupole interactions in the ground state or weak perturbations of the hyperfine interaction in the excited state.

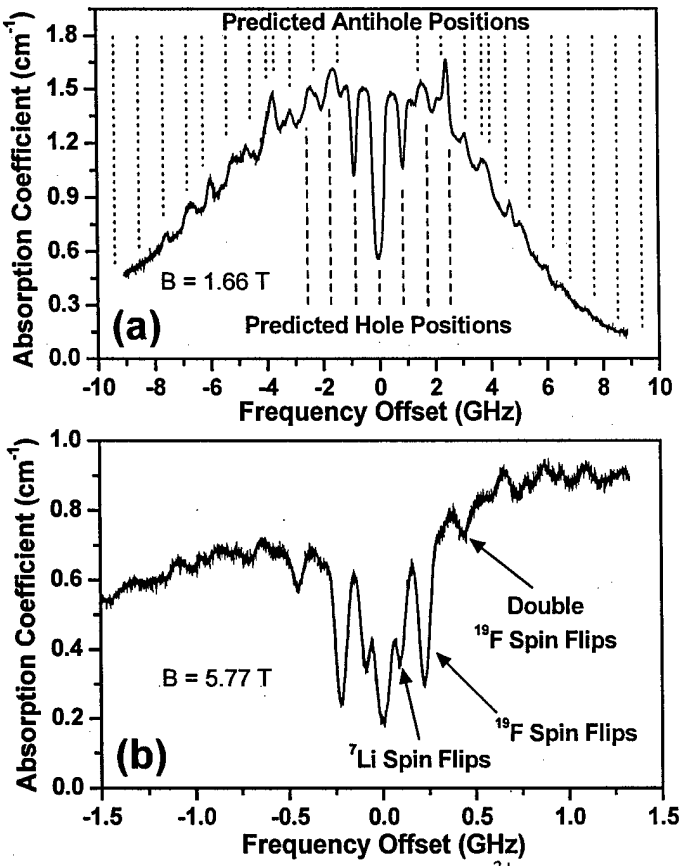

FIG. 29. Spectral hole burning in 1% Tb^{3+}:$LiYF_4$ at T = 1.6 K with E||c and B||c. a) Absorption spectrum after a hole has been burned at 20558.423 cm^{-1} with B = 1.66 T. Positions of holes and anti-holes predicted from the ground and excited state hyperfine splittings are indicted by dashed and dotted lines, respectively. b) Spectral hole burned at 20567.334 cm^{-1} for B = 5.77 T, with side-holes due to optically induced ^{7}Li and ^{19}F nuclear spin flips indicated on the plot.

As the magnetic field is increased, the spectral holes and anti-holes both develop additional structure due to the strong coupling to nuclear spins of neighboring ions, as shown in Fig. 29 (b) for 5.77 T. These nuclear spin-flip sidebands result from absorption transitions in which a nuclear spin flip of a neighboring ion is induced simultaneously with the electronic excitation. This mechanism allows electronic transitions to be excited by frequencies offset from resonance by the frequency splittings of neighboring nuclear spin states. In the time-domain,

this produces a strong echo envelope modulation of the photon echo decay that has been experimentally characterized and theoretically described for Tb^{3+}:$LiYF_4$. Spin-flip sidebands have also been observed in the spectral hole-burning and fluorescence line-narrowing spectra of Er^{3+}:$LiYF_4$. The sidebands in Tb^{3+}:$LiYF_4$ are much stronger than those observed in Er^{3+}:$LiYF_4$, indicating that Tb^{3+} couples more strongly than Er^{3+} to the neighboring spins.

By measuring the positions of the spin-flip sidebands as a function of the external field strength, we may determine the corresponding gyromagnetic ratios to identify the source of individual features. At these fields, the separations of the three pairs of side holes from the main hole are 17 MHz/T, 39 MHz/T, and 78 MHz/T, allowing us to assign the first two features to ^{7}Li and ^{19}F spin flips. The third feature exhibits a splitting that is exactly twice the ^{19}F splitting at all fields, indicating that it corresponds to transitions involving two simultaneous ^{19}F spin flips. Due to the chemical shifts produced by magnetic dipole-dipole and exchange interactions with the Tb^{3+} ion, the gyromagnetic ratios are noticeably different from the unperturbed values of 16.5 MHz/T and 40 MHz/T. In fact, studying these transitions with increased resolution using optically detected NMR will provide detailed structural information about the Tb^{3+} environment.

Analyzing the hole shapes in Fig. 29 (b), we find that the fundamental hole width is ~65 MHz, corresponding to an effective homogeneous linewidth of 33 MHz. This linewidth is much larger than both the homogeneous linewidth of 28 kHz measured from photon echo decays and the laser linewidth of ~1 MHz, indicating the presence of spectral diffusion over the timescale of the hole burning measurement. Although the large magnetic moment of Tb^{3+} results in a strong coupling between ions, this contribution to the spectral diffusion is rapidly frozen out for magnetic fields larger than ~0.5 T; consequently, the dominant source of spectral diffusion is nuclear spin flips of ^{19}F and ^{7}Li in the lattice. An estimate of the spectral diffusion broadening using the "method of moments" approach and approximating the crystal structure as a simple cubic arrangement of ^{19}F predicts a 24 MHz broadening for B||c due to magnetic dipole-dipole interactions with the ^{19}F nuclear spins. A similar calculation predicts an additional broadening of 6 MHz resulting from dipole-dipole interactions with the ^{7}Li nuclear spins. Thus, the calculated spectral diffusion due to ^{19}F and ^{7}Li nuclear spin flips is in excellent agreement with the observed linewidths.

For many applications, there is a strong motivation to develop photon-gated hole-burning materials so that the hole-burning process is only active when writing information into the inhomogeneous line, with no hole burning occurring during later readout or processing steps. One mechanism well suited to photon-gated hole burning is two-step photoionization of the rare-earth ion.

Because the $4f^N$ wavefunctions have very little spatial overlap with conduction band states, efficient ionization requires that the rare-earth ion be excited to a spatially extended $4f^{N-1}5d$ intermediate state that is degenerate with conduction band states. More restrictively, the $4f^N$ ground state must have an energy higher than that of the anion ligand states to prevent the tetravalent product from returning to a trivalent state by relaxation through electron transfer from the ligands. For an unperturbed site in a crystal lattice, this corresponds to the requirement that the $4f^N$ ground-state binding energy must be in the host band gap for the photoionization holes to be meta-stable.

To elucidate the photoionization process in rare-earth-activated $LiYF_4$, which has important consequences for lasers and phosphors as well as hole burning, we determined the energies of the Tb^{3+} $4f^8$ and $4f^7$5d states relative to the host bands in $LiYF_4$. In the following sections, results for the $4f^8$ and $4f^7$5d states and the effects of lattice relaxation on the photoionization dynamics are presented.

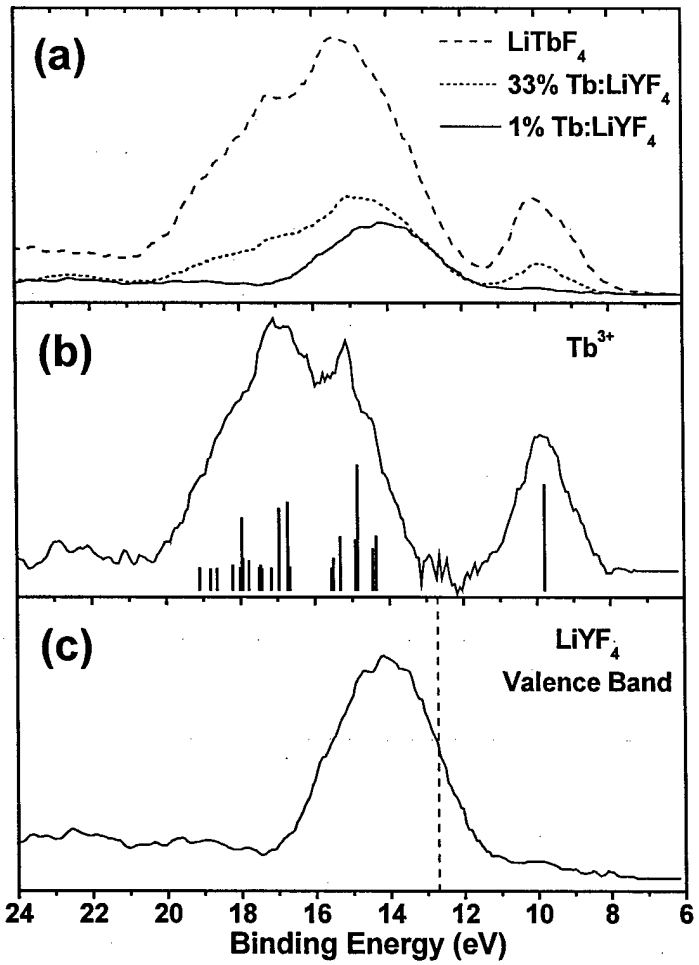

FIG. 30. a) X-ray photoemission spectra of $LiYF_4$ for three different Tb^{3+} concentrations. b) Extracted Tb^{3+} 4f electron spectrum, with underlying final-state structure represented by vertical bars. c) Extracted spectrum of the $LiYF_4$ valence band, with the position of the valence band maximum indicated by a dashed line.

To determine the relative binding energies of the Tb^{3+} 4f electrons and the valence band, x-ray photoemission spectra were measured for 1% Tb^{3+}:$LiYF_4$, 33% Tb^{3+}:$LiYF_4$, and stoichiometric $LiTbF_4$ grown by H. J. Guggenheim at AT&T Bell Laboratories. Photoemission spectra were obtained using a PHI Physical Electronics Model 5600ci ESCA measurement workstation in the Montana State University Imaging and Chemical Analysis Laboratory user facility. Photoemission was excited by Al Kα radiation (hν = 1486.6 eV) from a small spot-size source dispersed by a crystal monochromator. An electron flood gun was used to compensate positive sample charging and the sample was shielded by an electrically grounded mask to minimize the effects of stray electric fields. Electron binding energies were calibrated by placing the carbon 1s peak of adventitious hydrocarbon contaminants at a binding energy of 290 eV relative to the vacuum level.

Photoemission spectra of the three samples are plotted in Fig. 30 (a), where the increasing 4f electron contributions to the spectra are clearly observed as the concentration is increased. The Tb^{3+} 4f electron spectrum and the $LiYF_4$ valence band spectrum extracted by comparing the samples with 1% and 33% Tb^{3+} doping are shown in Fig. 30 (b) and Fig. 30 (c). The Tb^{3+} photoemission structure corresponds to the $4f^7$ final states of the ionized

system weighted by the photoemission transition probabilities to each possible final state. The underlying components of this final-state structure are represented by vertical bars, where the well-resolved component at lower binding energy corresponds to the minimum energy required to remove a 4f electron and leave the Tb^{4+} ion in the ^8S ground state. From the spectrum, we found that the 4f electron binding energy of Tb^{3+} is 9.8 eV.

By comparing the Tb^{3+} and valence band spectra in Fig. 30, it is clear that the Tb^{3+} $4f^8$ ground state lies above the valence band and is within the band gap of $LiYF_4$. To quantitatively determine the position of the valence band maximum from the measured spectrum, knowledge of the underlying density of states is required. Since band structure calculations are not available for $LiYF_4$, simple estimates must be made. The simplest approximation is to assume that the density of states and photoemission cross section are roughly uniform over some range of energies, with a sharp rise from zero at the valence band maximum. In fact, this type of density of states is a good approximation to the known density of states in LaF_3, a crystal that has many properties similar to $LiYF_4$. To fit the observed photoemission, the width of the uniform density of states was allowed to vary while the Gaussian broadening was restricted to values similar to those observed for other photoemission peaks in the spectrum. This approach described the shape of the observed valence band photoemission very well, further indicating that this simple density of states is a reasonable approximation. This procedure located the valence band maximum at ~12.7 eV, as shown in Fig. 30 (c) by the dashed line; however, the uncertainty in this value may be as large as several hundred meV because of the approximations involved. Combining this estimate for the valence band maximum with the Tb^{3+} 4f electron binding energy, we find that the Tb^{3+} ground state is in the band gap at ~2.9 eV above the valence band maximum.

To determine the position of the $4f^8$ levels relative to the conduction band, we must know the band-gap energy of the host crystal. For $LiYF_4$, the reflectivity measurements of Yang and DeLuca showed that the band gap is about 10.5 eV, a value very similar to those of LaF_3 and YF_3. More recent excitation measurements on $LiYF_4$ also support this value for the band gap. Thus, we estimate that the Tb^{3+} $4f^8$ ground state is 7.6 eV below the conduction band.

Once the energy of the $4f^8$ ground state relative to the host bands is established, measuring the $4f^8$–$4f^7$5d energy differences allows the energies of the $4f^7$5d states relative to the band states to be determined. The $4f^N$ to $4f^{N-1}$5d transition energies of rare-earth ions in $LiYF_4$ have been extensively studied and theoretically modeled, providing a clear picture of the $4f^7$5d energy level structure for Tb^{3+}:$LiYF_4$. However, because nearly all $4f^N$ to $4f^{N-1}$5d transitions occur in the vacuum ultraviolet, most studies have probed the absorption structure using excitation techniques. To investigate the magnitude of the $4f^8$ to $4f^7$5d absorption coefficients and oscillator strengths, we have measured the absorption spectrum of the lowest spin-forbidden ($^7F_6$ to ^9D) and spin-allowed transitions ($^7F_6$ to ^7D) for 1% Tb^{3+}:$LiYF_4$. To measure the ultraviolet absorption spectrum, the sample was held at 1.8 K in a Pope Scientific cryostat and light from a 30 W D_2 lamp was focused through the sample and collected by UV-grade quartz lenses. The transmitted light was dispersed using a McPherson 218 monochromator with 0.1 nm resolution and detected using an EMI 9558QB photomultiplier. To determine the absorption, the sample transmission was compared to the lamp spectrum recorded using the same optical arrangement but with the sample removed from the optical path.

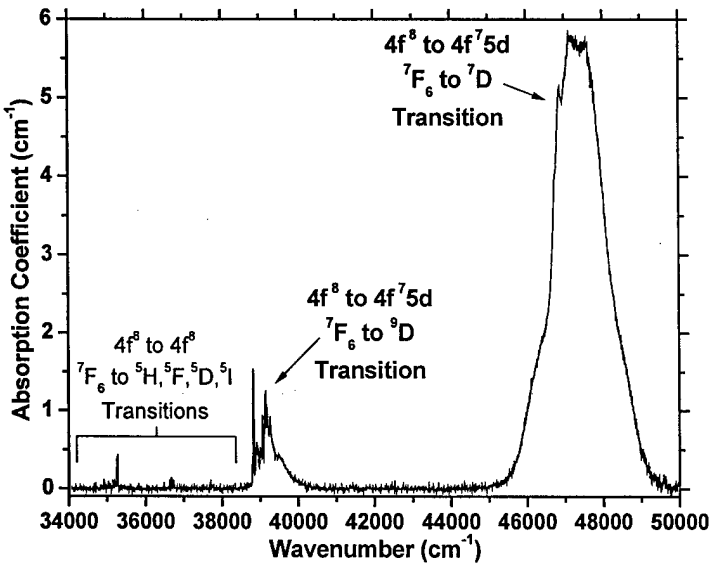

FIG. 31. UV absorption of 1% Tb:$LiYF_4$ at T = 1.8 K. The lowest spin-forbidden and spin-allowed $4f^8$ to $4f^7$5d transitions are clearly observed. Note that the spin-allowed transition absorbed too strongly to obtain an accurate measure of the peak absorption coefficient.

The ultraviolet absorption spectrum is plotted in Fig. 31. The weak features at low energy correspond to intraconfigurational $4f^8$ to $4f^8$ transitions, while the intense bands at 39300 cm^{-1} and 47400 cm^{-1} correspond to the lowest energy interconfigurational spin-forbidden and spin-allowed $4f^8$ to $4f^7$5d transitions. The peak absorption of the spin-allowed transition could not be accurately determined due to the strong absorption and the low throughput of the system at high energies so that the maximum absorption is larger than the value indicated on the plot. Zero-phonon lines were observed at 38820 cm^{-1} and 46850 cm^{-1}, in agreement with previous assignments. The barycenters of the strong phonon sidebands occur at about 500 cm^{-1} higher energy than the zero-phonon lines, corresponding to a relatively weak Stokes shift of ~1000 cm^{-1}. From the integrated absorption, we find that the total oscillator strength of the $^7F_6$ to ^{9}D spin-forbidden band is 3×10^{-6} and that the Debye-Waller factor is 0.06. For two-step photoionization hole burning, the gating transition would involve a spin-forbidden $4f^8$ ($^5D_4$) to $4f^7$5d (^{7}D) transition so that we expect the oscillator strengths to be significantly reduced. Using the free-ion parameters obtained by Carnall *et al.* to calculate intermediate coupling wavefunctions for the $4f^8$ configuration of Tb^{3+}, we found that $^5D_4$ includes a 2.8% admixture of $^7F_4$. Consequently, we estimate that excited-state absorption transitions from $^5D_4$ to the $4f^7$5d levels should be weaker than the corresponding transitions from $^7F_6$ by roughly a factor of 0.03. In fact, a value of 0.02 for the oscillator strength ratio is obtained when full calculations of the transition matrix elements are carried out. Since the $^7F_6$ to ^{9}D and ^{7}D transitions generally have an oscillator strength ratio of ~0.01, we expect the oscillator strength of the $^5D_4$ to ^{7}D gating transition to be similar to the value for the $^7F_6$ to ^{9}D transition.

Combining observed barycenter energies of the $4f^8$ to $4f^7$5d transitions with the $4f^8$ binding energy, we find that the energies of the lowest $4f^7$5d ^{9}D and ^{7}D states are about 2.7 eV and 1.7 eV below the conduction band.

So far, the values of the relative binding energies that we have considered correspond to unrelaxed Franck-Condon energy differences for a rigid lattice with the same spatial configuration as the $4f^8$ ground state, as would be appropriate for describing direct transitions from the $4f^8$

ground state. However, any transitions that occur through a series of absorption or relaxation steps involve much longer timescales that allow the lattice to react to changes in the electronic states. Because of electron-lattice interactions, the total adiabatic energy of the coupled ion-lattice system must be considered when determining energy differences and relaxation mechanisms between states with different electronic configurations. This effect is well known from optical spectroscopy, where stabilization of excited states through relaxation of the ligand configuration can produce large Stokes shifts between emission and absorption energies and can also cause nonradiative relaxation of excited states by mixing the wavefunction with excited configurations of lower energy states. These effects are traditionally described by viewing the total adiabatic energy of each state as a function of "configurational coordinates" that describe the spatial configuration of the ligands around the excited ion. The configurational coordinate most commonly considered is the change in the average ion-ligand distance due to "breathing mode" vibrations of the ligands. Furthermore, the approximations of harmonic ligand vibrations and a linear electron-lattice interaction are usually adopted so that the energy curves are simply quadratic functions of the configurational coordinate.

The importance of describing ionization processes using configurational coordinate diagrams was first recognized nearly fifty years ago by Dexter *et al.* This consideration of the relaxation energies is particularly important for describing ionization processes since contraction of the ligand configuration due to the change in valence is much stronger than the relaxation that occurs for localized excitations of the ion. In spite of this importance, very little is known about the effect of electron-lattice coupling on the ionization thresholds due to the difficulty of experimentally characterizing ionization processes in solids. However, the need to quantitatively understand and predict the effects of ionization on luminescence efficiency has motivated significant progress in this area for both phosphor and scintillator materials.

The estimated configurational coordinate diagram for Tb^{3+}:$LiYF_4$ is shown in Fig. 32. Under the usual approximation of a linear electron-lattice interaction, all of the energy curves have the same curvature. The lowest ^9D and all five ^7D crystal field levels of the $4f^7 5d$ configuration are shown, where the energies of the higher ^7D levels were obtained from van Pieterson *et al.* and the relaxation energy of 500 cm^{-1} was obtained from the optical spectra. The vertical ionization energy from $^7F_6$ is the value determined from the photoemission results. Unfortunately, very little is known regarding the magnitude of the relaxation energies for ionized states. For both Ce^{3+} and Tb^{3+} in YAG and YGG, analysis of luminescence quenching allowed Mayolet *et al.* to determine the approximate positions of the adiabatic energy curves for the ionized states, indicating that the Franck-Condon shifts for the ionized states were roughly three times larger than the shifts for the $4f^{N-1}5d$ levels. The accuracy of their estimates are supported by the remarkable agreement between the $4f^N$ vertical ionization energies predicted from the configurational coordinate diagrams and the values predicted from photoemission measurements on YAG and YGG, with the two very different approaches consistently agreeing to within a few hundred meV. Thus, assuming a similar scaling of the electron-lattice interaction, we have approximated the Franck-Condon shift for the ionized states in $LiYF_4$ as three times the value observed for the $4f^7 5d$ states. The corresponding curve for the ionization threshold is represented by the dotted line in Fig. 32, where the error bar indicates the estimated uncertainty in the position of the threshold due to the approximations used in the model and experimental uncertainty in the measured binding energies.

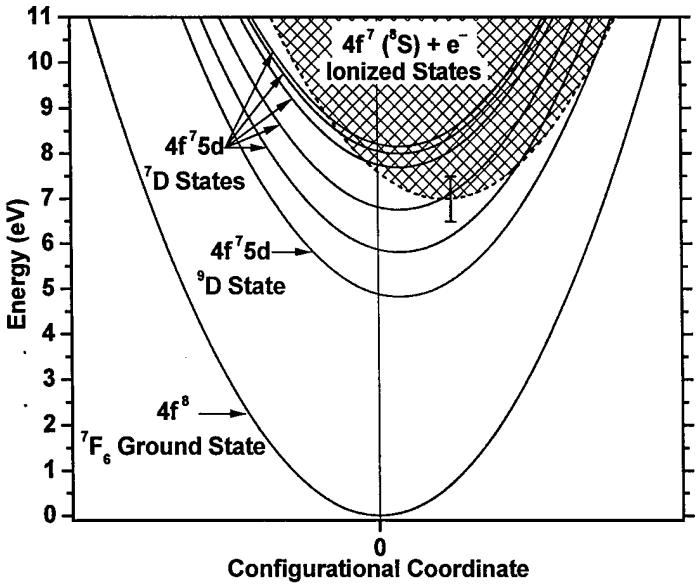

FIG. 32. Estimated configurational coordinate diagram for Tb^{3+}:$LiYF_4$. Adiabatic energy curves for discrete levels are represented by solid lines. The continuum of ionized states is indicated by the crosshatched region, with the ionization threshold curve given by the dotted line. The uncertainty in the position of the adiabatic ionization threshold is represented by the error bar.

In optical spectra, the lowest $^7F_6$ to ^9D and ^7D transitions exhibit well-resolved structure while the higher crystal field components show significant broadening that has been attributed to rapid relaxation through ionization—a conclusion that is supported by Fig. 32. The significant broadening of the second $^7F_6$ to ^7D transition indicates a very efficient relaxation, suggesting that the ionization threshold crosses the second ^7D crystal field level at an energy close to the minimum of the adiabatic energy curve, which is within the uncertainty of the ionization threshold given in Fig. 32. From these considerations, we would need to excite the system from the $^5D_4$ level into the second ^7D level to obtain ionization hole burning, requiring a gating energy of 34390 cm^{-1}, which might be generated using an ultraviolet lamp. A more subtle issue is how the position of the curves affects the lifetime of the ionized state. For efficient photon gating, the probability for geminate recombination must be minimized, requiring that the ionized state cannot rapidly relax to a lower energy $4f^7$5d state. Consequently, the precise position and shape of the ionization threshold curve can have significant consequences for photoionization hole burning. Unfortunately, uncertainty in the position of the ionization threshold prevents a quantitative analysis of this effect for Tb^{3+}:$LiYF_4$ at this time.

The importance of electron-lattice coupling when interpreting results from different experimental techniques is illustrated by evaluating each process using an adiabatic energy level diagram such as Fig. 32. If the ionization threshold is measured using direct absorption from the ground state, the value that would be obtained is the vertical energy difference. However, if an excitation technique such as photoluminescence, photoconductivity, or thermoluminescence is used, relaxation of the system can produce ionization at significantly lower energies so that the observed threshold can occur at energies as low as the adiabatic energy minimum of the ionized state. An excited-state absorption measurement from the lowest $4f^7$5d level would produce yet another value for the ionization threshold intermediate between the other two values. For $LiYF_4$, relatively weak electron-lattice coupling minimizes these effects so that values obtained by different methods would only vary by ~0.5 eV; however, the much stronger interaction in oxides could cause values obtained from different techniques to vary by more than 1 eV.

The $4f^N$ ground state energies of other rare-earth ions in $LiYF_4$ may be estimated from the results obtained for Tb^{3+} by applying the systematics of the 4f electron binding energies. When a rare-earth ion is incorporated into a solid, the 4f electron binding energy of the free ion (given by the free-ion ionization potential I) is shifted by interactions with the host so that the binding energy in the solid is given by $E_B = I - E_{shift}$. Because of their chemical similarity, all of the rare earths experience similar binding energy shifts in a particular material, with only a weak linear variation of E_{shift} occurring across the rare-earth series due to the effects of the lanthanide contraction.

From the measured 4f binding energy, we find a value of $E_{shift} = 29.6$ eV for Tb^{3+} in $LiYF_4$. Since we expect the values of E_{shift} to be similar among materials with the same anions and significantly different for materials with different anions, it is interesting to compare the Tb^{3+} binding energy shift in $LiYF_4$ to the values of 29.9 eV in LaF_3 and 31.4 eV in YAG and YGG. As an estimate for how the binding energy shift varies across the series, we may use the value of $\Delta E_{shift} = 0.162 \text{ eV} \times \Delta A$ measured in LaF_3, where ΔE_{shift} is the difference in the binding energy shift between rare-earth ions with a ΔA difference in atomic number. Using the free-ion ionization potentials determined either from the analysis of optical spectra or from the analysis of photoemission from solids, the value of E_{shift} for each ion can be used to determine the $4f^N$ ground-state binding energy. For example, this predicts a value of $E_{shift} = 28.6$ eV for Pr^{3+} in $LiYF_4$; therefore, using I = 38.98 eV, we estimate that the Pr^{3+} ground state has a 4f binding energy of 10.4 eV, or 2.3 eV above the valence band maximum. Our extrapolated value agrees well with previous studies that found the Pr^{3+} ground state to be ~1.9 eV above the valence band in $LiYF_4$.

The binding energies of the $4f^{N-1}5d$ levels for each rare-earth ion in $LiYF_4$ may be determined by combining the experimental $4f^N$ to $4f^{N-1}5d$ transition energies with the estimated $4f^N$ binding energies. However, a simple approximation is to assume that each $4f^{N-1}5d$ state has the same binding energy for all rare-earth ions in $LiYF_4$. This approximation is expected to be accurate to within about ±0.5 eV across the rare-earth series and is therefore useful as a rough estimate. Since the second ^7D level is the lowest energy $4f^7 5d$ level to be broadened due to relaxation through ionization, we would expect the same behavior to be observed for all rare-earth ions in $LiYF_4$. In fact, this is exactly what is observed in the experimental spectra. From these results, it is clear that understanding the energy level structure and ionization processes for one rare-earth ion also gives important insight into the behavior of all the other rare-earth ions in the same host material.

The Role of Symmetry in Spectral Hole Burning Materials

Symmetry Considerations Regarding Light Propagation and Light Polarization for Coherent Interactions with Ions in Crystals, Y. Sun, G. M. Wang, R. L. Cone, R. W. Equall, and M. J. M. Leask, Phys. Rev. B **62**, 15443-15451 (2000).

This paper describes the principles of our first patent. Optimum crystal orientation enhances transient response and efficiency in device applications.

Design and Characterization of Optical Memory Material $Eu^{3+}:Y_2SiO_5$

Temperature and Concentration Dependence of Optical Dephasing, Spectral Hole Lifetime, and Anisotropic Absorption in $Eu^{3+}:Y_2SiO_5$, Flurin Könz, Y. Sun, C. W. Thiel, R. L. Cone, R. W. Equall, R. L. Hutcheson, and R. M. Macfarlane, Phys. Rev. B. **68**, 085109 (2003) 9 pages.

Optical Dephasing by Disorder Modes in Yttrium Orthosilicate (Y_2SiO_5) doped with Eu^{3+}, R. M. Macfarlane, Y. Sun, R. L. Cone, C. W. Thiel, and R. W. Equall, J. Lumin. **107**, 310-313 (2004).

This material prepared by Scientific Materials Corporation is currently being used by several groups for quantum information applications and has been used in the design of a spectrally-multiplexed high capacity optical memory.

PERSONNEL SUPPORTED AND ASSOCIATED

Cone's group produced four Ph.D. graduates working on this AFOSR research project.

1) **Todd Harris** completed his Ph.D. in Physics in April 2001. His thesis was entitled, *Erbium-Based Optical Coherent Transient Correlator for the 1.5-Micron Communication Bands*. Harris had a postdoctoral position at IBM Almaden Research Center, San Jose, California, and has recently accepted a position as Research Engineer at SRI International, Menlo Park, CA. During his graduate study in our group, Harris developed analog optical signal processing device demonstrations at 1.5 μm using external cavity diode lasers he built and erbium doped fiber amplifiers. Harris characterized Er^{3+} compounds for 1.5 μm devices in photon echo measurements and Zeeman spectroscopy. The 1.5 μm device demonstrations included an optical header decoder for all-optical packet-switching and tests of code fidelity in all-optical correlators using bi-phase-shift-key codes(BPSK) and quadri-phase-shift-key codes (QPSK).
2) **Thomas Bottger** completed his Ph.D. in Physics on April 18, 2002. His thesis was entitled, *Laser Frequency Stabilization to Spectral Hole Frequency References in Erbium-Doped Crystals: Material and Device Optimization.* Bottger worked on development of our ultra-narrow band diode lasers stabilized to spectral holes. He also applied those lasers to studies of Er^{3+} spectral hole burning materials. Bottger worked for an additional year as a postdoc in our group and then accepted a tenure track faculty position, in August 2003, as Assistant Professor, Department of Physics, University of San Francisco, San Francisco, CA, where he is establishing a research program.
3) **Gregory Reinemer** completed his Ph.D. in Physics in January 2003. His thesis was entitled, *Optical Characterization of Perturbed and C_{3i} Sites in Rare-Earth Doped Oxides.* Reinemer characterized a number Er^{3+} hole burning materials and studied the effects of crystal structure defects in garnet crystal materials for spectral hole burning devices. Reinemer accepted a position as Visiting Assistant Professor, Department of Physics, Idaho State University, Pocatello, ID.
4) **Charles Thiel** held an NSF graduate fellowship and completed his Ph.D. in Physics in December 2003. His thesis was entitled, *Energies of Rare-Earth Ion States Relative to Host Bands.* Thiel worked on development of gated spectral hole burning materials and on sophisticated time-domain modeling of the frequency stabilization of diode lasers to spectral hole frequency references. Thiel carried out innovative UV electron photoemission spectroscopy that allowed us to determine the positions of the ion levels relative to the valence bands and conduction bands of the host crystals. That information allows us to design and select ideal candidate materials for gated hole burning. Gated materials containing Tb^{3+} ions were studied, and work on a number of other rare earth ions and hosts continues. This challenging work also has improved the general understanding of a wide range of other optical materials including lasers, phosphors for displays and illumination, and scintillators for imaging applications.

Senior personnel included

1) Postdoctoral fellow, **Dr. Geoff Pryde**, who completed his Ph.D. at Australian National University, Canberra, Australia, made valuable contributions to the group's program of laser stabilization to spectral holes during his two-year stay in our group.. On December 1, 2001, Dr. Pryde accepted a position in quantum computing.
2) Associate Research Professor, **Dr. Yongchen Sun**, worked full time on this project carrying out material development of spectral hole burning materials for frequency references.
3) Senior Research Scientist **Dr. Roger Macfarlane**, Emeritus Member of the Technical Staff of IBM Almaden Research Center joined the group on a part time basis year round in July 2002. Having Dr. Macfarlane as a member of the group accelerated the collaboration that we have had for many years.
4) **Dr. Thomas Bottger** began work as a Postdoctoral Fellow in May 2002. As noted above, he assumed a tenure track faculty position in August 2003 as Assistant Professor, Department of Physics, University of San Francisco, 2130 Fulton St, San Francisco, CA.
5) **Dr. Peter Sellin** began work as a Research Scientist working on frequency stabilization of lasers to spectral holes on September 1, 2003. He completed his Ph. D. with Professor Thomas Mossberg at the University of Oregon.
6) **Dr. Annabelle Collombet** joined the group as a Postdoctoral Fellow with a Lavoisier Fellowship from the French government. She completed her Ph.D. with Dr. Marie-France Joubert on Spectroscopy of Nd^{3+}-doped crystals and a study of their potential as tunable solid-state UV laser sources at Laboratoire de Physico-Chimie des Matériaux Luminescents, Université Lyon, France.
7) **Casey Dodge**, with at B.S. in Mechanical Engineering joined us as a Research Associate September 1, 2003.
8) **Dr. Charles Thiel** continued his research on modeling the laser stabilization to spectral holes and on hole burning material development as a Postdoctoral Fellow from January 2004.

Cone's group had six undergraduate students involved in this AFOSR research project.

1) **Anna Hagenston**, undergraduate student in Physics, received her B.S. in Physics in May 2001. Ms. Hagenston won the Dean's Award for Excellence in the College of Letters and Science in May 2000. Hagenston is now a graduate student at Yale on an NSF Graduate Fellowship.
2) **Michael Patterson**, undergraduate student in Physics, was involved in electronic construction projects including photodetectors for the laser stabilization systems and material characterization. He also installed and characterized a laser beam profile measurement system.
3) **Nolan Newkirk**, an undergraduate physics major at Oklahoma State University, participated in our group with support from an MSU "NSF Research Experience for Undergraduates" (REU) program for eight weeks during the Summer of 2000.
4) **Dustin Rich** an MSU mechanical engineering undergraduate participated in this project for two years, beginning work in our laboratory during the academic year September 2000 to May 2001. His contributions included utilizing Computer Numerically Controlled Machining (CNC) together with Computer Automated Drafting (CAD) to

manufacture diode laser and laser stabilization components. Rich also designed and machined components for a rotating sample handling apparatus designed for operation near absolute zero temperature and used for characterization of optical materials for the frequency references in a magnetic field. Rich spent the Summer 2002 as an intern at Boeing in Everett, WA, where he worked in 777 Tool Engineering and was involved in both design and production shop liaison activities. The internship provided valuable experience with engineering and business practice in the aviation industry. He returned to our group for the academic year 2002-2003. On graduation in May 2003, Rich accepted a position as an Assistant Shift Test Engineer at the Puget Sound Naval Shipyard, Bremerton, Washington, where he works in the Nuclear Test Engineering organization that is responsible for operations and testing of nuclear propulsion plant systems. Rich presented a poster at the MSU Optical Technology Conference in September 2002.

5) **Cooper McCann**, a Physics major from Pony, Montana, joined the group for summer research project on interferometric characterization of vibration in the cryostats used for laser stabilization from May through August 2002. McCann presented a talk on the results at the MSU OpTeC Conference. He completed his B.S. in Physics in May 2004 and began a job as laser technician at the local laser company AdvR.

6) **Ted Armstrong**, a in Physics at MSU, carried out undergraduate research on optical detector development during January – July 2003. During his senior year he characterized the scanning properties of diode lasers. He will begin medical school at the University of Minnesota in August 2004.

Though not working directly in our group, Dr. Galina Malovichko joined the MSU Physics department as an Associate Professor of Physics on August 30, 2002. Dr. Malovichko is an expert on $LiNbO_3$ and KTP and other electro-optical materials and has established EPR and ENDOR magnetic resonance facilities that nicely complement many of our capabilities. Collaborations will positively impact our research, and she and her group (3 Ph.D.'s) are a major resource for us.

PUBLICATIONS

Refereed Publications – 20

1. *Laser Frequency Stabilization using Regenerative Spectral Hole Burning,* N. M. Strickland, P. B. Sellin, Y. Sun, J. L. Carlsten, and R. L. Cone, Phys. Rev. B **62**, 1473-1476 (2000).
2. *Symmetry Considerations Regarding Light Propagation and Light Polarization for Coherent Interactions with Ions in Crystals,* Y. Sun, G. M. Wang, R. L. Cone, R. W. Equall, and M. J. M. Leask, Phys. Rev. B **62**, 15443-15451 (2000).
3. *Laser Stabilization at 1536 nm Using Regenerative Spectral Hole Burning*, P. B. Sellin, N. M. Strickland, T. Böttger, J. L. Carlsten, and R. L. Cone, Phys. Rev. B **63,** 155111-1 – 155111-7 (2001).
4. *Systematics of 4f Electron Energies Relative to Host Bands by Resonant Photoemission of Rare Earth Ions in Aluminum Garnets,* C. W. Thiel, H. Cruguel, H. Wu, Y. Sun, G. J.

Lapeyre, R. L. Cone, R. W. Equall, and R. M. Macfarlane, Phys. Rev. B **64**, 085107 (2001).

5. *Semiconductor Lasers Stabilized to Spectral Holes in Rare Earth Crystals,* R. L. Cone, T. Böttger, G. J. Pryde, N.M. Strickland, Y. Sun, P. B. Sellin, and J. L. Carlsten, in Physics and Simulation of Optoelectronic Devices IX, Yasuhiko Arakawa, Peter Blood, Marek Osinski, Editors, Proceedings of SPIE Vol. **4283**, 335-346 (2001).
6. *Systematics of 4f electron energies relative to host bands by resonant photoemission of rare earth doped optical materials,* C. W. Thiel, H. Cruguel, Y. Sun, G. J. Lapeyre, R. M. Macfarlane, R. W. Equall, and R. L. Cone, J. Lumin. **94-95**, 1-6 (2001).
7. *Diode laser frequency stabilization to transient spectral holes and spectral diffusion in* Er^{3+}*: Y_2SiO_5 at 1536 nm,* Thomas Böttger, Y. Sun, G.J. Pryde, G. Reinemer, and R.L. Cone, J. Lumin. **94-95**, 565-568 (2001).
8. *Numerical modeling of laser stabilization by regenerative spectral hole burning,* G. J. Pryde, T. Böttger, and R. L. Cone, J. Lumin. **94-95**, 587-591 (2001).
9. *Semiconductor Lasers Stabilized to Spectral Holes in Rare-Earth Crystals,* Thomas Böttger, Geoffrey J. Pryde, Nicholas M. Strickland, Peter B. Sellin, and Rufus L. Cone, Optics & Photonics News, **12,** #12, 23 (2001).
10. *Relating Localized Electronic States to Host Band Structure in Rare-Earth-Activated Optical Materials,* Charles W. Thiel, Herve Cruguel, Huasheng Wu, Yongchen Sun, Gerald J. Lapeyre, Rufus L. Cone, Randy W. Equall, and Roger M. Macfarlane, Optics & Photonics News, **12,** #12, 64 (2001).
11. *Semiconductor lasers stabilized to spectral holes in rare earth crystals to a part in* 10^{13} *and their application to devices and spectroscopy,* G. J. Pryde, T. Böttger, R. L. Cone, and R. C. C. Ward, J. Lumin. **98**, 309-315 (2002).
12. *Recent progress in developing new rare earth materials for hole burning and coherent transient applications,* Y. Sun, C. W. Thiel, R. L. Cone, R. W. Equall, and R. L. Hutcheson, J. Lumin. **98**, 281-287 (2002).
13. *Progress in Relating Rare Earth Ion 4f and 5d Energy Levels to Host Bands in Optical Materials for Hole Burning, Quantum Information, and Phosphors,* C. W. Thiel, Y. Sun, and R. L. Cone, Journal of Modern Optics **49**, 2399-2411 (2002).
14. *Coherent Integration of 0.5 GHz Spectral Holograms at 1536 nm using Dynamic Bi-Phase Codes,* Z. Cole, T. Böttger, Krishna Mohan, R. Reibel, W. R. Babbitt, R. L. Cone, and K. D. Merkel, Appl. Phys. Lett. **81**, 3525-3527 (2002).
15. *Programmable Sub-kHz Laser Frequency Stabilization at 1523 nm using Persistent Spectral Hole Burning,* Thomas Böttger, G. J. Pryde, and R. L. Cone, Opt. Lett. **28**, 200-202 (2003).
16. *Material Optimization of* Er^{3+}*:Y_2SiO_5 at 1.5 μm for Optical Processing, Memory, and Laser Frequency Stabilization Applications,* Thomas Böttger, Y. Sun, C. W. Thiel, and R. L. Cone, Proceedings of SPIE , Vol. 4988, 51-61 (2003).
17. *Temperature and Concentration Dependence of Optical Dephasing, Spectral Hole Lifetime, and Anisotropic Absorption in* Eu^{3+}*:Y_2SiO_5,* Flurin Könz, Y. Sun, C. W. Thiel, R. L. Cone, R. W. Equall, R. L. Hutcheson, and R. M. Macfarlane, Phys. Rev. B. **68**, 085109 (2003) 9 pages.
18. *Spectral Hole Burning and Energy Level Structure of* Tb^{3+}*:$LiYF_4$,* C. W. Thiel, Y. Sun, R. W. Equall, and R. L. Cone, J. Lumin. **107**, 236-244 (2004).

19. *Optical Dephasing by Disorder Modes in Yttrium Orthosilicate (Y_2SiO_5) doped with Eu^{3+}*, R. M. Macfarlane, Y. Sun, R. L. Cone, C. W. Thiel, and R. W. Equall, J. Lumin. **107**, 310-313 (2004).
20. *Proceedings of the 8th International Meeting on Hole Burning, Single Molecule, and Related Spectroscopies: Science and Applications,* Bozeman, MT, USA, 26 - 31 July 2003, Edited by: W. R. Babbitt, R. L Cone, A. Rebane, and R. W. Equall, J. Lumin. **107**, 1-373 (2004).

INTERACTIONS/TRANSITIONS

Participated in **AFOSR Workshop** organized by Kent Miller at SRI, Menlo Park, California, May 25-28, 2000.

Participated in **Montana Spectral Hole Burning Workshop** at Big Sky, Montana, July 9-12, 2000.

A. Presentations and Participation at Meetings and Conferences

Conference Organization – 12

1. PROGRAM COMMITTEE, 31st Winter Colloquium on The Physics of Quantum Electronics, Snowbird, Utah, January 7-11, 2001.
2. ORGANIZING COMMITTEE, Third Annual Meeting of the Northwest Section of the American Physical Society, University of Washington, Seattle, Washington May 25 - 26, 2001.
3. INTERNATIONAL ADVISORY COMMITTEE, 13th International Conference on Dynamical Processes in Excited States of Solids / Conférence Internationale Dynamique des Etats Excités dans les Solides, Université Claude Bernard Lyon1, Lyon, France, July 1 - 4, 2001
4. PROGRAM COMMITTEE, The Texas A & M 2001 Workshop on Laser Physics and Quantum Optics – Ramsey Fest, Jackson Hole, Wyoming, July 29 - August 3, 2001.
5. PROGRAM COMMITTEE, 7th International Meeting on Hole Burning, Single Molecule, and Related Spectroscopies, Academia Sinica, Taipei, Taiwan, November 18 - 23, 2001
6. Rufus Cone presided over the session on Atomic, Molecular, and Optical Physics at the Third Annual Meeting of the Northwest Section of the American Physical Society, University of Washington, Seattle, Washington May 25 - 26, 2001.
7. Rufus Cone presided over the session on Dynamics of Highly Excited States of Solids 13th International Conference on Dynamical Processes in Excited States of Solids / Conférence Internationale Dynamique des Etats Excités dans les Solides, Université Claude Bernard Lyon1, Lyon, France, July 1 - 4, 2001.
8. PROGRAM COMMITTEE, 7th International Meeting on Hole Burning, Single Molecule, and Related Spectroscopies, Academia Sinica, Taipei, Taiwan, November 18 - 23, 2001
9. PROGRAM COMMITTEE, 32nd Winter Colloquium on The Physics of Quantum Electronics, Snowbird, Utah, January 6-10, 2002.

10. CONFERENCE ORGANIZATION, 8th International Meeting on Hole Burning, Single Molecule, and Related Spectroscopies: Science and Applications – HBSM 2003, July 27 to 31, 2003, Bozeman, MT.

    Rufus Cone, Randy Babbitt, and Aleksander Rebane, together with Randy Equall of Scientific Materials Corporation, hosted the 8th International Meeting on Hole Burning, Single Molecule, and Related Spectroscopies: Science and Applications, 'HBSM 2003,' on July 26 - 31, 2003, in Bozeman, Montana. The HBSM Conference is held regularly to disseminate the latest developments in high-resolution optical spectroscopy of solids: spectral hole burning, single molecule spectroscopy, photon echoes and related topics. The main conference themes included: hole-burning materials and mechanisms, photon echoes and coherent transients, photophysics and photochemistry, single molecule detection and spectroscopy, novel microscopies, optical storage and signal processing, optical dephasing and spectral diffusion, time and space domain holography, biological systems, nanosystems and nano-optics, and multi-photon and nonlinear effects. There were 100 participants from 13 countries. The conference was sponsored by The Montana State University Physics Department, The Montana State University Spectrum Lab, and Scientific Materials Corporation and was supported by Air Force Office of Scientific Research and Scientific Materials Corporation.

11. INTERNATIONAL ADVISORY AND PROGRAM COMMITTEE, , 8th International Meeting on Hole Burning, Single Molecule, and Related Spectroscopies: Science and Applications July 27 to 31, 2003, Bozeman, MT. Cone has been in this role for the past three conferences; this activity is distinct from that of being the Conference Organizer.
12. INTERNATIONAL ADVISORY COMMITTEE, International Conference on Dynamical Processes in Excited States of Solids, Christchurch, New Zealand, August 3-8, 2003.

Invited Conference Talks – 17

1. INVITED WORKSHOP PRESENTATION, *New Spectral Hole Burning Devices and Spectral Hole Burning Materials,* R. L. Cone and Y. Sun, AFOSR Workshop, SRI International, Menlo Park, California, May 25, 2000.
2. INVITED CONFERENCE TALK, *Rare Earth Materials for Lasers, Spectral Hole Burning and Stabilized Lasers,* R. L. Cone and Y. Sun, Townes Festival 2000, Teton Village, Wyoming, July 31 - August 4, 2000
3. INVITED PLENARY CONFERENCE TALK, *Spectroscopy of rare earth materials from 20 Hz to hundreds of electron volts,* R. L. Cone, 31st Winter Colloquium on The Physics of Quantum Electronics, Snowbird, Utah, January 7-11, 2001.
4. INVITED CONFERENCE TALK, *Semiconductor Lasers Stabilized to Spectral Holes in Rare Earth Crystals,* R. L. Cone, T. Böttger, G. J. Pryde, N.M. Strickland, Y. Sun, P. B. Sellin, and J. L. Carlsten, Photonics West - Optoelectronics 2001, in the Symposium on Physics and Simulation of Optoelectronic Devices IX (OE09), January 20-26, 2001.
5. INVITED CONFERENCE TALK, *Systematics of 4f Electron Energies Relative to Host Bands by Resonant Photoemission of Rare Earth Doped Optical Materials,* C. W. Thiel, H. Cruguel, Y. Sun, G. J. Lapeyre, R. M. Macfarlane, R. W. Equall, and R. L. Cone, International Conference on Dynamical Processes in Excited States of Solids, Lyon, France, July 1-4, 2001.

6. INVITED PLENARY CONFERENCE TALK, *Level Structure of Rare Earth Ions in Solids, Overview, Examples From Spectroscopy,* R. L. Cone, The 2001 Workshop on Laser Physics and Quantum Optics – Ramsey Fest, Jackson Hole, Wyoming, July 29 - August 3, 2001.
7. INVITED TALK, *Optical Devices Based on Spectral Hole Burning Materials,* Rufus L. Cone, Physics Colloquium, University of Georgia, October 11, 2001.
8. INVITED TALK, *New Rare Earth Materials for Hole Burning and Coherent Transient Applications,* Y. Sun, C. W. Thiel, R. L. Cone, R. W. Equall, and R. L. Hutcheson, 7th International Meeting on Hole Burning, Single Molecule, and Related Spectroscopies, Academia Sinica, Taipei, Taiwan, November 18 - 23, 2001.
9. INVITED PLENARY CONFERENCE TALK, *Overview of Rare Earth Materials for Quantum Information Applications,* Rufus L. Cone, 32nd Winter Colloquium on The Physics of Quantum Electronics, Snowbird, Utah, January 6-10, 2002.
10. INVITED TALK, *Progress in Relating Rare Earth Ion 4f and 5d Energy Levels to Host Bands in Optical Material Design for Hole Burning, Quantum Information, and Phosphors,* C. W. Thiel, Y. Sun, and R. L. Cone, 32nd Winter Colloquium on The Physics of Quantum Electronics, Snowbird, Utah, January 6-10, 2002.
11. INVITED TALK, *Lasers Stabilized to Regenerative Spectral Holes: Experiment, Modeling, and Material Optimization,* Thomas Böttger, G. J. Pryde, C. W. Thiel, Y. Sun, and R. L. Cone, 32nd Winter Colloquium on The Physics of Quantum Electronics, Snowbird, Utah, January 6-10, 2002.
12. INVITED TALK, *Spectroscopy of Rare Earth-Doped Materials for Hole Burning Devices and Laser Frequency Stabilization,* La Societe Francaise de Physique, Section Rhone-Loire, Universite Lyon I, Lyon, France, March 28, 2002.
13. INVITED TALK, *Energies of $4f^N$ and $4f^{N-1}5d$ States Relative to Host Bands in Rare-Earth-Activated Optical Materials,* C. W. Thiel, Y. Sun, and R. L. Cone, 23rd Rare Earth Research Conference, University of California, Davis, California, July 14-18, 2002.
14. INVITED TALK, *Coherent Spectroscopy of Er^{3+}-Doped Crystals for 1.5 μm Optical Signal Processing and Laser Frequency Stabilization,* R. L. Cone, Y. Sun, Thomas Böttger, G. Reinemer, C. W. Thiel, T. L. Harris, G. J. Pryde, N. M. Strickland, R. W. Equall, R. L. Hutcheson, R. C. C. Ward, and Glynn D. Jones, 23rd Rare Earth Research Conference, University of California, Davis, California, July 14-18, 2002.
15. INVITED TALK, Ultra-narrow spectral holes in rare-earth-doped crystals as sub-kHz frequency references for active stabilization of diode lasers at 1.5 μm and 793 nm, R. L. Cone, Thomas Böttger, C. W. Thiel, P. B. Sellin, G. J. Pryde, and Y. Sun, 227th American Chemical Society National Meeting, Anaheim, CA, March 28 - April 1, 2004.
16. INVITED TALK, Measuring and modeling energies of rare-earth ion states relative to host bands in optical materials, C. W. Thiel, Y. Sun, and R. L. Cone, 227th American Chemical Society National Meeting, Anaheim, CA, March 28 - April 1, 2004.
17. INVITED TALK, Spectral holeburning and optical coherent transients in rare-earth ions, Y. Sun, C. W. Thiel, and R. L. Cone, 227th American Chemical Society National Meeting, Anaheim, CA, March 28 - April 1, 2004.

Contributed Conference Talks – 50

1. *Optical Spectroscopy Of Perturbed Sites In Rare Earth Garnets,* G. Reinemer, G.M. Wang, C. W. Thiel, Y. Sun, R. L. Cone, R. M. Macfarlane, R. W. Equall, and R. L. Hutcheson, Northwest Section Meeting of the American Physical Society, Eugene, Oregon, May 19-20, 2000.
2. *Stabilized Lasers and Hole Burning Materials,* R. L. Cone, T. Böttger, G. J. Pryde, and N. M. Strickland, Workshop on Applications of Spectral Hole Burning 2000, Big Sky, Montana, July 9-12, 2000.
3. *New Studies of Materials,* Y. Sun, G. J. Pryde, C. W. Thiel, Flurin Könz, G. Reinemer, T. L. Harris, R. L. Cone, R. W. Equall, R. L. Hutcheson, Workshop on Applications of Spectral Hole Burning 2000, Big Sky, Montana, July 9-12, 2000.
4. *Lasers Stabilized at 1.5 Microns,* G. J. Pryde, T. Böttger, and R. L. Cone, Workshop on Applications of Spectral Hole Burning 2000, Big Sky, Montana, July 9-12, 2000.
5. *Spectroscopy of Rare Earth Materials from 20 Hz to Hundreds of Electron Volts,* R. L. Cone, Y. Sun, G. J. Pryde, .A. Braud, C. W. Thiel, T. L. Harris, T. Böttger, G. Reinemer, G. J. Lapeyre, R. W. Equall, and R. L. Hutcheson, 2000 Optical Science and Laser Technology Conference, Montana State University, Bozeman, Montana, August 14-15, 2000.
6. *Systematics of Rare Earth Crystal Band Structure by Photoemission for Design of Laser and Hole Burning Materials,* C. W. Thiel, Y. Sun, R. L. Cone, G.J. Lapeyre, and R.W. Equall, 2000 Optical Science and Laser Technology Conference, Montana State University, Bozeman, Montana, August 14-15, 2000.
7. *Stabilizing Lasers* to *Spectral Holes: Experiments, Materials, and Simulations*, G. J. Pryde, T Böttger, and R. L. Cone, 2000 Optical Science and Laser Technology Conference, Montana State University, Bozeman, Montana, August 14-15, 2000.
8. *Laser Materials for LIDAR Applications,* A.Braud, S. Ermeneux, C. Maunier, R. W. Equall, R. L. Hutcheson, R. L. Cone and R. Moncorge, 2000 Optical Science and Laser Technology Conference, Montana State University, Bozeman, Montana, August 14-15, 2000.
9. *Photon Echo Characterization in the Electro-Optic Material Er^{3+}:KTP at 1.5 Microns,* G. Reinemer, T Böttger, Y. Sun, and R. L. Cone, 2000 Optical Science and Laser Technology Conference, Montana State University, Bozeman, Montana, August 14-15, 2000.
10. *Laser Frequency Stabilization at 1.5 μm Using Spectral Hole Burning,* T. Böttger, G. J. Pryde, P. B. Sellin, N. M. Strickland, J. L. Carlsten, and R. L. Cone, Optical Society of America Annual Meeting, Providence, Rhode Island, Oct 22 - 26, 2000.
11. *Numerical studies of frequency stabilization using transient spectral holes in rare-earth crystals,* G. J. Pryde, T. Böttger and R. L. Cone, Optical Society of America Annual Meeting, Providence, Rhode Island, Oct 22 - 26, 2000.
12. *Rare Earth Spectroscopy, Materials for Spectral Hole Burning Devices, and Laser Frequency Stabilization to Ultranarrow Spectral Holes,* R. L. Cone, T. Böttger, and G.J. Pryde, Atomic Physics Seminar, Physics Department, Yale University, October 27, 2000.
13. *Systematics of rare earth crystal band structure by photoemission for design of laser and hole burning materials,* C. W. Thiel, H. Cruguel, Y. Sun, G. J. Lapeyre, R. L. Cone, H.

Wu, R. W. Equall, R. M. Macfarlane, 31st Winter Colloquium on The Physics of Quantum Electronics, Snowbird, Utah, January 7-11, 2001.

14. *Compact laser frequency stabilization at 1.5μm using spectral hole burning,* G. J. Pryde, T. Böttger, and R. L. Cone, 31st Winter Colloquium on The Physics of Quantum Electronics, Snowbird, Utah, January 7-11, 2001.
15. *Nd-Doped Mixed Scandium Garnets for Improved Laser Performance and Compositional Tuning From 937 to 946 nm,* A. Braud, F. S. Ermeneux, Y. Sun, R. L. Cone, R. W. Equall, R. L. Hutcheson, C. Maunier, R. Moncorge, N.P. Barnes, H.G. Gallagher and T.P. Han. Conference on Advanced Solid-State Lasers 2001, Seattle, Washington, January 28-31, 2001.
16. *Er^{3+} $^4I_{15/2}$ and $^4I_{13/2}$ Levels and Magnetic g-Tensors for C_2 and C_{3i} Sites in Y_2O_3 by 1.5 μm Diode Laser Spectroscopy,* G. Reinemer, T. L. Harris, Y. Sun, R. L. Cone, and R. W. Equall, March Meeting of the American Physical Society, Seattle, Washington, March 12-16, 2001.
17. *Compact Laser Frequency Stabilization at 1.5μm Using Spectral Hole Burning,* T. Böttger, G.J. Pryde, N. M. Strickland, and R. L. Cone, 2001 Quantum Electronics and Laser Science Conference, Baltimore, Maryland, May 6-11, 2001.
18. *Er^{3+} $^4I_{15/2}$ and $^4I_{13/2}$ Levels and Magnetic g-tensors for C_2 and C_{3i} Sites in Y_2O_3 by 1.5 μm Diode Laser Spectroscopy*, G. Reinemer, T. L. Harris, Y. Sun, R. L. Cone, and R. W. Equall, Third Annual Meeting of the Northwest Section of the American Physical Society, University of Washington, Seattle, Washington May 25 - 26, 2001.
19. *Spectral hole and laser dynamics: What happens when a laser is stabilized to a regenerative spectral hole frequency reference?,* G. J. Pryde, T. Böttger and R. L. Cone, International Conference on Dynamical Processes in Excited States of Solids, Lyon, France, July 1-4, 2001.
20. *Site Occupancy Determination in Pr^{3+}:Y_2SiO_5 by Optical Nutation and Absorption,* Y. Sun, F. Könz, R. L. Cone, and R. W. Equall, International Conference on Dynamical Processes in Excited States of Solids, Lyon, France, July 1-4, 2001.
21. *Spectral Diffusion at 1.5 microns in Er^{3+} Compounds Measured with a Diode Laser Frequency Stabilized to a Spectral Hole,* T. Böttger, G. J. Pryde, G. Reinemer, Y. Sun, and R. L. Cone, International Conference on Dynamical Processes in Excited States of Solids, Lyon, France, July 1 - 4, 2001.
22. *Systematics of 4f Electron Energies Relative to Host Bands in Rare Earth Doped Optical Materials,* Charles W. Thiel, Condensed Matter Physics Seminar, Montana State University, Bozeman, MT, January 31, 2001.
23. *Overview of Cone/Sun Group Efforts on Material Design and Characterization and on Laser Frequency Stabilization to Spectral Holes,* R. L. Cone, Y. Sun, G. J. Pryde, T. L. Harris, C. W. Thiel, T. Böttger, G. Reinemer, G. J. Lapeyre, R. W. Equall, and R. L. Hutcheson, Optical Science and Laser Technology Conference, Bozeman, MT, August 22, 2001.
24. *Measurement and Control of Spectral Diffusion at 1.5 Microns in Er^{3+} Materials for Spectral Hole Burning Applications,* T. Böttger, G. J. Pryde, G. Reinemer, Y. Sun, R. L. Cone, and R. W. Equall, Optical Science and Laser Technology Conference, Bozeman, MT, August 22, 2001.
25. *Magnetic Field Suppression of Optical Dephasing for Er^{3+}:Y_2O_3 and Measurement of Magnetic g-Tensors for C_2 and C_{3i} Sites by 1.5 Micron Diode Laser Spectroscopy,* G.

Reinemer, T. L. Harris, Y. Sun, R. L. Cone, and R. W. Equall, Optical Science and Laser Technology Conference, Bozeman, MT, August 22, 2001.

26. *Compact Frequency Stabilized Laser at 1.5 Micron Using Spectral Hole Burning,* T. Böttger, G.J. Pryde, N. M. Strickland, and R. L. Cone, Optical Science and Laser Technology Conference, Bozeman, MT, August 22, 2001.
27. *Energy Level Structure of Rare-Earth-Activated Laser, Phosphor, and Scintillator Materials Probed by Electron Photoemission,* C. W. Thiel, H. Cruguel, Y. Sun, G. J. Lapeyre, R. L. Cone, R. W. Equall, R. L. Hutcheson, and R. L. Cone, Optical Science and Laser Technology Conference, Bozeman, MT, August 22, 2001.
28. *Model for Optimizing Spectral Hole Burning Laser Frequency References,* G. J. Pryde, T. Böttger and R. L. Cone, Optical Science and Laser Technology Conference, Bozeman, MT, August 22, 2001.
29. *Progress in Rare Earth Materials for Hole Burning and Coherent Transient Applications,* Y. Sun, C. W. Thiel, G. J. Pryde, T. L. Harris, T. Böttger, G. Reinemer, R. L. Cone, R. W. Equall, and R. L. Hutcheson, Optical Science and Laser Technology Conference, Bozeman, MT, August 22, 2001.
30. *Semiconductor Lasers Stabilized to Spectral Holes in Rare Earth Crystals to a Part in 10^{13} and Their Application to Devices and Spectroscopy,* G. J. Pryde, T. Böttger, Y. Sun, and R. L. Cone, 7th International Meeting on Hole Burning, Single Molecule, and Related Spectroscopies, Academia Sinica, Taipei, Taiwan, November 18 - 23, 2001.
31. *Material Optimization of Er^{3+}:Y_2SiO_5 at 1.5 μm for optical processing, memory, and laser frequency stabilization applications,* Thomas Böttger, Y. Sun, C. W. Thiel, and R. L. Cone, Photonics West, Advanced Optical Data Storage, San Jose, CA, January 2003.
32. *Locating the electronic states of rare-earth ions relative to host band states for the development of photon-gated hole burning materials,* C. W. Thiel*, Y. Sun, and R. L. Cone, 8th International Meeting on Hole Burning, Single Molecule, and Related Spectroscopies: Science and Applications, Bozeman, MT, July 27 – 31, 2003.
33. *Spectral Diffusion in Erbium-Doped Transient Spectral Hole Burning Materials,* C. W. Thiel, T. Böttger, Y. Sun*, and R. L. Cone, 8th International Meeting on Hole Burning, Single Molecule, and Related Spectroscopies: Science and Applications, Bozeman, MT, July 27 – 31, 2003.
34. *Optical Dephasing by Disorder Modes in Yttrium Orthosilicate (YSO) doped with Eu^{3+},* R. M. Macfarlane, Y. Sun, R. L. Cone, C. W. Thiel and R. W. Equall, 8th International Meeting on Hole Burning, Single Molecule, and Related Spectroscopies: Science and Applications, Bozeman, MT, July 27 – 31, 2003.
35. *Transient and Permanent Spectral Hole-Burning in Erbium-Doped Glasses,* L. Bigot, S. Choblet, A-M. Jurdyc, B. Jacquier, T. Böttger, Y. Sun, and R. L. Cone, 8th International Meeting on Hole Burning, Single Molecule, and Related Spectroscopies: Science and Applications, Bozeman, MT, July 27 – 31, 2003.
36. *Spectral hole burning with a mode-locked laser,* Joe A. Fischer, Thomas Böttger, Mingzhen Tian, R. L. Cone, and Wm. Randall Babbitt, 8th International Meeting on Hole Burning, Single Molecule, and Related Spectroscopies: Science and Applications, Bozeman, MT, July 27 – 31, 2003.
37. *New Aspects of Line Broadening in YAG Laser Materials,* G. Reinemer, Y. Sun, R. L. Cone, and R. W. Equall, Optical Science and Laser Technology Conference, Bozeman, MT, September 13-14, 2002.

38. *Energies of $4f^N$ and $4f^{N-1}5d$ States Relative to Host Bands in Rare-Earth-Activated Optical Materials,* C. W. Thiel, Y. Sun, and R. L. Cone, Optical Science and Laser Technology Conference, Bozeman, MT, September 13-14, 2002.
39. *Spectroscopy of Er^{3+}:Y_2SiO_5 - A 1.5 Micron Spectral Holography Processing Material and Laser Wavelength Reference,* Thomas Böttger, C. W. Thiel, Y. Sun, and R. L. Cone, Optical Science and Laser Technology Conference, Bozeman, MT, September 13-14, 2002.
40. *Interferometric Characterization of Sample Vibration in Optical Cryostats,* C. P. McCann, C. W. Thiel, Y. Sun, and R. L. Cone, Optical Science and Laser Technology Conference, Bozeman, MT, September 13-14, 2002.
41. *Rotating Sample Holder for Angle-Dependent Optical Studies,* Dustin Rich, Norman Williams, G. Reinemer, and R. L. Cone, Optical Science and Laser Technology Conference, Bozeman, MT, September 13-14, 2002.
42. *Material Optimization of Er^{3+}:Y_2SiO_5 at 1.5 μm for optical processing, memory, and laser frequency stabilization applications,* Thomas Böttger, Y. Sun, C. W. Thiel, and R. L. Cone, Photonics West, Advanced Optical Data Storage, San Jose, CA, January 2003.
43. *Locating the electronic states of rare-earth ions relative to host band states for the development of photon-gated hole burning materials,* C. W. Thiel*, Y. Sun, and R. L. Cone, 8th International Meeting on Hole Burning, Single Molecule, and Related Spectroscopies: Science and Applications, Bozeman, MT, July 27 – 31, 2003.
44. *Spectral Diffusion in Erbium-Doped Transient Spectral Hole Burning Materials,* C. W. Thiel, T. Böttger, Y. Sun*, and R. L. Cone, 8th International Meeting on Hole Burning, Single Molecule, and Related Spectroscopies: Science and Applications, Bozeman, MT, July 27 – 31, 2003.
45. *Optical Dephasing by Disorder Modes in Yttrium Orthosilicate (YSO) doped with Eu^{3+},* R. M. Macfarlane, Y. Sun, R. L. Cone, C. W. Thiel and R. W. Equall, 8th International Meeting on Hole Burning, Single Molecule, and Related Spectroscopies: Science and Applications, Bozeman, MT, July 27 – 31, 2003.
46. *Transient and Permanent Spectral Hole-Burning in Erbium-Doped Glasses,* L. Bigot, S. Choblet, A-M. Jurdyc, B. Jacquier, T. Böttger, Y. Sun, and R. L. Cone, 8th International Meeting on Hole Burning, Single Molecule, and Related Spectroscopies: Science and Applications, Bozeman, MT, July 27 – 31, 2003.
47. *Spectral hole burning with a mode-locked laser,* Joe A. Fischer, Thomas Böttger, Mingzhen Tian, R. L. Cone, and Wm. Randall Babbitt, 8th International Meeting on Hole Burning, Single Molecule, and Related Spectroscopies: Science and Applications, Bozeman, MT, July 27 – 31, 2003.
48. *Overview of Cone/Sun Group Activities on Optical Material Design and Characterization,* R. L. Cone, Y. Sun, C. W. Thiel, Thomas Böttger, Gregory Reinemer, Peter B. Sellin, and Annabelle Collombet, Optical Science and Laser Technology Conference, Bozeman, MT, September 19-20, 2003.
49. *Transient and Permanent Spectral Hole Burning in Er^{3+}-Doped Glasses,* Y. Sun, T. Böttger, R. L. Cone, L. Bigot, Alcatel; S. Choblet, A-M. Jurdyc, and B. Jacquier, Optical Science and Laser Technology Conference, Bozeman, MT, September 19-20, 2003.
50. *Optimizing Erbium doped materials for optical processing, memory, and laser frequency stabilization applications at 1.5 μm,* T. Böttger, C. W. Thiel, Y. Sun, and R. L. Cone,

2004 Conference on Lasers and Electro-Optics/International Quantum Electronics Conference, San Francisco, CA, May 16-21, 2004.

B. Consultative and Advisory Functions

Cone's group served as advisors on crystal design and characterization to **Scientific Materials Corporation of Bozeman, MT, an AFOSR SBIR Phase II contractor**. A number of new materials were developed and characterized in this role. Cone's group also worked to enhance linkage of Scientific Materials to other groups in the Spectral Hole Burning community. Together Scientific Materials and Cone's group served a primary role as material developers and providers for application and advancement of spectral hole burning technology.

Todd Harris and Rufus Cone participated in a technical meeting on the **IBM – Montana State University Spectral Hole Burning Storage Review**, IBM Amaden Research Center, San Jose, California, September 17-20, 2000. The Eu:Y_2SiO_5 spectral hole burning / holographic storage material has been developed and refined by our group.

Dr. Yongchen Sun traveled to IBM Almaden Research Center for optical experiments with Michael Jefferson, Roger Macfarlane, and Peter Sellin, January 17-23, 2001. He also attended the **IBM – Montana State University Spectral Hole Burning Storage Review** at IBM Almaden Research Center, San Jose, California, January 18-19, 2001.

Visitors to our Research Group

Professor Neil B. Manson of the Laser Physics Centre , Research School of Physical Sciences and Engineering, Institute of Advanced Study of The Australian National University visited our laboratory from July 8 – 29, 2000; Manson, Pryde, and Cone began experiments on electromagnetically-induced transparency in Er^{3+}-doped rare earth crystals.

Dr. Matt Sellars of the Laser Physics Centre , Research School of Physical Sciences and Engineering, Institute of Advanced Study of The Australian National University visited our laboratory on July 12-14, 2000, following the Workshop on Applications of Spectral Hole Burning 2000 held at Big Sky, Montana.

Stefan Kröll, University of Lund, Sweden, visited our laboratory on July 12-14, 2000, following the Workshop on Applications of Spectral Hole Burning 2000 held at Big Sky, Montana. Stefan Kröll, Yongchen Sun, and Richard Meltzer discussed ongoing joint experiments on and analysis of the coherence properties of the hole burning material Pr^{3+}:Y_2SiO_5. The dependence of instantaneous spectral diffusion effects on photon echo excitation pulse 1 and pulse 2 is being investigated and correlated with phonon dynamics associated with the excited Pr^{3+} ions.

Advice on spectral hole burning materials was provided to **Professor W. Randall Babbitt**, AFOSR grantee.

Advice on spectral hole burning materials was provided to **Professor Kelvin Wagner** at the University of Colorado.

Professor Marlan Scully invited Cone to participate in the ONR/Texas A&M Workshop on Quantum Optics and Winter Colloquia on the Physics of Quantum Electronics. There is broad interest in rare earth materials for new quantum optical phenomena such as quantum information, electromagnetically induced transparency, lasing without inversion, and quantum computing.

Dr. R. M. Macfarlane of IBM Almaden Research Center San Jose, California, visited our laboratory for experiment collaboration many times throughout this project.

Dr. Michael Jefferson of IBM Almaden Research Center San Jose, California, visited our laboratory for several days in February 2001.

There were regular interactions with the interdisciplinary groups of the MSU Optical Technology Center (OpTeC).

Professor Marlan O. Scully visited the Cone/Sun Group and Spectrum Lab from March 16-20, 2001. Discussions centered on electromagnetically-induced transparency (EIT), laser stabilization and modeling, better ways to characterize laser linewidths, fine details of rare earth ion energy levels relevant to EIT, and conference organization. Marlan Scully is Burgess Distinguished Professor of Physics, Director of the Center for Theoretical Physics, and Director of the Institute of Quantum Studies, Texas A&M University, College Station, Texas. Professor Scully presented two Physics/Spectrum Lab Colloquia entitled,

- "*Stopping Light via Hot Atoms*," March 19, 2001
- "*Extracting Work from a Single Thermal Bath: The-One-Atom Quantum Heat Engine*," March 20, 2001.

Professor Uwe Happek, Department of Physics and Astronomy, University of Georgia, visited Rufus Cone, Charles Thiel, and Yongchen Sun on May 2-6, 2001. Happek presented a Physics Colloquium entitled, "*Photoconductive Studies of Optical Materials*," on May 4, 2001.

Dr. J. L. Hall, Fellow of the Joint Institute of Laboratory Astrophysics, Boulder, CO, visited MSU on August 24, 2001. Rufus Cone and Geoff Pryde, discussed their latest experimental results as he visited our laboratory. Hall has greatly helped the groups of Professors Cone and Carlsten with their programs in laser frequency stabilization involving, respectively, spectral hole frequency references and enhanced continuous wave stimulated Raman scattering.

Professor Jun Ye, Fellow of the Joint Institute of Laboratory Astrophysics, National Institute of Standards and Technology, and Physics Department University of Colorado, visited our group on December 13-14, 2001. Ye presented a Physics Colloquium entitled, *Time meets frequency: Coherent optical waveform generation and optical frequency synthesis.*

Professor Marlan Scully of Texas A&M visited January 15 and March 14-16, 2002.

Professor Robert Boyd of the Institute of Optics, University of Rochester, visited January 31 - February 2, 2002.

Dr. Michael Jefferson of IBM Almaden Research Center San Jose, California, visited our laboratory for several days in March 2002.

Professor Dan Boye, Davison College, visited April 4 – 7, 2002.

Dr. Todd Harris visited from IBM Almaden Research Laboratory, June 7, 2002, for discussions of spectral hole burning materials for data storage.

Dr. Yehoshua Kalisky, of ELOP (Electrooptics Industries Ltd), Rehovot Israel, visited our group for the month of July 2002 to carry out experiments on Yb^{3+}:YAG grown by Scientific Materials. Dr. Yehoshua Kalisky was a Sabbatical Visitor.

Dr. Laurent Bigot of Alcatel Research, Marcoussis, France, and **Dr. Bernard Jacquier** and **Dr. Anne-Marie Jurdyc** of the Laboratoire de Physico-Chimie des Matériaux Luminescents, Université Claude Bernard Lyon I, Lyon, France, visited our group during July 20 – 26, 2002, for spectral hole burning experiments on erbium-doped glasses used in commercial fiber amplifiers for telecommunications.

Dr. Phil Hobbs of IBM Yorktown visited August 15-20, 2002, for discussions of laser stabilization.

Dr.Fredy Meixner of the University of Siegen, Germany, visited August 21, 2002.

Professor Jürgen Schaefer of the Inst. fur Phys. und Zentrum fur Mikro- und Nanotechnologien, Technische Univ. Ilmenau, Germany visited on Sept 24, 2002.

One hundred scientists visited Bozeman and our laboratories for the **8th International Meeting on Hole Burning, Single Molecule, and Related Spectroscopies: Science and Applications – HBSM-2003**, July 27-31.

Dr. Laurent Bigot of Alcatel Research, Marcoussis, France, visited our group during August 1-14, 2003, for spectral hole burning experiments on erbium-doped glasses used in commercial fiber amplifiers for telecommunications.

Travel and Lab Visits

Geoff Pryde, Tom Böttger, Rufus Cone attended the Optical Society of America Annual Meeting in Providence, Rhode Island, October 22-26, 2000. Tom Böttger attended a short course on *Fiber-Optic Amplifiers* given by Douglas W. Hall, Corning, Inc.

Geoff Pryde, Tom Böttger, and Rufus Cone visited the Atomic Physics Laboratories at Yale University on October 27, 2000.

Rufus Cone, Charles Thiel, and Geoff Pryde, traveled to Snowbird, Utah, for the 30th Winter Colloquium on the Physics of Quantum Electronics, January 7 - 11, 2001.

Yongchen Sun traveled to IBM Almaden Research Center for optical nutation experiments with Michael Jefferson, Roger Macfarlane, and Peter Sellin, January 17-23, 2001.

Yongchen Sun attended the Spectral Hole Burning Storage Review at IBM Almaden Research Center with Alan Craig, Kent Hill, and Peter Sellin of The Spectrum Lab, January 18-19, 2001.

Rufus Cone and Tom Böttger attended Photonics West 2001 in San Jose, CA, January 22-28, 2001.

Tom Böttger, Geoff Pryde, and Rufus Cone visited Jean-Louis Legouet and Ivan Lorgere at Laboratoire Aimé Cotton, University of Paris, South in Orsay, France on June 28-30, 2001, for discussions of spectral hole burning devices including a microwave/radio frequency spectrum analyzer, chirped tunable lasers, our frequency stabilized lasers using spectral hole burning, and hole burning materials developed at MSU.

We also had fruitful discussions on applications of spectral hole burning to dispersion control and multiplexing in optical fibers with Kelvin Wagner of the University of Colorado ECE Department while there.

Charles Thiel, Geoff Pryde, and Yongchen Sun visited the Laboratoire Physico-Chimie des Matériaux Luminescents at the Université Claude Bernard Lyon 1, Lyon, France, on July 5, 2001, after attending the International Conference on Dynamical Processes in Excited States of Solids, July 1 - 4, 2001, at the Université Claude Bernard Lyon 1, Lyon, France. Rufus Cone and Tom Böttger also attended the conference.

Tom Böttger and Rufus Cone visited the Max Planck Quantum Optics Laboratory in Garching, a suburb of Munich, Germany, on July 5, 2001; ultrastable lasers and Fabry-Perot cavities, atomic frequency standards, mode-locked lasers, and optical frequency comb instrumentation were discussed.

Tom Böttger and Rufus Cone visited the diode laser company Toptica Photonics in Martensreid, Germany, a suburb of Munich, on July 6, 2001, to discuss opportunities for cooperation and product development (Toptica Photonics was TUI Optics).

Rufus Cone traveled to the University of Georgia Oct 10-12, 2001, for discussions with Professors Uwe Happek, Richard Meltzer, William Dennis, Bill Yen, and David Landau at the Physics Department of the University of Georgia, Athens, Georgia.

Rufus Cone and Yongchen Sun visited Academia Sinica in Taipei, Taiwan, for the 7th International Hole Burning, Single Molecule, and Related Spectroscopies Conference, November 16-24, 2001. Sun traveled to Hong Kong, where he visited Dr. Huasheng Wu, and to China where on Dec 5 he presented a talk at Henan Normal University.

Rufus Cone traveled to Lyon, March 23 –29, 2002, to serve on a Ph.D. thesis committee on development of rare earth doped materials.

Tom Böttger traveled to San Jose, CA, for Photonics West 2003. He also visited IBM Almaden Research Center and the University of California at Berkeley.

Tom Böttger visited the Physics Department at Westminster College in Salt Lake City, UT, and was offered a tenure-track Assistant Professor of Physics position on the faculty.

Tom Böttger presented a Physics Colloquium at University of San Francisco, Thursday February 13, 2003, entitled *"Diode Lasers Stabilized to Spectral Holes and Material Optimization of* Er^{3+}*:*Y_2SiO_5 *at 1.5 Microns."* He accepted a tenure-track Assistant Professor position in the Physics Department there. Tom will be setting up a diode laser laboratory and will visit our laboratory with undergraduate research students in the summers. This will be an important and fruitful source of new graduate students.

Rufus Cone, Yongchen Sun, and Charles Thiel presented invited talks at the American Chemical Society Meeting, March 18 – April 1, 2004.

Thesis Defenses

Todd Harris completed his Ph.D. thesis defense on April 11, 2001. His thesis was entitled, *Erbium-Based Optical Coherent Transient Correlator for the 1.5-Micron Communication Bands.*

Thomas Bottger completed his Ph.D. thesis defense on April 18, 2002. His thesis was entitled, *Laser Frequency Stabilization to Spectral Hole Frequency References in Erbium-Doped Crystals: Material and Device Optimization.*

Gregory Reinemer completed his Ph.D. thesis defense on January 24, 2003. His thesis was entitled, *Optical Characterization of Perturbed and* C_{3i} *Sites in Rare-Earth Doped Oxides.*

Charles Thiel completed his Ph.D. thesis defense on November 24, 2003. His thesis was entitled, *Energies of Rare-Earth Ion States Relative to Host Bands.*

Personnel Transitions

Dr. Todd Harris had a postdoctoral position at IBM Almaden Research Center, San Jose, California, and recently accepted a position as Research Engineer at SRI International, Menlo Park, CA.

Dr. Thomas Böttger was a Postdoctoral Fellow in the group for one year and on July 1, 2003, accepted a tenure-track Assistant Professor position in the Physics Department at the University

of San Francisco, San Francisco, California. Tom will be setting up a diode laser laboratory and inherited considerable laboratory equipment.

Dr. Gregory D. Reinemer, in February 2003 accepted a position as Visiting Assistant Professor of Physics in the Department of Physics and Astronomy at Idaho State University, Pocatello, Idaho.

Dr. Charles Thiel is a Postdoctoral Fellow in our group.

Postdoctoral fellow **Dr. Geoff Pryde** accepted a position in quantum computing on December 1, 2001.

Anna Hagenston, undergraduate Physics student, received her B.S. in Physics in May 2001. Ms. Hagenston won the Dean's Award for Excellence in the College of Letters and Science and is now a graduate student at Yale on an NSF Graduate Fellowship.

Michael Patterson, undergraduate Physics student, received his B. S. in Physics in May 2003 and is a Ph. D. student in Complex Biological Systems at MSU.

Dustin Rich received his B. S. in Mechanical Engineering in May 2003 and accepted a position as an Assistant Shift Test Engineer at the Puget Sound Naval Shipyard, Bremerton, Washington, where he works in the Nuclear Test Engineering organization that is responsible for operations and testing of nuclear propulsion plant systems.

Cooper McCann, undergraduate Physics student from Pony, Montana, received his B. S. in Physics in May 2004 and began a job as laser technician at the laser company AdvR in Bozeman, Montana.

Ted Armstrong, undergraduate Physics student from received his B. S. in Physics in May 2004 and will begin medical school at the University of Minnesota in August 2004.

Technology Transitions

Transition

Customer:
Scientific Materials Corporation
Ralph Hutcheson and Randy W. Equall
310 Icepond Road
PO Box 786
Bozeman, MT 59715
Phone: (406) 585-3772
Fax: (406) 585-8606

&

The Spectrum Lab
Montana State University
Bozeman, MT 59717

Result:
Three US Patents have been licensed by Scientific Materials Corporation.

1. United States Patent 6,407,831. *Coherent interaction of optical radiation beams with optical-electronic materials of generalized crystal symmetry.* Inventors: Rufus L. Cone (Bozeman, MT), Guangming Wang (Marlborough, MA), Yongchen Sun (Bozeman, MT), Randy W. Equall (Bozeman, MT), issued June 18, 2002.
2. United States Patent 6,516,014. *Programmable Frequency Reference for Laser Frequency Stabilization, and Arbitrary Optical Clock Generator, Using Persistent Spectral Hole Burning,* J. L. Carlsten, R. L. Cone, P. B. Sellin, N. M. Strickland, issued February 4, 2003.
3. United States Patent 6,654,394. *Laser Frequency Stabilizer Using Transient Spectral Hole Burning,* J. L. Carlsten, R. L. Cone, P. B. Sellin, N. M. Strickland, issued November 25, 2003.

Application:
This technology is used for high bandwidth **Radar Signal Processing** by spectral hole burning (SHB) and optical coherent transients. This technology incorporates our material design and our laser stabilization to spectral holes. The same SHB material acts as signal processor and as laser frequency reference.

Transition

Customer:
Scientific Materials Corporation
Ralph Hutcheson and Randy W. Equall
310 Icepond Road
PO Box 786
Bozeman, MT 59715
Phone: (406) 585-3772
Fax: (406) 585-8606

&

The Spectrum Lab
Montana State University
Bozeman, MT 59717

Result:
Laser stabilization to spectral holes – art and realization of optics, electronics, and mechanics.

Transition

Customer:
Scientific Materials Corporation
Ralph Hutcheson and Randy W. Equall
310 Icepond Road
PO Box 786
Bozeman, MT 59715
Phone: (406) 585-3772
Fax: (406) 585-8606

Result:
Our characterization of optical crystals has led to understanding of the impacts that the crystal growth process has on the active properties of the materials. Improvements and new products have resulted.

Application:
These products are for solid state lasers, opto-electronic applications, and spectral hole burning signal processors. The products are used by AFRL and by AFOSR contractors and grantees as well as the broader laser and electro-optics industries.

- Spectroscopy samples were supplied by Scientific Materials to Philip Hemmer at AFRL based on our work.
- Spectral hole burning samples were supplied by Scientific Materials to numerous other AFOSR-supported researchers based on our work.
- Laser gain media were supplied by Scientific Materials to Ken Dindorf and Harold Miller at Kirtland AFB.
- Laser gain media were supplied by Scientific Materials for Wright Patterson Air Force Base for 2 micron LIDAR. This LIDAR related laser development work involves collaboration of Scientific Materials with Coherent Technologies Inc in Boulder, CO.
- Work on crystal growth techniques for $YAlO_3$ impacted various projects for 2 micron LIDAR.
- We have explored crystal defect sites in rare earth doped garnets in collaboration with Scientific Materials.
- Our developments of the concept of 'single Rabi frequency orientations' for spectral hole burning materials such as Tm^{3+}:YAG and Er^{3+}:Y_2SiO_5 were used by the groups of Philip Himmer, Tom Mossberg, William Randall Babbitt, MSU Spectrum Lab, Stefan Kröll, and Jean-Louis LeGouet.
- We made improvements to Eu^{3+}:Y_2SiO_5 used by MSU Spectrum Lab and IBM Almaden Research Center for optical data storage development.
- We developed a method for determining the occupation of individual crystal sites.
- We helped with the development of Y_2O_3 crystal growth and crystal characterization. This material has superior thermal properties for laser use.

We developed and characterized a number of new spectral hole burning materials for optical correlators, memories, and other signal processing applications. With Scientific Materials we actively participated in the design of new materials. We cooperatively optimized the material properties through the close interaction with Scientific Materials made possible by our location;

by providing rapid feedback. Adjustments were made to the synthesis process, leading to development of better quality materials.

The hole burning materials have been transferred to several other research groups at MSU, leading to significant advancements in their AFOSR and DoD funded programs:

- Professor W. R. Babbitt's group on optical signal processing has exploited the technology in sophisticated demonstrations of correlators and true-time delay generators and RF spectrum analyzer project.
- Dr. Kris Merkel and Dr. Alan Craig have used a Ti:S laser stabilized to spectral holes to demonstrate the accumulation of complex correlator signals for optical signal analysis.
- Groups in France, Sweden, and Australia have applied our materials and techniques in their development of optical correlators, memories, and rf spectrum analyzers.
- Scientific Materials Corporation provides the hole burning materials we have developed to the commercial market.

Transition

Customers:
Scientific Materials Corporation
310 Icepond Road
PO Box 786
Bozeman, MT 59715
Phone: (406) 585-3772
Fax: (406) 585-8606

&

The Spectrum Lab
Montana State University
Bozeman, MT 59717

Result:

Single-Eu^{3+}-isotope $^{151}Eu^{3+}:Y_2SiO_5$ and $^{153}Eu^{3+}:Y_2SiO_5$ crystals were designed and characterized for high capacity optical memories.

Application:

The $Eu^{3+}:Y_2SiO_5$ crystals doped with only the ^{151}Eu isotope extend the data storage time to several weeks in high-density optical data storage devices based on spectral hole burning. They also optimize storage density by using the minimum hyperfine splitting.

Transition

Customers:
Scientific Materials Corporation

310 Icepond Road
PO Box 786
Bozeman, MT 59715
Phone: (406) 585-3772
Fax: (406) 585-8606

&

The Spectrum Lab
Montana State University
Bozeman, MT 59717

Result:
Er^{3+}:Y_2SiO_5 crystals for real-time optical signal correlators in the 1.5 micron band and ultrastable lasers stabilized to spectral holes

Application:
The spectral hole burning materials and principles of spatial-spectral holography provide real-time correlator devices for multi-GHz signal processing at 1536 nm. The active Er^{3+}:Y_2SiO_5 crystal material has been optimized for composition, crystal orientation, signal bandwidth, and purity for processing signals at up to 10 GHz bandwidth. The same material has provided frequency references for stabilizing the frequency of the diode laser used in these devices.

NEW DISCOVERIES, INVENTIONS, PATENT DISCLOSURES

Three US Patents Issued

1. United States Patent 6,407,831. *Coherent interaction of optical radiation beams with optical-electronic materials of generalized crystal symmetry.* Inventors: Rufus L. Cone (Bozeman, MT), Guangming Wang (Marlborough, MA), Yongchen Sun (Bozeman, MT), Randy W. Equall (Bozeman, MT), issued June 18, 2002.

2. United States Patent 6,516,014. *Programmable Frequency Reference for Laser Frequency Stabilization, and Arbitrary Optical Clock Generator, Using Persistent Spectral Hole Burning,* J. L. Carlsten, R. L. Cone, P. B. Sellin, N. M. Strickland, issued February 4, 2003.

3. United States Patent 6,654,394. *Laser Frequency Stabilizer Using Transient Spectral Hole Burning,* J. L. Carlsten, R. L. Cone, P. B. Sellin, N. M. Strickland, issued November 25, 2003.

HONORS AND AWARDS

Rufus Cone was made a **Fellow of the American Physical Society.**

Charles Thiel was chosen by the MSU Physics Department for the 2004 Graduate Achievement Award.

Anna Hagenston, an MSU physics undergraduate participating in this project in our laboratory, won the Dean's Award for Excellence in the College of Letters and Science in May 2000.

Dustin Rich, an MSU mechanical engineering undergraduate participating in this project in our laboratory, won the **William E. Parkins Engineering-Physics Award at Montana State University** in April 2001. Following the award, Rich was quoted as saying, "Working with people of varied backgrounds and being involved in following a concept through all the stages of design and manufacture has been exciting and a great learning experience."

Ted Armstrong, an MSU physics undergraduate participating in this project in our laboratory, won the Alpha Lambda Delta Senior Book Award for the highest grade point average of an undergraduate at MSU – 4.00.